UNIVERSITY OF NAIROBI

INSTITUTE OF NUCLEAR SCIENCE AND TECHNOLOGY

ENHANCEMENT OF X-RAY IMAGES FOR INDUSTRIAL APPLICATIONS

Njogu, Peter Kimani

S56/71531/2014

B. Eng. in Electrical and Electronics Engineering

(Moi University)

A thesis submitted in partial fulfilment for the Degree of Master of Science in Nuclear Science in the Institute of Nuclear Science and Technology in the University of Nairobi.

November, 2016

DECLARATION AND APPROVAL

Declaration

This thesis is my original research work. It has not been presented for a degree in any other university.

Name: Njogu, Peter Kimani

Registration number: S56/71531/2014

Signature: ……..…….… Date:……

Approval

This thesis has been presented for examination with our approval as the university supervisors.

1. Mr. David M. Maina,
   Institute of Nuclear Science and Technology,
   University of Nairobi, Kenya.

   Signature: ……..…….… Date:……..……

2. Prof. Michael J. Gatari,
   Institute of Nuclear Science and Technology,
   University of Nairobi, Kenya.

   Signature: ……..…….… Date:……..……

3. Prof. Elijah M. Mwangi,
   School of Engineering,
   University of Nairobi, Kenya.

   Signature: ……..…….… Date:……..……

ORIGINALITY DECLARATION

Name of student: NJOGU, PETER KIMANI

Registration Number: S56/71531/2014

College: COLLEGE OF ARCHITECTURE AND ENGINEERING

School: INSTITUTE OF NUCLEAR SCIENCE AND TECHNOLOGY

Course Name: MASTER OF SCIENCE IN NUCLEAR SCIENCE

Title of the work: ENHANCEMENT OF X-RAY IMAGES FOR INDUSTRIAL APPLICATIONS

DECLARATION

1. I understand what Plagiarism is and I am aware of the University's policy in this regard.
2. I declare that this THESIS is my original work and has not been submitted elsewhere for examination, award of a degree or publication. Where other people's work or my own work has been used, this has properly been acknowledged and referenced in accordance with University of Nairobi's requirements.
3. I have not sought or used the services of any professional agencies to produce this work.
4. I have not allowed, and shall not allow anyone to copy my work with the intention of passing it off as his/her own work.
5. I understand that any false claim in respect of this work shall result in disciplinary action, in accordance with University Plagiarism Policy.

Signature…… Date …….

DEDICATION

I dedicate this work to my adoring wife Caroline Reseccah and my beautiful daughter Ivanna for their unconditional support, encouragement and for what they have taught me:

"Success often comes to those who dare to act".

ACKNOWLEDGEMENTS

First, I would like to show my appreciation to Prof. Elijah Mwangi for his guidance, reassurance and continuous support throughout my research period. Although I did not meet his expectation sometimes, he was still ready to assist and encourage me. His challenges let me reflect and find my real problems. It was an invaluable encounter that only Prof. Mwangi's student can appreciate. The rigorous research attitude I have learned from him has benefited and will continue to benefit every aspect of my life.

I am also appreciative to my other supervisors, Mr. David Maina and Prof. Michael Gatari, for their valuable suggestions and help. This research would not have been easy to conduct without the help that they always offered me willingly. My appreciation also goes to the Institute staffs for their unending support.

I am highly indebted to Quality Inspectors Limited and Kenya Bureau of Standards for allowing me to use their equipment and their unreserved cooperation and assistance during data collection. I also acknowledge the 20 observers who contributed in the subjective measurements test evaluation. I appreciate you for accepting to participate in the study.

I am grateful to the National Commission for Science, Technology and Innovation (NACOSTI) for their research endowment fund that made this research possible.

Thanks also to the International Science Programme, Uppsala University, Sweden, and International Atomic Energy Agency (IAEA) for their research support to the Institute of Nuclear Science and Technology.

Lastly, I am thankful to my family members for the boundless support and absolute love they have accorded me during my research period.

Kimani Njogu,
November, 2016.

ABSTRACT

In metallic structures, defects are usually manifested as cracks, surface wear, poor weld spots and slag inclusions. The timely detection of such faults is useful in preventive maintenance routines. Various researchers have shown that manual inspection on structures is unreliable, because the human visualization process is susceptible to inaccuracies and can be biased. Hence, manual results lack reliability and consistency. This hampers with the entire process of preventive maintenance. Similarly, manual inspection is costly and consumes a lot of time. This has given way to the development of numerous automated techniques for defect detection. This thesis is developing a simple and efficient technique for automatic defect detection on digital radiographic images for industrial application. Otsu's and percolation thresholding and segmentation algorithms have been used in developing the proposed algorithm.

In addition, it is desirable that images should be in a form in which information can be extracted easily, interpreted and where necessary permit for further image processing. In this thesis various image enhancement techniques have been reviewed so as to improve on the contrast of digital radiographic images obtained from the industrial sector. These techniques involve diverse procedures such as histogram equalization, contrast stretching, edge sharpening and noise reduction. These processes are achieved by using both the frequency and spatial domains. This investigation involves the use of both techniques and aim at improving existing algorithms. One of the envisaged approaches is the use of histogram based contrast enhancement supplemented by some wavelet based noise suppression technique. This eliminates low contrast and improves the degraded features.

MATLAB based computer simulations have been applied in determining the efficacy of the proposed algorithms. The radiographic images used were obtained from Quality Inspectors Limited, Kenya Bureau of Standards and from various internet sites which contain images used by other researchers. A total of sixty two images and sixteen templates were used. Both subjective and objective techniques have been applied to determine the usefulness of the suggested techniques. The performance of these algorithm, which involved image denoising using wavelets, image enhancement to improve on the image contrast and automatic defect detection, are better in comparison to existing defect detection techniques and the outcomes achieved were remarkable in regard to the rate of defect detection and the defects identified such as cracks, weld pores and slag inclusions.

TABLE OF CONTENTS

ABBREVIATIONS AND ACRONYMS

2-D - Two Dimensional

AHE - Adaptive Histogram Equalization

BBPHE - Background Brightness Preserving Histogram Equalization

BPBHE - Brightness Preserving Bi- Histogram Equalization

CCTV - Closed-Circuit Television

CHE - Classical Histogram Equalization

CLAHE - Contrast Limited Adaptive Histogram Equalization

CoC - Coefficient of Correlation

CPU - Central Processing Unit

CR - Computed Radiography

DFT - Discrete Fourier Transform

DHE - Dynamic Histogram Equalization

DSIHE - Dualistic Sub-Image Histogram Equalization

DWT - Discrete Wavelet Transform

GB - Giga-Byte

GIF - Graphics Interchange Format

HVS - Human Visual System

IPT - Image Processing Toolbox

IQA - Image Quality Assessment

JPEG - Joint Photographic Experts Group

KEBS - Kenya Bureau of Standards

MATLAB - MATrix LABoratory

MMBEBHE - Minimum Mean Brightness Error Bi-Histogram Equalization

MSE - Mean Square Error

NC - Normalized Correlation

NCC - Normalized Cross Correlation

NDT - Non-Destructive Testing

PNG - Portable Network Graphics

PSNR - Peak Signal to Noise Ratio

QIL - Quality Inspectors Limited

RAM - Random Access Memory

RMSHE - Recursive Mean Separate Histogram Equalization

ROI - Region of Interest

RT - Radiographic Testing

SSET - Sewer Scanner and Evaluation Technology

SSIM - Structural Similarity Index Measure

LIST OF FIGURES

LIST OF TABLES

CHAPTER ONE

INTRODUCTION

1.1 Background

Engineering components require testing to ensure their reliable performance during their service life without premature failure. Some of these components function in hostile environments such as in corrosive atmosphere, extreme temperatures and high pressure, which may reduce their service life. Hence, these components must be subjected to several non-destructive tests to ensure that they are free from defects. In engineering, Industrial Non-Destructive Testing (NDT) is concerned with all techniques that examine, test, detect and evaluate materials for defects or discontinuities that may affect the usefulness or serviceability of an object without causing any physical damage to the material. In industries, NDT has found application in raw materials examination prior to processing, process control by assessing materials throughout the processing phase, examination of finished products and assessment of structures and products when in use (Hellier, 2003).

Since the 1950's to date, unparalleled innovation and development of NDT technology has been witnessed through new resources and instrumentation. The capability to interface modern apparatus with supercomputers has had a considerable influence on this technology. This has made it possible to store huge amounts of data with nearly instant archival capability. In the present day's usage, NDT can be broken into several categories where it plays a crucial role in quality control at various stages of manufacturing, process design for materials, material property measurements and online process control (Satish *et al.*, 2013). Moreover, NDT is essential in determining the continued safe operation of machines and has found applications in the analysis of the machine inner parts which are undetectable to the naked eye (Domingo, 2014). The main advantage of NDT is that the assessment procedure yields no detrimental effects on the material or structure being tested. This therefore, ensures that the structural components and systems accomplish their function in a reliable and cost effective manner (Satish *et al.*, 2013).

The NDT expertise has grown and advanced to incorporate numerous highly developed techniques being used nowadays. These inspection techniques include radiography tests, ultrasonic tests, visual tests, thermal infrared tests, penetrant tests, magnetic particle tests, eddy current tests and acoustic emission tests. Some of which are limited by their performance and feasibility outside laboratory setting. For example, film development in radiography tests relied on laboratory processing and reading (Hellier, 2003).

One of the most effective method of NDT is Radiographic Testing (RT) which relies on either X-ray energy or gamma ray energy in determining material properties or indicating the presence of material discontinuities which are either on the surface or concealed. In RT applications, the radiation beam is forced to penetrate through the test object. The energy within the radiation beam is reduced in proportion to the thickness of the material and the occurrence of any defect within the test object is detected. Basically, an image with added information relating to the internal structure of the test object is produced. Any defect reduces the amount of attenuation and this has a direct relationship to the X-ray energy attenuation of the sound material immediately adjacent the void. Equally, if there is a high-density inclusion within the test object the level of attenuation will be increased. The X-ray energy left after attenuation is recorded by an imaging device and from this information a two-dimensional X-ray image is produced. This is recorded on a radiographic film where it is later processed, examined by using a film viewer and then analysed. The image thus produced is permanent in nature and cannot be modified. However, modern advancement in imaging technology has steered the development of advanced techniques such as digital radiography which are being explored as alternative to film radiography.

Digital radiography is a method of obtaining a digitized radiographic image of an object, which can be displayed on a computer monitor. It makes use of a special phosphor coated flexible imaging plate that is exposed to the radiation beam. Then, the image plate is scanned in a special scanner, called Computed Radiography (CR) Blade, to produce electronic images. This technique does not include any wet chemical processing, hence there is no associated chemical hazard. In addition, digital radiographs can be stored in wide variety of storage devices and has the ease of availability. Moreover, the image obtained is immediately available for real-time operation and manipulation. However, these images have a range of distortion achieved during the process of acquiring the

image, processing the image, compressing it, storing it, transmitting it and finally when reproducing the image. Subsequently, it is very important that image quality assessment be performed for the various image processing techniques in use. In order to find answers to problems facing digital radiography a lot of software simulations and testing are required. A good illustration of such modern image processing software is MATLAB (MATrix LABoratory). This is a powerful, high level language that integrates programming, computation and visualization in a user-friendly environment where it is possible to represent problems and solution in familiar mathematical notations (Gonzalez and Woods, 2008; MathWorks, Inc, 2009). This software uses application-specific toolboxes which are used to perform specialized computations like control systems, signal processing, wavelets, neural networks, image processing and simulation. With this software it is possible to interact with complex image processing functions and interactive tools that are used to analyse digital images such as image enhancement, noise reduction, image transformation, colour manipulation and region of interest manipulation (Solomon and Breckon, 2011).

1.2 Problem Statement

A major problem in the industrial sector is the low development in image enhancement despite the progress that has been witnessed in the medical field. Industrial radiographs are of low contrast and the images produced are unsharp which leads to poor image clarity. Besides, conventional radiography produces images on film which are permanent in nature. This format does not allow easy modification to be done on the image.

Most X-ray images have important details of information obscured due to factors such as poor illumination, low resolution, noise, fading and geometrical distortions (Gonzalez and Woods, 2008). The existing enhancement algorithms cannot remove these effects by themselves.

In industries, defect fatigues on working machines are the most common types of fractures and develop after a large number of load applications on the machine. This can lead to reactor failure, derail of trains, pipeline to burst and machine breakdown if not identified during routine maintenance. Also, in aircrafts, the main structural problems are corrosion detection and fatigue cracks which are not visible and these can cause damages that can lead to a plane crash. Moreover, in industries dealing with plastics, manufacturers are forced to cut prototypes so as to measure or analyse concealed defects.

Such a challenging task consumes a lot of time and is an expensive affair. Alloy casting produced for industrial automotive applications sometimes contain discontinuities and non-homogeneous regions within the work piece which are dangerous for the overall roadworthiness. Besides, welding processes contain some flaws such as lack of fusion, porosity, inclusion and cracks which can be disastrous.

Radiographs are inspected by skilled personnel who can recognize variations in film density due to flaws in the presence of non-uniform background and other unwanted image features. The success in detecting the flaw signals is limited by the sensitivity of the operator sight. Additional factors affecting successful inspection include eye strain and operator fatigue which result in poor detection performance. These factors contribute to the fluctuating quality of inspection achieved in the conventional radiographic inspection process.

The commercial nature of some image processing software leads to the main problem of practical non-usability for scientific work, like image filtering and image enhancement. This is because the user has no control of any kind over the algorithms used in the functions and there are practically no references about any scientific background or its implementation in to the algorithms. For example, adobe photoshop image processing is a preferred method among law enforcement forensic experts for digital enhancement of latent fingerprints. However, there is no defined procedure of how to enhance an image. Also, the exact steps used during photoshop may deliberately remove some crucial information which might exclude a suspicious person. Hence the need to use scientific image analysis packages that can be relied on (Carasso, 2013).

To overcome the challenges of human error in identify defects in an image, even where you have trained operators, an algorithm for crack detection has been formulated. This identifies defects and evaluates them as either acceptable or they are rejected in reference to a design programme for acceptance or rejection. In addition, a combination of various procedures are required so as to improve on image contrast. In this research, various image enhancement procedures have been proposed for enhancing such images.

1.3 Justification and Significance of the study

The research aims at improving X-ray images obtained from any industrial inspection to provide better differentiation of available defects and to automate the procedure

identifying defects. The applied image processing techniques do not increase the inherent image content, rather they manipulate the image to improve its visibility. Digital X-ray imaging has its application ranging from simple welding in pipes to the most complex applications in threat detection at security checkpoints and cracks inspection in aircrafts.

Today, X-ray imaging provides a powerful and an advanced tool to plastic manufacturers for the authentication of their products. By enhancing the clarity of the images obtained, it is possible to recognise product inconsistencies and issues with the design. This ensures lot-to-lot uniformity and gives an accurate and comprehensive measure of inner components. Another important aspect is the increase in speed of product qualification, troubleshooting and analysis. This therefore prevents loss of material, manpower and time leading to increase in production. Besides, since it is possible to identify defects and inclusions quickly, schedules and manufacturing processes are not badly affected. Moreover, NDT assists in accelerating the time required in completing a project since it decreases the time required to qualify production parts. In addition, it is probable to overlook assembly details in assembly analysis through observation. However, with improved clarity of the images defects are analysed and reviewed easily without segmentation.

Preventive maintenance gives information whether certain parts are still satisfactory for use thus enabling the manufacturer to plan for their replacement. This also leads to predictable production, fewer repairs, less accidents in the field of safety and lower operating costs.

Additionally, radiographic images are not easy to interpret. This is due to the fact that during the film developing process some artifacts might be added making it problematic to identify the real defects. Some artifacts may even result in masking of discontinuities. By using digital images, these problems are eliminated. Also, since radiation dose requirement is less in imaging plates, it may be used in combination with battery operated pulse X-ray machine for remote field application. The equipment used are portable, thus improving efficiency (Das *et al*., 2013).

The image produced by digital radiography is available in digital format and can be processed by several image enhancement technique to extract more information. Also, digital radiography does not include the use of chemicals for film processing, hence there

is no associated chemical hazard. In addition, the images obtained can be stored in wide variety of storage devices such as compact discs, flash disks and hard disks and can be retrieved easily and faster. Moreover, the image obtained is immediately available for real-time operation and manipulation.

In industrial structures, discontinuities are undesirable as they reduce the strength of the structure to unacceptable levels affecting their functionality, dependability, and their lifespan.

1.4 Objectives

This research has its main objectives of developing an image enhancement technique that can improve the clarity of X-ray images used in the industrial sector and to automate the process of defect detection.

Specific objectives:

i) To obtain a suitable histogram-based and edge-preserving image enhancing algorithm,
ii) To perform noise reduction in X-ray images using Discrete Wavelet Transform (DWT),
iii) To sharpen images in order to reveal details in a more contrasted manner,
iv) To develop an algorithm for automatic defect detection in pipe images.

1.5 Scope of study

This thesis focusses on industries that rely on X-rays for their NDT inspection in their day-to-day operations specifically in alloy casting inspection, cargo inspection, food products analysis, automotive parts inspection, cracks and welds quality control in pipeline companies, aviation industry for corrosions and cracks in aircrafts and forensic investigators. Additionally, it can resolve the issue of having to rely only on trained operators to identify defects.

The study does not cover the identification of cracks in terms of their length or the number of cracks available in a certain cluster.

1.6 Thesis Organization

This first chapter gives a brief introduction to X-ray imaging and its application in Non-Destructive Testing (NDT). A statement of the problem has been made, justification and

significance of this research to the engineering field, the objectives as well as the scope of the research are also presented in this chapter.

Chapter two covers some of the literature on digital image enhancement techniques and imaging automation process. It presents the background relevant for understanding the digital image enhancement techniques. It begins with a broad overview of various image assessment techniques in general. It then briefly introduces the methodology for automated image-based inspection. Recent works that are related to this study have also been highlighted in the chapter.

In chapter three, the theoretical aspects of image enhancement are presented. They are divided into either spatial or frequency domain methods. The spatial domain enhancement procedures presented are contrast stretching, histogram processing, spatial filtering, as well as the theory in image segmentation. The frequency domain enhancement methods presents the two-dimensional Fourier and Wavelet Transforms. Also frequency domain filtering, image denoising and wavelets thresholding methods are expounded.

The fourth chapter presents the materials and methods that were used in carrying out the research. There is an explanation of the different algorithms of the various phases of image processing and analysis and their application in automatic crack detection.

Computer simulation experimental results obtained during the research are presented in chapter five. These have been used to prove the effectiveness of our algorithms. The simulations have done using MATLAB.

Chapter six gives the thesis conclusions and proposes some advances and guidelines of future research work.

A published reference document and appendices are included at the end of this thesis.

CHAPTER TWO

LITERATURE REVIEW

2.1 Overview

Images are two-dimensional, *f(x, y),* or three-dimensional, *f(x, y, z),* mathematical representation made of different gray intensities. The *f* represents the amplitude while *x*, y and *z* are the spatial coordinates. When these values are finite, a digital image is obtained (McAndrew, 2004). A combination of these finite elements with specific values and locations are called picture elements (pixels). According to Gonzalez and Woods (2008), these images are categorized in four broad types according to their pixel format: gray-scale images, binary images, true colour images and indexed images.

Firstly, gray-scale or intensity images are data matrices whose values represent shades of gray. They have a pixel range that is limited by the available resolution of the bits (Solomon and Breckon, 2011). For instance, the gray-scale image values can have integer values of [0, 255] for an 8-bit image or [0, 65535] for a 16-bit image. Secondly, a binary image uses a single bit to symbolise each pixel. In a binary image, the pixels exist either in the on or off states. This gives the representation two colours available of either white or black. Since it is not possible to characterise the in-between pixels in a binary image, this restricts their usage in photography. Thirdly, a true-colour image is represented by an M by N by 3-data matrix of colour pixels, which characterize the red, blue and green constituents of the image at precise spatial sites. The image formed has similar integer values range of [0, 255] for an 8-bit image or [0, 65535] for a 16-bit image. Lastly, indexed images have integers of data matrix and colour-map matrix representing the colour in the image. These two components assist in direct mapping of pixels intensity values to colour-map values (Gonzalez and Woods, 2008).

Digital image processing origin is closely tied to the advancement of digital computers. This is because, digital imaging require massive computational power and storage space that are purely dependent on the development of digital computers and their auxiliary machineries. The first powerful computers to carry out meaningful image processing tasks can be traced back to the early 1960s. This advancement was brought about by research in space exploration. From then to date, image processing has full-grown solidly

into two major areas: enhancement of visual information for analysis; and data processing so as to store it better, transmit it and represent it for better cognition.

2.2 Image processing

Image processing is a technique for manipulating a digital image with the intention of extracting additional information or producing another representation of the same image (Gonzalez and Woods, 2008). The motivations behind image processing fall into either the removal of unwanted signal components corrupting the image hence improving on the image appearance; or the extraction of information from an image for further computer processes. As such, image processing produces a resultant image that is better in comparison to the original image for some predefined applications. This is important, because it shows that the techniques discussed are problem-oriented (Sinha and Fieguth, 2006).

The whole process of image processing is summarised in Figure 2.1. The various approaches applicable to images are shown.

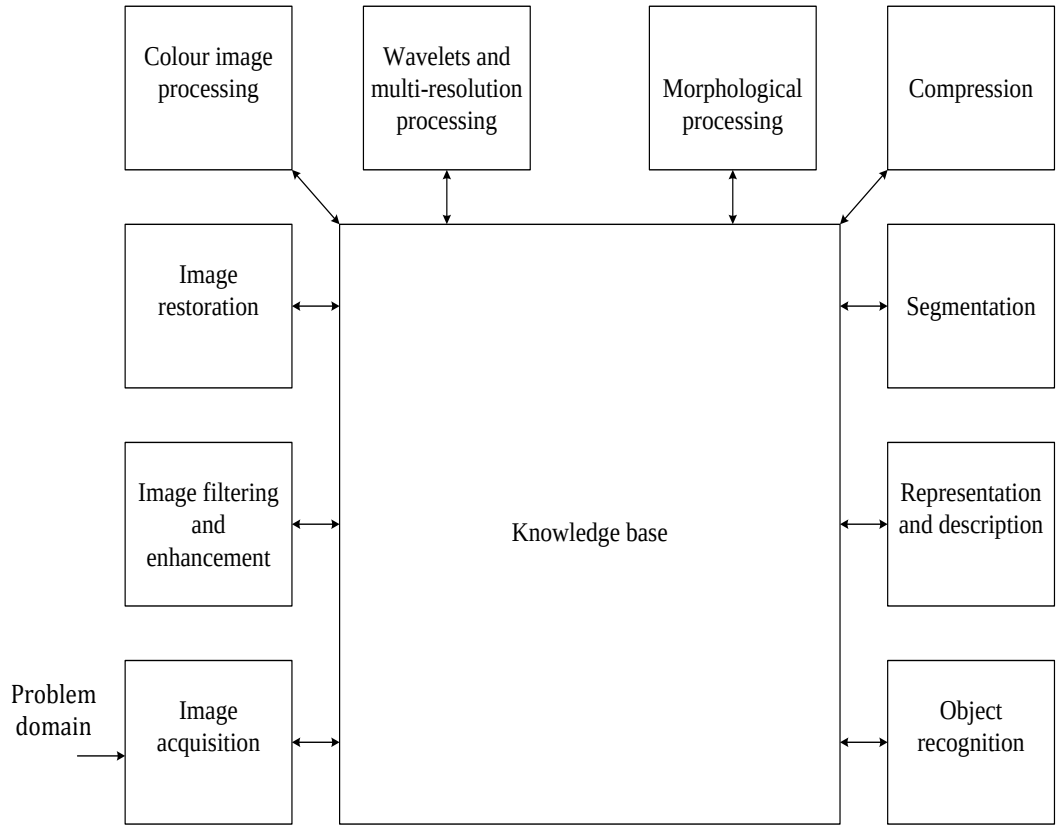

Figure 2.1: Major imaging methodologies (Gonzalez and Woods, 2008).

Image acquisition: this is the process of obtaining an image by combining an illumination source and a sensor which either reflects or absorbs the energy from the source. The image is then converted to a manageable entity. For example, to visualize a gray-scale image, the information from the sensor is converted into a pixel in the range of [0, 255] for an 8-bit image. Such values are interpreted as the amount of light received by a cell during that specific exposure time.

Image enhancement: it involves manipulation of an image so as to obtain a more appropriate image for a specific application. By suppressing the unwanted distortions in the background, it is possible to obtain an improved image where obscured details are revealed or certain features, like cracks, are highlighted. This improves the visual appearance of the image (McAndrew, 2004). This shows that this methodology is problem-oriented. It has application in the medical arena and in other applications like military surveillance, industrial inspections, aviation industry, geology, meteorology, astronomy and in entertainment.

Image restoration: this technique attempts to reconstruct a corrupted image from previous understanding of the degradation procedure used. It entails formulation of a standard that produces optimal results (Gonzalez and Woods, 2008). This technique involves the use of mathematical and probabilistic models in testing the reconstruction of the image, resulting in an objective measurement.

Colour image processing: colour simplifies object identification and extraction. In addition, it is possible for humans to differentiate countless colour intensities as compared to just a hundred gray-shades. This simplifies the entire process of image analysis since additional information can be found in a colour image.

Wavelets: these are functions of varying frequency and limited duration. These techniques make the wavelet transform more practical than the Fourier transform in computing spectral information that does not have previous and future information about its signal over the entire time domain. In addition, wavelets will decompose data without gaps or overlap and the decomposition process is reversible. Wavelets are localized in both frequency and time and find their applications in image denoising and compression.

Image compression: this entails data reduction to fewer bits without corrupting the quality of the image to intolerable levels (Solomon and Breckon, 2011). This permits the

storage of more images in a specified memory space and decreases the necessary bandwidth for transmission.

Morphological image processing: this deals with important operations that are used for extracting useful image components which are used to represent and describe region shape, such as boundaries. In this technique, the input is an image but the outputs are attributes of the image extracted using tools such as morphological filtering, thinning and pruning.

Image segmentation, representation and description: image segmentation subdivides a digital image into various regions of similar attributes (McAndrew, 2004). The level of segmentation is specific to a given problem. In that case, the process of segmentation is stopped after identifying the regions of interest. An accurate segmentation procedure makes the process of image recognition and analysis simple and has very high chances of succeeding. On the other hand, representation involves the use of the raw data yielded by segmentation techniques for further computer processing. A section can be represented either by using its external characteristics or in terms of its internal characteristics. Description, instead, deals with digging out some image attributes resulting in some quantitative information being acquired from an image.

Object recognition: this entails identifying a specific element in an image by using particular tags called descriptors. In the real world, machines cannot recognise objects by themselves and they require some algorithmic descriptions to enable them recognize objects. Implementing these tasks on machines is an intricate task.

2.3 Application of digital image techniques

Image processing for human interpretation found their ways into medical diagnosis in the late 1960s. Besides medicine space exploration, radiographic images have found applications in numerous fields. For example, computer algorithms are being used to improve image contrast and change its intensity levels into colour for easier interpretation. This has found its usage in industries, airports and medical fields mostly dealing with X-rays. Similar techniques are used by geographers when studying aerial and satellite images. Moreover, image processing techniques have found applications in archaeological sites for restoration of blurred pictures of rare artifacts that have been damaged or lost after being photographed. Other related fields where image processing

has found applications are astronomy, nuclear medicine, law enforcement and defence (Weeks, 1998).

In addition, these techniques are being used in areas dealing with machine perception or computer vision. This extracts suitable information from an image for computer processing. It has found its usage in automatic character recognition, automatic fingerprints processing and product assembly and inspection.

Some of the techniques in section 2.2 have been utilized in this thesis to assist in the enhancement and automation of defect detection mostly in pipes. The techniques to emphasize on and develop algorithm are segmentation and contrast enhancement methodologies as discussed below and in later chapters.

2.4 Contrast Stretching

Contrast stretching operates by increasing the difference between the darkest and brightest pixel ranges of a gray-image to full range (Gonzalez and Woods, 2008). This results in the expansion of the brightness values, making it easier for an image to be presented efficiently to an expert for analysis (Singh *et al*., 2013). This process can be denoted as shown below for an 8-bit gray-scale image;

$$g(x,y) = \frac{255}{f_{max} - f_{min}}[f(x,y) - f_{min}]; for\ 0 \leq f_{min} < f_{max} \leq 255 \quad (2.1)$$

where;

f_{min} and f_{max} represents the smallest and largest pixel levels respectively,

$f(x,y)$ and $g(x,y)$ represents the original and the enhanced images respectively.

Contrast stretching is mostly done by using histogram based approaches. For example, Khan and Chai (2012) proposed an image improvement procedure using dual-energy X-ray for hand luggage at airports. In the proposed algorithm, they combined low and high energy images, de-noised them and finally enhanced the merged image using histogram techniques. This was aimed at improving image contrast. The resultant image retains all the necessary details and has a significant noise reduction. This makes the process of detection easier for luggage screeners and brings a reduction in the number of false alarms raised during luggage inspection. Their approach was found to be very

appropriate for luggage screeners in spotting contraband items in comparison to conventional methods.

Longkumer *et al.* (2014) gives a comparison of the various histogram equalization techniques and gives their merits and demerits. They include Adaptive Histogram Equalization (AHE), Classical Histogram Equalization (CHE), Recursive Mean Separate Histogram Equalization (RMSHE), Brightness Preserving Bi- Histogram Equalization (BPBHE) and Background Brightness Preserving Histogram Equalization (BBPHE). On comparing them it was discovered that BBPHE provides a better and scalable brightness preservation for images with poor contrast and avoids unwanted noise.

Rajesh *et al.* (2011) did a comparative analysis of the different enhancement techniques frequently employed in industries. They investigated the Contrast Limited Adaptive Histogram Equalization (CLAHE) technique, the Dynamic Histogram Equalization (DHE) technique and the Dualistic Sub-Image Histogram Equalization (DSIHE) method. The comparison was by using both subjective and objective criterion. The subjective factor used was the visual quality while the objective factors used were Peak Signal to Noise Ratio (PSNR) and Normalized Correlation (NC). The CLAHE procedure was found to give better output in terms of PSNR and DSIHE gives the best results when considering the absolute mean brightness error.

Jin *et al.,* (2011) developed an industrial image de-noising and enhancement system by using wavelets and histograms. Since most of the X-ray image pixels are found on the low frequency spectrum and very few pixels, if any, are on the high frequency range, their techniques called Contrast Limited Adaptive Histogram Equalization (CLAHE) handled low contrast and poor details effectively. They found out that the results of enhanced images had more information details and became clearer.

Rajput *et al.,* (2012) suggested a routine of enhancing medical images based on histogram equalization using non-linear techniques and discrete wavelet transform. This routine enhanced the lower and higher contrast spectrums in both the spatial and the frequency domain. Using the proposed routine, they observed better results of PSNR compared to the simple histogram technique. These results showed that the proposed technique enhanced image contrast and also maintained image quality.

2.5 Image Thresholding

This is an image processing technique that produces images in binary form by applying a particular threshold degree on the image pixels available. This concept is mostly used for gray-scale images, though it has started being used in colour images. The threshold can be fixed manually at an exact point or automatically through an algorithm. It then converts pixels below the set threshold to black and those pixels above the threshold to white. This is seen as separating an image into foreground and background values with minimal overlapping regions (Romen *et al*., 2011). It has its applications in document image analysis, where it extracts printed characters; in scene processing, for target detection and in quality material inspection, where defective parts are defined.

Sezgin and Sankur (2004) conducted a research on the various image thresholding techniques. They characterized them into six clusters depending on the information they were utilising. They included clustering-based approaches, histogram shape-based approaches, object attribute-based approaches, the spatial approaches, entropy-based approaches and local approaches. They finally carried out their performance comparison. They observed that, for NDT images, the best thresholding techniques were the entropy-based and clustering-based approaches. Likewise, in terms of document binarization they realized that the clustering-based and the local-based approaches were the best performing techniques. They also observed that no single approach was successful by itself. As such, to obtain a robust thresholding approach, they explored the option of combining several thresholding techniques.

2.6 Edge detection

Edge detection involves the use of mathematical and algorithmic methods for detecting pixels that lie along object boundaries in an image where it exhibits discontinuities. It is possible to clearly show, on an image, a set of associated curves indicating the image boundaries by using edge detectors. Thus, the results produced by the edge detection algorithm are often a reduced set of filtered data, which omit irrelevant information while preserving the properties of the image (Anandakrishnan and Baboo, 2014). Moreover, in an image edges may be used to quantify object sizes and isolate certain items from the image background. This aids in objects recognition and classification.

Juneja and Sandhu (2009) compared the numerous image edge detection methods that are in use in imaging. They identified that the Canny's algorithm is superior to all other

operators under most situations. This is because the technique detects both weak and strong edges. In addition, they identified that on visual perception Prewitt, Roberts and Sobel provided poor feature edge maps compared with other techniques.

Further investigations by Vinoth and Jayalakshmi (2014) on analysis of edge detection algorithms and denoising filters on digital X-ray images confirmed the superiority of the Canny edge detector. They attempted to analyse the performance of various filters over different types of noise while evaluating the performance of various edge detecting algorithms. From their comparison, they resolved that the Canny edge detector is an efficient algorithm in identifying edges even though it has a higher computational complexity when compared to others algorithms like Sobel, Log, Roberts and Prewitt.

MathWorks, Inc, (2009) also emphasises that the most powerful edge detection technique available so far is the Canny technique. This is because the algorithm is ideal in terms of detecting edges, localizing them and in the number of responses. This algorithm employs a multi-stage technique in identifying a variety of edges and is hardly affected by noise and tends to recognise true but weak edges.

2.7 Noise reduction

Noise reduction involves the removal of noise in an image while retaining the important information, irrespective of the frequency contents. It can also involve the recovery of crucial information in a degraded image. This section presents some of the published methods that have been proposed for noise suppression.

A method for modifying wavelets coefficients to eliminate noise from data has been developed by Ruikar and Doye (2011). Their method provides superior edge resolution, better contrast stretching in the spatial domain and preserves background information. In addition, it is a computationally faster.

Sahu and Parsai (2012) have described the various image fusion techniques that have been in operation. They have demonstrated the application of spatial domain fusion and transform domain fusion. They found out that the wavelet transform is an important algorithm in image fusion since it offers quality in the spectral content of the fused image. It was proved that a combination of spatial fusion and wavelet techniques produces superior fused image. This is because such a combination improves their

performance in comparison to individual techniques. This has its application in medical imaging, remote sensing, computer vision, and robotics.

Pai *et al.* (2015), proposed a method of enhancing and sharpening medical colour images using wavelet transform followed by image sharpening. Since medical images are sensitive to contrast and quality, they applied wavelets transform for noise reduction before using the Laplacian operator to obtain the sharpened and enhanced images. From their findings it was showed that this method did enhance image details and also preserved image edges effectively.

2.8 Some Relevant Works

Some of the recently published works that are related to the enhancement and automation of crack detection algorithms proposed in this thesis are summarised in this section.

Saravanan and Kumar (2014) made a sound study of the various contrast enhancement techniques used so far. They found out that the global histogram enhancement technique has some limitations such as a significant change in brightness and washed out appearances. To counter these hitches, a number of histogram equalization systems that conserves the mean brightness were developed. They found out that the Minimum Mean Brightness Error Bi-Histogram Equalization (MMBEBHE) routine is superior when it comes to brightness preservation followed by the Recursive Mean-Separate Histogram Equalization (RMSHE) routine. It was also identified that the RMSHE has the highest value for average information content, which shows abundance of details in the output image. Besides, RMSHE had an improved visual quality as well as the highest contrast improvement value. Further, they found out that Dynamic Histogram Equalization (DHE) eliminates dominance and masking of small features of the input image.

Domingo (2014) presents a summary of computer vision algorithms used in X-ray imaging for non-destructive testing. They find their application in baggage screening, automotive parts inspection, quality control of welds and in food product analysis. In his research, he observed that some areas like casting inspections in industries are fully automated while applications like baggage inspections in airports are not automated since human inspections are still being relied on. Other areas like weld inspections in industries are semi-automated. Domingo noted that by automating a system one achieves

objectivity and reproducibility for every test. Though, the complexity of installation and the inflexibility to any change in the evaluation process limits most systems.

Santhi *et al.* (2012) has proposed an automation model for crack detection in pavements using edge detection techniques. Conventionally, skilled workers were involved in cracks detection in pavements. This proved to be an inefficient and expensive affair. To avoid these inefficiencies, an automated technique for crack detection was proposed and the results displayed on a screen. The method used adaptive thresholding technique to detect the available cracks. However, this algorithm had a limitation in that the image used had to be pre-processed to get a squared gray-scale image before any detection was done. In addition no comparison to established algorithms was investigated.

Sinha and Fieguth (2006) proposed a methodical image segmentation procedure that inspects scanned images automatically from underground pipes. Naturally, the pipeline infrastructure deteriorate with time after installation and because a complete overhaul of the entire infrastructure is not economical, the utility operators requires a way to monitor the state of the pipes. The proposed approach is effective in areas lacking uniform brightness. Besides, the process of morphological segmentation is helpful in distinguishing between cracks and holes. However, it was difficult to classify defects by their severity.

Karsten *et al.* (2011) did a comparison of three contrasting crack detection procedures namely percolation thresholding, template matching and sheet filtering by using Hessian Eigenvalues. From their analysis, they proposed the use of template matching on thin cracks.

Halfawy and Hengmeechai (2014) developed an algorithm for an effective pattern recognition system that supports defects detection automation and classification of pipe flaws in images gotten from conventional sewer closed-circuit television (CCTV). They relied on histograms of sloping gradients and support vector machine to identify defects. This valuable tool ensured quality, accuracy, and consistency of the condition data, while decreasing the time and cost of the assessment process. This algorithm also addressed the issue of background noise and non-uniform illumination conditions. In addition, the algorithm they developed relied on known features where the classifier is trained using known patterns of the defect under investigation. The method was only applicable on a

few defects and they proposed that it could be extended to defects like corrosion, cracks and fractures.

Iyer and Sinha (2005) did a proposal of automating defects detection on sanitary sewer pipelines by relying on procedures like mathematical morphology and contrast enhancement. The two researches dealt with two systems of inspection in their work: the sewer scanner and evaluation technology (SSET) and the closed-circuit television (CCTV) technology. By using these systems, they developed a crack detection algorithm which performed fairly well in identifying major cracks. The limitations to this method was its reliance on skilled operators and missing on small cracks.

Yamaguchi *et al.* (2008) introduced an image-based tactic to identify cracks on concrete surfaces by using percolation thresholding. Initially accurate crack detection could not be achieved by image-based tactics since concrete surface encompasses several sorts of noises and shading. From their assumptions, cracks are made of thin interconnected textures. They therefore had to look for a technique that could extract a continuous texture of the connectivity of intensities. They identified the percolation model which was very effective with unclear cracks detection. Analysis using quantitative procedures proved the technique is superior compared to previous methods.

Khurana and Awasthi (2013) proposed a technique which could recognize multi-objects in an image. Normally object detection is an intricate process and mostly detects single objects. The two scholars envisaged developing an algorithm for detecting multiple objects in an image using different templates simultaneously in a less complex manner. They used global features and shape based methods. The resulting algorithm is efficient and robust and correctly identifies the required objects.

Sargunar and Sukanesh (2010) developed an algorithm for detecting slag inclusion and porosity in boilers by using pattern recognition methods. The system was used in automatic weld inspection and in training of quality inspectors in the welding industry. This technique increased the inspection speed and improved the accuracy of detection. The algorithm developed had restrictions on the classes of weld defects it could identify.

Finally, Thiruganam *et al.* (2010) proposed a segmentation method of radiographic welds combining global and local techniques of thresholding. In addition, the proposed algorithm gives the defect count. This method significantly improves the efficiency in

terms of computational complexity since it only processed the regions of interest (ROI) instead of the whole image. The filtering procedure used assisted in the fast execution during defect count and improved on the computational time. This concept can also be implemented in object recognition.

2.9 Proposed Method

The main purpose of this thesis is to come up with an algorithm that automatically detects cracks and then enhances them for improved contrast and clarity. A comparison with other proposed algorithm has been made in order to identify the knowledge gaps that exist.

Sinha and Fieguth (2006) were able to develop an image segmentation system for analysis of scanned images for underground pipes. However in their work they did not integrate a way of indicating the severity of the crack. The algorithm proposed in this thesis incorporates a way of indicating the severity by having to set a threshold. If the crack is above a certain threshold, it is severe and the system will indicate.

It has been shown by several researchers that defects identification is dependent mainly on the operator's experience. However this makes the entire process to be error prone and subjective. It is therefore unreliable and inconsistent hence making it impossible for preventive maintenance to be carried out with certainty (Domingo, 2014). This thesis comes up with a simple and efficient techniques of indicating to the operator in words the presence or absence of a crack.

Santhi *et al.*, (2012) in their model had a limitation in that they had to perform a preliminary image processing so as to acquire a squared gray-scale image. In our research, the image does not require to be converted to a specific size. In addition, their work has no report of the comparison to other existing algorithms. However, our research is based on comparing with other scholars work to avoid duplications.

Halfawy and Hengmeechai (2014) algorithm had a limitation that it was only applicable in detecting a few defects and they proposed that it could be extended to defects like corrosion, cracks and fractures. This research incorporates all these defects.

Enhancement techniques are specific and problem-oriented in that the best enhancement technique used to enhance one type of image for a given application may not be the best technique to enhance another image for a different application. Thus, in this research,

various enhancement techniques have been used and the best selected in areas of contrast conservation, preservation of the mean information content and prevention of dominance and masking of small features of the input image.

Finally, Structural Similarity Index Measure (SSIM) has been incorporated as an objective measurement technique since it makes better the Peak Signal to Noise Ratio (PSNR) technique that is inconsistent with the Human Visual System (HVS). Therefore, SSIM checks at the structural changes in information of the image and considers this as image degradation. This is true from the fact that pixels have strong interdependencies mostly when they are spatially close (Sampat *et al.*, 2009).

CHAPTER THREE

THEORETICAL ASPECTS OF IMAGE ENHANCEMENT TECHNIQUES

3.1 Overview

Image enhancement makes the resultant image better in comparison to the native image for specific applications as presented in Figure 3.1. This can be achieved by using two ways. First, displaying the image in a suitable manner such that the information carried is maximal and the desired information is extracted. Second, processing the image so as to retain the informative part and discard the rest. The second method requires a definition of the informative part, and this makes the enhancement techniques specific (Galatsanos *et al.*, 2003).

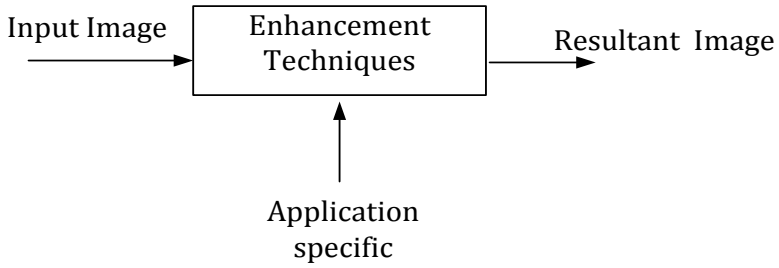

Figure 3.1: Application specific image enhancement

The enhancement techniques used are categorised into two methods: the spatial and the frequency domains (Weeks, 1998). The spatial procedures work on the image pixels directly. However, the frequency domain procedures operate by first transforming an image to a particular domain, performing image enhancement in that domain, and finally performing the inverse transformation to obtain the image in spatial domain.

3.2 Spatial Domain Image Enhancement Techniques

The spatial domain method is used to manipulate the image pixels to achieve the desired enhancement either by using intensity transformations or by spatial filtering. The intensity transformation is designed to operate on a single pixel of an image and is majorly used in image thresholding and contrast manipulation. On the other hand, spatial filtering is a two-dimensional convolution process which is more computationally efficient and involves the usage on fewer processing resources in comparison to the frequency domain techniques.

Spatial domain enhancement techniques can be classified as single-pixel process, neighbourhood operation or geometric spatial transformation.

a) Single-pixel process

This is a simple process that modify the individual pixels of a digital image based on their intensity (Gonzalez and Woods, 2008). This type of process may be denoted by the following expression;

$$s = T(z) \tag{3.1}$$

where;

z and s represents pixel intensities of original and processed images respectively,

T represents the gray-level transformation function.

b) Neighbourhood operation

This assess the features of an area surrounding a particular location. For example, the pixels mean value of a rectangular neighbourhood of size $m \times n$ centred at (x, y) can be computed through set S_{xy} as shown below in Equation 3.2 and Figure 3.2.

$$g(x, y) = \frac{1}{mn} \sum_{(r,c) \in S_{xy}} f(r, c) \tag{3.2}$$

where r and c represents rows and columns of the pixels in set S_{xy}.

This technique produces a matching pixel for the output image as in the input image coordinates depending on the specified operation being performed on the input image.

Figure 3.2: Local averaging using neighbourhood processing

c) Geometric spatial transformation

This technique modifies the spatial relationship amongst the image pixels and it consists of two processes: coordinates spatial transformation and intensity interpolation. As such, geometric transformation deals with the modification of pixels in an image without affecting its colour. The transformation of coordinates is indicated mathematically as;

$$g(x,y) = T[f(x,y)] \tag{3.3}$$

where;

$f(x,y)$ and $g(x,y)$ are the native and resultant images respectively and,

T represents the transformation operator which scales, rotates, translates or shears a set of coordinate points.

Geometric spatial transformation can be used for scaling, rotating, translating or shearing a set of coordinate particular points from an image. This depends on the value of the transformation operator matrix T (Gonzalez and Woods, 2008).

3.2.1 Contrast Stretching

Contrast stretching uses the principal of increasing the range between the brightest and darkest pixels of a gray-scale image to full range. It maps the lowest gray-levels in an image to zero and the highest levels to 255 (for an 8-bit image) (Gonzalez and Woods, 2008). The outcome is an expansion of image contrast range and the image become desirable to the observer (Singh *et al*., 2013).

3.2.1.1 Linear Contrast Stretching

This happens by uniformly expanding the pixel values to fill the full range of the output image [0, L-1]. This is mostly restricted to linear mapping of input to output values and is indicated mathematically as:

$$s = \left(\frac{max - min}{f_{max} - f_{min}}\right)(r - f_{min}) \tag{3.4}$$

where;

min and max represents the desired smallest and largest gray-levels of the resultant image ([0-255] for an 8-bit image),

f_{min} and f_{max} represents minimum and maximum gray-levels of original image,

r and s represents the original image and the mapped output values respectively.

Linear contrast stretching can be divided into two classes: simple identity and negative transformation.

a) Simple identity transition

This involves a direct mapping of pixels of the native image to the resulting image as presented in the Figure 3.3. This figure displays an implementation of linear contrast stretching transformation using a histogram. In the original plot, the pixel values range from 84 to 153 and the resulting image is of low contrast. In the stretched plot, a linear stretch involves moving the 84 value to 0 and the 153 pixels to 255; all intermediate values are stretched proportionately.

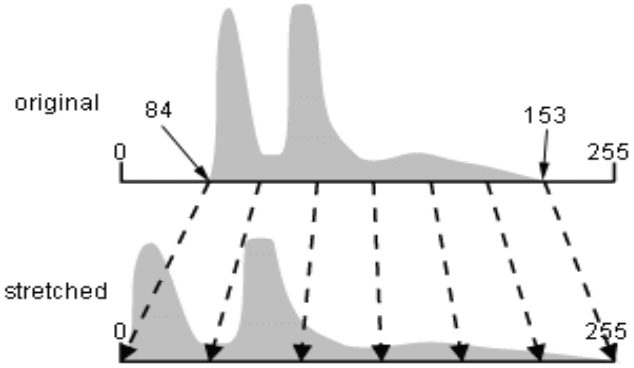

Figure 3.3: Histograms showing original and enhanced image

b) Negative transformation

This is an inversion of the identity transform above. Here, every pixel value from the primary image is subtracted from $(L-1)$ and the result set onto the output. So what happens is that, the lighter intensity values are converted to darker pixels and the darker pixels are converted to lighter intensity values. This is indicated mathematically as;

$$s = (L-1) - r \tag{3.5}$$

where;

r and s represents the original image and mapped output values respectively.

3.2.1.2 Non-Linear Contrast Stretching

This technique does not stretch image pixels linearly. As such they do not occupy uniformly the full pixel range. The common non-linear contrast stretching methods currently in use are piece-wise stretching, logarithmic stretching, power law stretching and Gaussian stretching.

a) Piece-wise linear stretching

Piece-wise linear stretching expands different parts of the histogram by different amounts as shown in the Figure 3.4. Here the *r* values are the input pixels on the horizontal plane while the *s* values are the output pixels on the vertical plane. The figure has three line sections which are used in expanding the input pixels range. By modifying any line sections the output image contrast is modified.

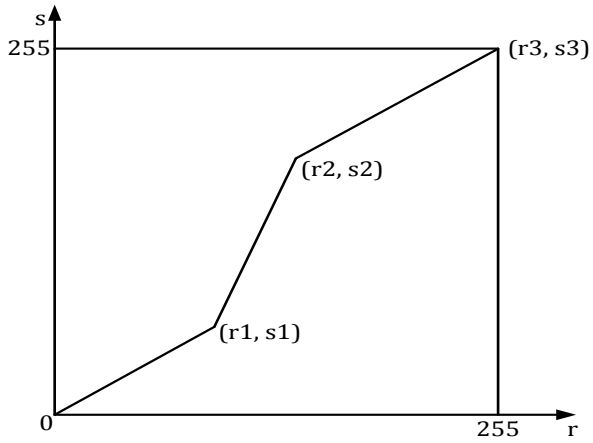

Figure 3.4: Showing an 8-bit Piecewise Linear Contrast Stretching process

Piece-wise linear stretching can be conveyed as:

$$g(x,y) = \begin{cases} ar, & 0 < r \leq r1 \\ br + s_{r1}, & r1 < r \leq r2 \\ cr + s_{r2}, & r2 < r \leq 255 \end{cases} \tag{3.6}$$

where;

$g(x,y)$ is the stretched image,

s_{r1} and s_{r2} are the respective y-intercepts,

a, b, and c are slopes constants for the respective regions and,

255 is the maximum intensity value for an 8-bit image.

This technique is useful in images with bi-modal histograms. The region superimposed by the two histograms may be compressed, while the histogram peaks may be enhanced differently. However, this techniques requires considerable number of user inputs in its application (Gonzalez and Woods, 2008).

b) Logarithmic, Power law or Gaussian stretching

Logarithmic stretching involves widening the smaller pixel values to a broader spectrum. This improves the information enclosed in the darker pixels, while compressing the information in the lighter pixels. Logarithmic stretching is conveyed by;

$$g(x,y) = c\log_{10}\left(1 + f(x,y)\right) \tag{3.7}$$

where;

f and g are the intensity levels of the native and resultant images respectively,

c represents a positive constant.

The power law performs its stretching in an opposite way compared to the logarithmic stretching. High pixel values are stretched to a wider range improving the information contained in their pixels, while the low pixel values are compacted. The power law is conveyed mathematically as;

$$g(x,y) = c\,[f(x,y)]^n \tag{3.8}$$

where c and n are positive constants.

The Gaussian contrast stretching modifies the input pixel values to fit into a normal distribution curve between [0, 255] limits of an 8-bit image. This improves the contrast in the darker and lighter areas of the input image at the expense of the contrast in the middle spectrum. The techniques is achieved by using:

$$g(x,y) = \frac{1}{2\pi\sigma^2}\, e^{-(x^2+y^2)/2\sigma^2} \tag{3.9}$$

where;

x and y represents the coordinates of the image and,

σ represents the standard deviation of the Gaussian distribution.

3.2.2 Histogram Processing

A histogram represents data distribution in a given entity graphically. In image processing, a histogram represents graphically the variations of the gray-values in digital

image (Jin *et al.* 2011). It is obtained by the orderly counting of all the number of pixels of every gray-level from black to white. The whole process is implemented by first iterating through all possible gray-level values available. Then pixels with a particular value are grouped together before storing the results in a table or displaying them in a chart.

Taking an example of an image with L possible intensity values of range [0, L-1], the resultant image histogram is given mathematically by;

$$h(r_k) = n_k \tag{3.10}$$

where;

r_k represents the value of kth gray-element and,

n_k represents the specific pixel numbers of the image having gray-level r_k.

The above function can be normalized by dividing through with the total pixels and the summation of these normalized components is equal to unity. This is obtained as;

$$p(r_k) = {}^{n_k}/_{(MN)} \quad ; \; for \;\; k = 0, 1, 2, \dots, L-1 \tag{3.11}$$

where;

N and M represent the columns and rows respectively.

Histogram manipulation is used effectively in image enhancement through a technique known as histogram equalization. The main effect of equalization in an image is to increase the dynamic range and obtain higher image contrast (Rajput *et al.,* 2012). The information obtained after enhancement is used in other image analysis techniques like image segmentation.

The histogram shape provides key information in regard to image quality and the likelihood of enhancement. For example, the histogram of a low quality image is normally narrow while that of a high quality image is wide (Longkumer *et al*., 2014). Histogram techniques are crucial role in the enhancement of the perceived brightness and contrast of an image.

3.2.2.1 Histogram Equalization

This technique is similar to contrast stretching. The difference is that contrast stretching requires user input in its operation while histogram equalization is exclusively automatic

(McAndrew, 2004). The main aim of performing histogram equalization is to achieve a smooth histogram since theoretically a smooth histogram contains the largest amount of information (Galatsanos *et al.*, 2003). This technique when used enhances image brightness and improves its contrast. This is achieved by distributing the gray-levels within an image and raising the probability of occurrence of the gray-levels. This therefore makes features that were not visible in the original image observable since it distributes the gray-levels uniformly. This allows images to be compared equally without bias due to perceived contrast and brightness differences (Weeks, 1998).

The general form of histogram equalization is;

$$s_k = \frac{(L-1)(r_k - r_{kmin})}{(r_{kmax} - r_{kmin})} \quad ; for \quad k = 0, 1, 2 \ldots, L-1 \tag{3.12}$$

where;

r and s are the input and output pixels of the image,

L is the image pixels,

r_{kmin} and r_{kmax} are the minimum and maximum input image gray-values.

Enhancement techniques are problem-oriented in that the best enhancement technique used to enhance one type of image for a given application may not be the best technique to enhance another image for a different application. In addition, enhancement techniques cannot be generalised because the observer is the final evaluator as to how good a particular technique works.

3.2.2.2 Algorithms used in histogram equalization

Histogram equalization operates by re-mapping the gray-levels in an image. This may introduce some irritating artifacts on the image. Different brightness preserving techniques have been proposed to overcome these drawbacks. Some are discussed below.

a) Classical Histogram Equalization

Classical Histogram Equalization (CHE) operates by levelling the histogram. This is done by widening the range of the smallest and the largest gray-pixels through a techniques called the image cumulative density function. Through CHE, image intensity is usually better distributed within the histogram and CHE operation is simple in implementation and computationally fast. However, this technique alters the image brightness significantly, and produces an image that is flooded by very dark or very

bright pixel values. This lowers the visual worth of the resultant image leading to contrast loss and the technique does not preserve image brightness (Saravanan and Kumar, 2014).

b) Adaptive Histogram Equalization

The Adaptive Histogram Equalization (AHE) technique is an automated improvement procedure that enhances image contrast. It divides an image into several distinct sections before equalizing them separately (Carasso, 2013). Neighbouring sub-blocks are now combined using a technique called bilinear interpolation so as to eradicate artifacts that were induced artificially (Rajesh *et al*., 2011). This technique is appropriate at improving the pixel neighbourhood brightness and brings out extra details as compared to CHE. On the other hand, this method is *c*omputationally intensive and it could lead to noise amplification (Jin *et al.,* 2011).

c) Brightness Preserving Bi-Histogram Equalization

The Brightness Preserving Bi-Histogram Equalization (BPBHE) technique does its operation by dividing a histogram into twofold centred on the original image mean brightness. The sub-histograms obtained are equalised autonomously through HE (Longkumer *et al*., 2014). By using this technique, the resultant image mean brightness is preserved as the original mean brightness is retained. This method, therefore, overcomes brightness preservation problem and enhances images without producing unnecessary artifacts (Saravanan and Kumar, 2014).

d) Recursive Mean-Separate Histogram Equalization

The Recursive Mean-Separate Histogram Equalization (RMSHE) technique gives an improved version of the BPBHE and CHE techniques. It performs image decomposition recursively until multiple sub-histograms are obtained. Then, histogram equalization is applied individually to all sub-histogram until a flat histogram and the required brightness are achieved. BPBHE is comparable to RMSHE when the recursion value is unity. Conventionally, to achieve more brightness preservation then the number of recursions have to increase significantly. Therefore, RMSHE achieve a higher brightness preservation value by performing more recursions (Raju *et al.,* 2013). The mean output $E(Y)$ of RMSHE with repeated application where r equals n is;

$$E(Y) = {((2^n - 1)X_m + X_G)}/{2^n} \tag{3.13}$$

where,

X_m represents the input mean weight and,

X_G represents the middle gray-level weight.

The output image brightness is best preserved here and the output image has improved visual quality. Besides, RMSHE has the highest value for average information content, which indicates richness of details in the enhanced image (Saravanan and Kumar, 2014).

e) Dynamic Histogram Equalization

The Dynamic Histogram Equalization (DHE) procedure subdivides the original histogram into several sub-histograms with no dominating component in them. Then, equalization is achieved based on the cumulative distribution of the histogram values. Thus, by using DHE better image contrast is obtained with controlled pixel range of the dark and bright values. It also eliminates the likelihood of compressing low spectrum constituents which may lead to having a washed out appearances on the image leading to loss of details. Thus, this method ensures that image details are preserved uniformly and there are no severe artifacts. (Singh *et al*., 2013).

3.2.3 Spatial Filtering and Correlation

Image filtering is a technique used to enhance an image by suppressing certain frequency components. Since filtering is a neighbourhood operation, the resultant image is obtained by applying some procedures to the pixels in the surrounding neighbourhood. The main image operations implemented using spatial filtering are image smoothing, image sharpening, and edge enhancement. Spatial filtering is divided into either linear filtering or nonlinear filtering depending on the spatial filters used (Gonzalez and Woods, 2008). Figure 3.5 can be used to represent the filtering process, where an image, $f(x, y)$, is passed across an impulse response system, $h(x, y)$, thus producing a resultant image, $g(x, y)$, that is filtered.

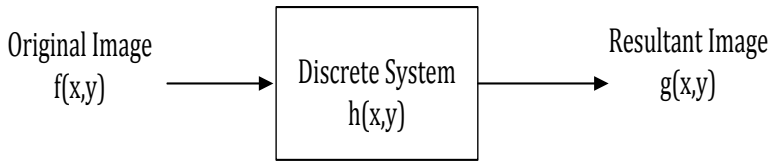

Figure 3.5: Functional representation of spatial filtering

When performing spatial filtering, two concepts emerge: correlation and convolution (Gonzalez and Woods, 2008).

3.2.3.1 Correlation

Correlation is a technique used to establish whether a linear relationship exists between two variables. It is done by sliding a filter mask on a primary image then summing the products of every site. It has mainly found its usage in localizing features appearing in both images.

The correlation coefficient of two variables is:

$$g(x,y) = \sum_{i=1}^{m}\sum_{j=1}^{n} f(i,j)h(x+i,y+j) \tag{3.14}$$

where

$f(x,y)$ and $h(x,y)$ represents original image and mask respectively.

Equation 3.14 is evaluated for the entire displacement points of x and y so that all elements of h visit every pixel of f, where f is assumed to be larger than h. This is done in a pixel–by– pixel basis looking for locations where h finds a correspondence in f (Tsai and Lin, 2003). The correlation of the two functions will be maximum if the two points match. This process is called matching by correlation or template matching. In image processing, this technique has applications in remote sensing, computer vision, medical imaging, and in industrial inspection.

Cross-correlation is frequently used in place of correlation to show that the images being correlated are different. This is as opposed to autocorrelation, which refers to a single image operation (Gonzalez and Woods, 2008). Normalized Cross-Correlation (NCC) is a ratio that assesses the extent of resemblance amongst two images. In comparison to cross-correlation, NCC is less affected by linear variations of the illumination amplitude between two images. Besides, NCC has a small range of between 1 and -1.

The NCC between the reference template and the primary image is obtained as (Gonzalez and Woods, 2008);

$$\gamma(x,y) = \frac{\sum_i \sum_j \left[h(i,j) - \bar{h}(i,j)\right]\left[f(x+i,y+j) - \bar{f}\,(x+i,y+j)\right]}{\sqrt{\left\{\sum_i \sum_j \left[h(i,j) - \bar{h}(i,j)\right]^2 \sum_i \sum_j \left[f(x+i,y+j) - \bar{f}(x+i,y+j)\right]^2\right\}}} \tag{3.15}$$

where;

$h(i,j)$ and $f(i,j)$ are the reference template and native images respectively,

$\bar{h}$ represents the pixels average value of the mask and,

$\bar{f}$ represents the pixels average of original image.

The NCC has the value of γ close to unity if there is a strong positive linear relationship between the image and the mask. A value of γ close to negative unity indicates that the two images have the same shape except that they have the opposite signs. A value of $\gamma = 0$ shows that they are completely uncorrelated (Kaur *et al,* 2012).

3.2.3.2 Convolution

Convolution is a neighbourhood operation that calculates the weighted sum of neighbouring input pixels in order to obtain the output pixels. This is done by using a convolution kernel called a filter. This is the normal correlation filter having been rotated 180 degrees. The convolution among two functions is given as;

$$f(x,y) * h(x,y) = \sum_{i=1}^{m}\sum_{j=1}^{n} f(i,j)h(x-i,y-j) \tag{3.16}$$

where;

the minus sign on the right flip shows the filter mask has been rotate by 180^0;

$f(x,y)$ and $h(x,y)$ are the native and mask images respectively,

3.2.4 Image Segmentation

This technique involves subdividing an image into various regions enabling the separation of some objects from the background. It is classified into three ways. The first is image thresholding that applies a pre-set gray-level threshold criteria to sub-divide an image into various sections. The second technique deals with edges which are obtained using discontinuities between gray-level regions. Object edges are crucial as they are used to extract features and hence recognize and identify any object. Finally, the last technique separates an image into numerous sections using a desired criteria.

3.2.4.1 Image Thresholding

This is an image segmentation technique that attempts to categorize and obtain the required target from its background using the image gray-level distribution. For this to be successful a threshold has to be fixed either manually at an exact point or automatically

through an algorithm. It then converts pixels below the set threshold to black and those pixels above the set threshold to white. This is seen as separating an image into foreground values (black) and background values (white) with minimal overlapping regions (Romen *et al*., 2011). It is represented mathematically by;

$$g(x,y) = \begin{cases} G_a, & f(x,y) \leq T \\ G_b, & f(x,y) > T \end{cases} \tag{3.17}$$

where;

$G_a$and G_b represents the gray-levels in the resultant binary image.

T represents the set threshold,

This technique is characterized into either by global or local thresholding methods. First, global thresholding involves the setting of threshold value whereby the pixels below the set threshold fit in one phase and the other pixels fit in the second phase. This is clearly illustrated in Equation 3.18. This technique of thresholding is mostly used in images found to have uniform contrast distribution between the foreground and background (Romen *et al*. 2011). This method is very fast in its operation but it has some minimal noise along the image borders. This can be eliminated by using local thresholding (Gonzalez and Woods, 2008).

Global thresholding is represented by;

$$g(x,y) = \begin{cases} 0 \;\; if \;\; f(x,y) \leq T) \\ 1 \qquad\quad otherwise \end{cases} \tag{3.18}$$

where;

T represents the set-threshold value,

$g(x,y)$ represents resultant image and

$f(x,y) \in [0,1]$ are the intensity values of the original pixels.

Local thresholding splits the original image into various sub-images each with a different threshold. At pixel levels, local thresholding yields superior results in comparison to global thresholding, particularly for images with varying contrast levels. This method achieves excellent outcomes even on acutely corrupted images. Nonetheless, this technique is computationally slow since image feature extraction from local neighbourhood is computed for each pixel of the image (Weeks, 1998). Equation 3.19

explains the process of local thresholding. The image is segmented into three gray-regions G_a, G_b and G_c.

$$g(x,y) = \begin{cases} G_a, & 0 \le f(x,y) < T_1 \\ G_b, & T_1 \le f(x,y) < T_2 \\ G_c, & T_2 \le f(x,y) \le G_{max} \end{cases} \quad (3.19)$$

where G_{max}represents the maximum image gray-level value.

a) Otsu's Thresholding

Otsu's technique is a global thresholding process that was proposed by N. Otsu in 1979 (Otsu, 1979) making it the oldest technique in segmentation of images. It is popular and widely used because it is simple in its operation with little computational requirements. It operates by splitting an image into two: the objects and the background. By looking for the biggest variance amongst the two classes, automatic threshold can be performed. This is done by performing several iterations for all the threshold values possible and then computing the degree of pixel spread. The purpose of this calculation is to locate the minimum threshold point for the summation of the background and foreground pixels. It also checks for the point where the variance is maximum. This is important since a well-thresholded class must be unique in terms of pixel intensity values (Gonzalez and Woods, 2008).

Taking an image with pixel size $M \times N$ and intensity points ranging from [0 - L-1]. Let n_i denote the total pixel numbers with intensity i. Then, the normalized histogram with components $p_i = {}^{n_i}/_{MN}$, is obtained as;

$$\sum_{i=0}^{L-1} p_i = 1 \qquad p_i \ge 0 \quad (3.20)$$

Considering a case of bi-level thresholding, $T(k) = k, 0 < k < L-1$, provides a threshold which divides the input image into two classes $C_1$and C_2, where C_1 contains the initial pixels in the array $[0, k]$ and C_2 contains the pixels in the other array $[k+1, L-1]$ (Liao *et al.*, 2001). The probability, $P_1(k)$, of a pixel being in class C_1 is given as:

$$P_1(k) = \sum_{i=0}^{k} p_i \quad (3.21)$$

Equally, the probability of class C_2 happening is given by:

$$P_2(k) = \sum_{i=k+1}^{L-1} p_i = 1 - P_1(k) \tag{3.22}$$

The effectiveness of a threshold value at a specific level k is obtained as:

$$\eta = {\sigma_B}^2 \Big/ {\sigma_G}^2 \tag{3.23}$$

where ${\sigma_G}^2$ is the global variance. The intensity variance of all the image pixels is obtained by:

$${\sigma_G}^2 = \sum_{i=0}^{L-1} (i - m_G)^2 \, p_i \tag{3.24}$$

m_G is the global mean denoted as:

$$m_G = \sum_{i=0}^{L-1} i p_i \tag{3.25}$$

and ${\sigma_B}^2$ gives the variance of between-class and is clearly indicated as:

$${\sigma_B}^2 = P_1 \, (m_1 - m_G)^2 + P_2 (m_2 - m_G)^2 \tag{3.26}$$

where m_1 and m_2 represents the mean pixel intensity values of class C_1 and C_2 respectively.

From these computations, the farther the two means m_1 and m_2 are from each other, the larger ${\sigma_B}^2$ will be. Therefore, the optimal threshold value, k, should maximize the between-class variance. The above formulas can easily be extended for multi-level thresholding of any digital image (Liao *et al.*, 2001).

b) Percolation Thresholding

Percolation is a model founded on some natural occurrences like liquid infiltration and is very effective in describing numerous phenomena such as electricity conductivity in materials, ferromagnetism and the spread of epidemics (Yamaguchi *et al.,* 2008). Percolation theory involves the study of discrete objects and their association with each

other. This is specifically done by investigating image clusters, their statistics and properties.

For percolation to occur, it must originate from a primary location before spreading to the neighbouring environs in relation to a possibility p. This probability measures the ease of percolation to the surrounding areas. The regions with the highest value of p are easily infiltrated. As the infiltration process is repeated, the area covered grows progressively up to the border (Yamaguchi, 2008). Generally, for percolation to occur the critical probability must be higher than 0.5927 otherwise percolation is highly unlikely. This value has been determined empirically (Sukop *et al.*, 2002). In image processing based-percolation model, the points with interconnected and identical values of gray-levels are percolated and finally produce an image cluster (Zhong *et al*, 2015).

Percolation thresholding entails four stages. The first stage fixes the size of the local window and sets the first pixels at the middle of this local window. These primary pixels belong to an infiltrated area of D_p, and for percolation to occur the initial threshold value is fixed to the original brightness of the pixels. The second stage updates the threshold T as indicated below:

$$T = \max\left(\max_{p \in D_p}(V(p)), T\right) + \omega \tag{3.27}$$

where;

ω represents the acceleration parameter, which accelerates percolation and,

$V(p)$ represents pixel brightness.

In the third stage, the eight neighbouring pixels of the area D_p are indicated in the area D_c. Those pixels whose intensity is below the set threshold are infiltrated and made to be part of the area D_p. Else, the pixels that have the lowest intensity in D_c are made to be part of D_p. Finally, for termination to occur D_p has to reach the borderlines of the local window. Else, the entire process goes back to stage two. Therefore, the final D_p neighbourhood is demarcated, and the percolation process forms the required cluster. By describing the percolated (D_p), the focal pixel obtained is assessed to determine whether it belongs to a defect. This is done by using the circularity (F_c) which is a characteristic of the area D_p and is given by:

$$F_c = {4C_{count}}\Big/{(4{C_{max}}^2)} \tag{3.28}$$

where,

C_{count} represents the pixel numbers of cluster D_p and,

C_{max} represents the percolated cluster circum-circle diameter.

The F_c value is close to zero if the pixels at the centre of the local window fits the crack area. This makes the percolation area to grow in linear dimensions. Otherwise, if F_c is near 1, the pixels at the center belongs to the background (Zhong *et al*, 2015).

The percolation thresholding process can be improved by modifying the acceleration parameter, ω. The improved parameter ω' is given as;

$$\omega' = F_c . \omega \tag{3.29}$$

Therefore, the threshold equation is updated equally by;

$$T = \max\left(\max_{p \in D_p}(V(p)), T\right) + \omega' \tag{3.30}$$

This accelerated algorithm considers all the pixels connectivity and decreases the redundant procedures of the percolation process and improves on the time required to detect a crack.

3.2.4.2 Edge detection

Edges in images occur due to discontinuities along the image boundaries (Gonzalez and Woods, 2008). They therefore form the structure of an object and indicate the borderline created by overlapping objects. Therefore by identifying these edges accurately, the objects in an image can be precisely identified and measured.

Edge detection, refers to the various mathematical and algorithmic methods by which pixels that fall along the boundaries of an image are mapped (Anandakrishnan and Baboo, 2014). The results produced by the edge detection algorithm are often a reduced set of data, which omits some information such as irrelevant data, but preserves the major properties of the image (Anandakrishnan and Baboo, 2014). Therefore, edge detection considerably decreases the amount of data to be processed in an image but preserves the

essential properties of the image for additional image processing. Moreover, edges can be used in measuring object sizes and in isolating specific objects from their background.

Edge detection has wide application in machine vision gauging, processing medical images, de-noising medical images, brain tumour detection, vehicle distance tracking, vehicle number plate tracking and industrial inspection. The ability to identify each individual object uniquely is a requirement for applying it in different areas. In order to identify the objects and classify them, it is required that the edges in the image be identified. The identification process covers the edge detection methods for the recognition of fine details and removal of irregularities obtained by the analyses of edges (Anandakrishnan and Baboo, 2014).

There are three main edge detection methods used in the spatial domain. These are;

a) Gradient based edge detection

This technique recognises edges by identifying the maxima and the minima first derivatives of the image pixels. This is done by calculating the partial derivatives of the pixels at every site in the image. Some of the commonly used gradient operators include Sobel, Prewitt and Robert's (Gonzalez and Woods, 2008).

The first order derivative expression of $f(x,y)$ can be summarised by;

$$\nabla f(x,y) = \begin{Bmatrix} \frac{\partial f(x,y)}{\partial x} \\ \frac{\partial f(x,y)}{\partial y} \end{Bmatrix} \tag{3.31}$$

With its associated magnitude represented as:

$$|\nabla f(x,y)| = \sqrt{\left(\frac{\partial f(x,y)}{\partial x}\right)^2 + \left(\frac{\partial f(x,y)}{\partial y}\right)^2} \tag{3.32}$$

whereas its gradient orientation is given by;

$$\theta(x,y) = tan^{-1}\left(\frac{\partial f(x,y)}{\partial y} \Big/ \frac{\partial f(x,y)}{\partial x}\right) \tag{3.33}$$

Gradient based edge detection techniques have two major drawbacks; they have fixed kernel filters and coefficient sizes making it difficult to adapt them to specific images; the technique is sensitive to noise.

b) Laplacian based edge detection

The relative size of the second derivative can be used in the detection of edges. Unlike the first derivative magnitude, which produces only one pulse per edge, the second derivative produces two pulses per edge. Of these two derivatives, the second is much more sensitive to the detection of edges.

For this technique to locate edges in an image, it has to get the zero crossings from the second derivative of $f(x, y)$ (Juneja and Sandhu, 2009). It expands the one-dimensional derivative using the Laplacian operator. This is represented as;

$$\nabla^2 f(x, y) = \frac{\partial^2 f(x, y)}{\partial x^2} + \frac{\partial^2 f(x, y)}{\partial y^2} \tag{3.34}$$

Its basic idea is that its first derivative of intensity values should be greater in magnitude than a specified threshold value and its second derivative should have a zero crossing.

c) Canny's edge detection algorithm

Previously, classical operators like Robert's, Prewitt and Sobel were used for edge detection but they did not give satisfactory results as they are highly sensitive to noise therefore leading to detection of false and unsharp edges. John F. Canny (1986), proposed a new edge detection algorithm known as Canny's edge detection algorithm. This algorithm provides good detection, good localization and minimal responses and is considered as an ideal edge detector algorithm. However, this algorithm is expensive in terms on computational complexity in comparison to other classical operators.

The Canny technique operates based on a specific principles. The first criterion is that of low error rate. This is major since no edges arising from the image should be missed and that the technique should not respond to non-edges. The second one concerns edge points' localization where by the distance identified by the detector between the edge pixels and the actual edges need to be minimum. Finally, the technique should only respond to a single edge (Gonzalez and Woods, 2008).

By using the above principles, the Canny's edge detector smoothens the image first so as to remove noise. Then, it highlights regions with high spatial derivatives and suppress

image pixels that are not peak levels. By using hysteresis, the gradient array is reduced further so as to trail the remaining pixels which have not been suppressed. It sets to zero magnitude below the first threshold and makes edges from magnitude that are above the high threshold.

3.3 Frequency Domain Image Enhancement Techniques

This section gives an overview of the frequency domain image processing techniques in the Fourier and wavelet transforms. The frequency domain approach has the advantages of ease with which one can view and manipulate the frequency structure of an image and the ease with which it's possible to apply the distinct transformed domain properties. The basic limitations are the inability to enhance an image uniformly and the many challenges encountered during image enhancement automation.

Frequency domain techniques manipulate the orthogonal transforms of an image and not the image itself and they process an image based on its frequency content. They operate by first transforming an image according to an orthogonal transformation like the Discrete Fourier Transform (DFT) or Discrete Wavelet Transform (DWT). The transformed image is then multiplied with a transfer function of an appropriate filter. By performing the inverse transformation, it is possible to obtain the enhanced image in spatial domain as presented in Figure 3.6. This domain permits frequency operations on an image, enabling content having high frequency, like edges, to be easily enhanced.

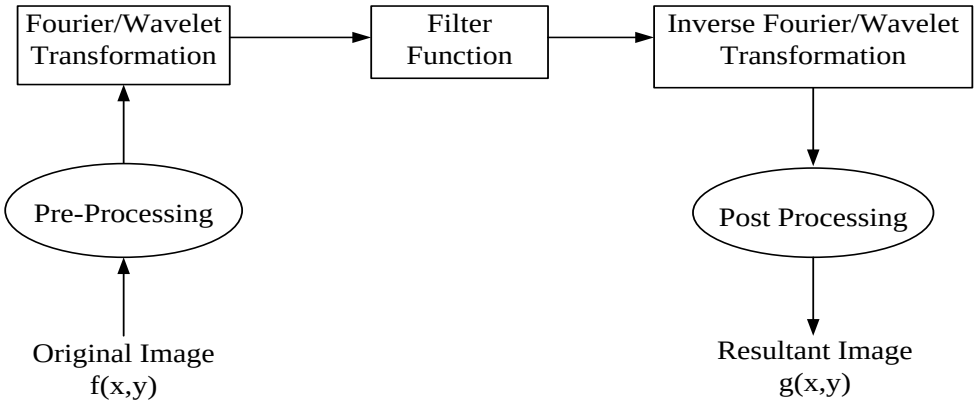

Figure 3.6: Process by frequency domain

3.3.1 Fourier Transform

This is used to represent an image as the summation of its complex exponents of changing phases, frequencies and magnitudes. Fourier transform is indispensable in areas

like linear filtering where it offers significant flexibility in planning and implementation of filters used in image enhancement, image restoration and image data compression (Gonzalez and Woods, 2008). When both the function and its Fourier transform are replaced with discretized counterparts, then the Discrete Fourier Transform (DFT) is formed. From these frequency components, the entire image is assembled into a spatially correct image and then reconstructed by an inverse Fourier transform process. This makes it convenient for computer manipulations.

Mathematically, Fourier transform originates from Fourier's theorem which states that a continuous function $f(t)$ which is periodic may be indicated by the summation of its cosine and sine terms, each with a particular coefficient for its amplitude and phase. This function is written as $F(u)$ and it is the aggregate of each frequency term in u that must be summed from the function $f(t)$. It is given as:

$$F(u) = \int_{-\infty}^{+\infty} f(t)\ e^{-j2\pi ut} dt \tag{3.35}$$

Fourier transform has a very significant characteristics in that, having the function $F(u)$, it is possible to obtain the function $f(t)$ in spatial domain, as shown below:

$$f(t) = \int_{-\infty}^{+\infty} F(u)\ e^{j2\pi tu} du \tag{3.36}$$

where $f(t)$ represents a real function and $F(u)$ is complex and periodic.

When dealing with finite sampled points, the integrals boundaries from minus infinity to plus infinity are summarized to a summation of terms having increasing frequency. Therefore, when applied to distinct data sets of finite intervals, the Fourier transform is modified to the Discrete Fourier Transform (DFT) and it is written as:

$$F(u) = \sum_{x=0}^{N-1} f(x)\, e^{-\frac{j2\pi ux}{N}} \ ; u = 0, 1, 2 \ldots, N-1 \tag{3.37}$$

where;

N is uniformly spaced and rely on the number of points sampled.

The summation of both positive and negative infinity is substituted by the integration of 0 to $N-1$ since this is a finite set of data. Similarly, the inverse transform is performed as;

$$f(x) = \frac{1}{N}\sum_{u=0}^{N-1} F(u)\, e^{\frac{j2\pi ux}{N}} \quad ; \quad x = 0, 1, 2 \ldots, N-1 \tag{3.38}$$

The function $f(x)$ has been reconstructed by addition of the discrete frequency component u from 0 to *N*–1.

For digital images, a two-dimensional transform is used in resolving the spatial frequency constituents of x and y. This is achieved by a direct extension from one-dimensional functions to two-dimensional ones in both cases of the continuous and the discrete values. This is done by replacing the 1-D functions with 2-D functions and summing over the two variables.

The 2-D DFT function of $f(x, y)$ is:

$$F(u, v) = \sum_{x=0}^{M-1}\sum_{y=0}^{N-1} f(x, y)\, e^{-j2\pi(^{ux}/_{M} + ^{vy}/_{N})} \tag{3.39}$$

where

u range is represented as [0- $M-1$] and v range is represented as [0 -$N-1$] and,

$M \times N$ represents the original image size.

Similarly, the inverse 2-D DFT is obtained through;

$$f(x, y) = \frac{1}{MN}\sum_{u=0}^{M-1}\sum_{v=0}^{N-1} F(u, v)\, e^{j2\pi(^{ux}/_{M} + ^{vy}/_{N})} \tag{3.40}$$

The high-frequency contents available in Fourier transform is contributed by the availability of sharp transitions and edges in an image while the low frequency contents are responsible for the overall look of an image over smooth areas. By filtering out the unwanted frequencies, one can obtain the enhanced image by applying the inverse Fourier transformation.

By applying the above functions, it is possible to convert an image from one domain to the other multiple times without degradation. This is because the DFT functions are exact descriptors and not approximations of a precise function. This capability of their usage without the likelihood of any data loss support their applicability in image processing (Gonzalez and Woods, 2008).

3.3.2 Frequency Domain Filtering

Frequency domain filtering is done by changing the image transform and then calculating its inverse so as to retrieve the de-noised image. Considering an image, $f(x, y)$, its simplest filtering function can be written as;

$$g(x, y) = \Im^{-1}[H(u, v)F(u, v)] \tag{3.41}$$

where;

$\Im^{-1}$ represents inverse DFT,

$F(u, v)$ represents input image DFT,

$g(x, y)$ is the filtered image and,

$H(u, v)$ is the filter function.

The filtering function, $H(u, v)$, is modified appropriately to either obtain the low-pass filters or the high-pass filters (Gonzalez and Woods, 2008). A low-pass filter attenuate high-frequency components like noise and other sharp intensity transitions hence achieving a smoothing operation. In contrast, a high-pass filter attenuate low-frequency components enabling one to achieve image sharpness and improve the edges. So, one is the opposite of the other.

3.3.2.1 Image smoothing using frequency domain

Noise contributes to the high-frequency bit in an image. By using low-pass filters, smoothing can be accomplished through high-frequency attenuation. The filtering equation remains as in Equation 3.41, with the filter function, $H(u, v)$, being the affected part. There are two types of low-pass filters of interest. These are the Butterworth and the Gaussian types.

A Butterworth low-pass filter has its high values approaching an ideal filter operation. Considering one with order n, its transfer function can be represented by:

$$H(u,v) = \frac{1}{1 + [D(u,v)/D_0]^{2n}} \tag{3.42}$$

where;

D_0 represents the set threshold referred to as the cut-off frequency,

$D(u,v)$ is the operational distance frequency.

The Gaussian low-pass filter is represented as:

$$H(u,v) = e^{-D^2(u,v)/2{D_0}^2} \tag{3.43}$$

where;

$D(u,v)$ represents the operational distance frequency,

D_0 represents the set threshold referred to as the cut-off frequency.

This filtering has its application in the printing and publishing industry, where it is used in the numerous pre-processing functions, including unsharp masking.

3.3.2.2 Image sharpening using frequency domain

Image sharpening is realised by using high-pass filters. Here low-frequency constituents are attenuated without affecting high-frequency constituents (Gonzalez and Woods, 2008). Its equation is written as;

$$H_{HP}(u,v) = 1 - H_{LP}(u,v) \tag{3.44}$$

where $H_{LP}(u,v)$ is the function of the low-pass filter.

There are two types of high-pass filters of interest. These are Butterworth and Gaussian filters. The Butterworth transfer function with order n can be represented by:

$$H(u,v) = \frac{1}{1 + [D_0/D(u,v)]^{2n}} \tag{3.45}$$

where $D_0$is the cut-off frequency.

The high-pass filter of a Gaussian function is written as:

$$H(u,v) = 1 - e^{-\frac{D^2(u,v)}{2{D_0}^2}} \tag{3.46}$$

where $D_0$is the cut-off frequency.

3.3.3 Wavelet Transform

Conventionally, the Fourier transform has found its application to a great extent in signal analysis. In particular it very helpful when examining the constituents of a stationary signal. However, the Fourier transform does not represent a non-stationary signal adequately. These non-stationary signals can be analysed effectively by using a technique called the wavelet transform which uses wavelets (Sifuzzaman *et al.,* 2009).

A wave is an oscillation occurring in time or space. Fourier analysis is a wave analysis. Alternatively, a wavelet is a small wave-like function which can used to scale or translate another function. In addition, it has its energy concentrated in time and frequency. As shown in Figure 3.7 below, wavelet functions integrate to zero, 'waving' above and below the x-axis. Equation 3.47 also shows a wavelet function has zero average.

$$\int_{-\infty}^{+\infty} \Psi(t)dt = 0 \tag{3.47}$$

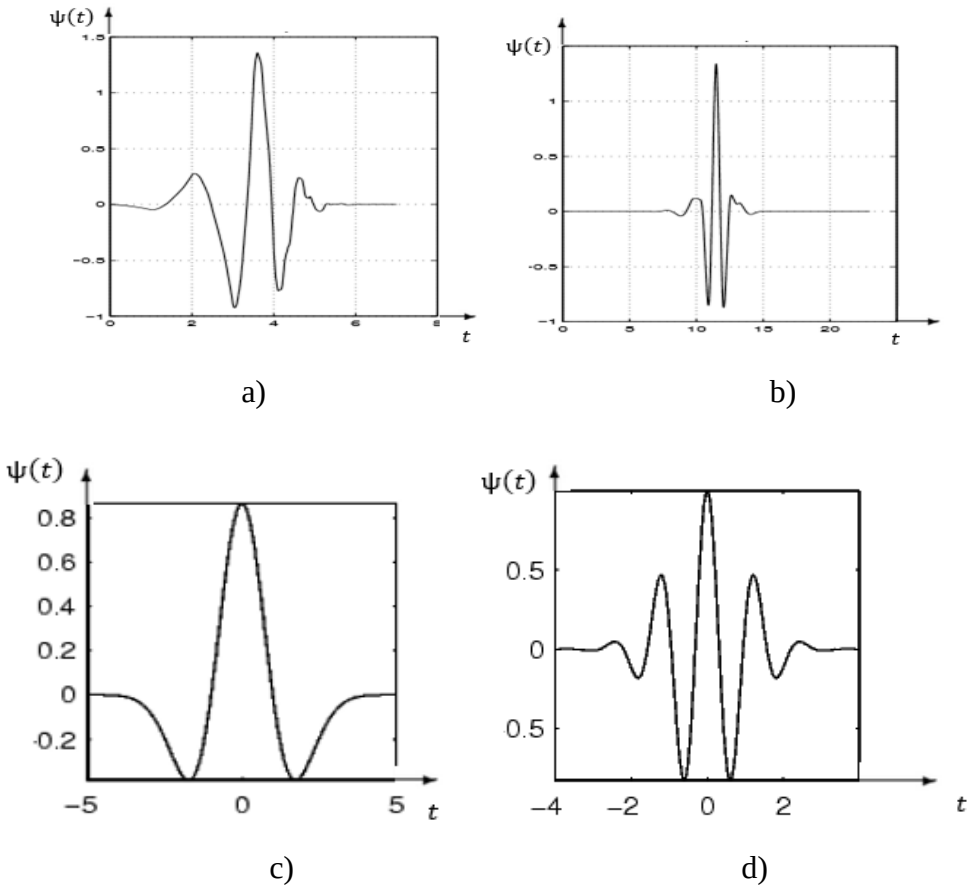

Figure 3.7: Diverse wavelet functions (a) Daubechies D4 (b) Coiflet order 4 (c) Mexican-hat (d) Morlet wavelet functions

Wavelets offer a mechanism of performing transient scrutiny of non-stationary and time-changing occurrences. It has an oscillating wave-like characteristic and it's capable of allowing instantaneous frequency and time mathematical analysis making wavelets essential tools in signal analysis.

The wavelet transform is able to provide the frequency and time details of any signal instantaneously. It also focuses the signal energy into smaller quantity of wavelet factors which have excellent time-frequency localization properties. It can also decompose a signal into simple function sets gotten from the mother wavelet through translation and dilation processes as shown below:

$$\Psi_{a,b}(t) = \frac{1}{\sqrt{a}}\,\Psi\frac{(t-b)}{a} \tag{3.48}$$

where;

a and b indicate the scaling and translation processes respectively,

Ψ is the mother wavelet.

Wavelet transform can be divided into two as either orthogonal or non-orthogonal wavelets. Orthogonal wavelets have their applications in discrete wavelet transforms where they decompose signals into arrays of small functions that are perpendicular to their translations and scaling. They returns data vectors of the similar or lower coefficients. They have their application in signal processing and signal compression. Non-orthogonal wavelets on the other hand have their applications in continuous wavelet transform functions where they returns an array that is one dimension larger than the input (Gonzalez and Woods, 2008).

3.3.3.1 Discrete Wavelet Transform

The Discrete Wavelet Transform (DWT) crumbles signals into mutually orthogonal set of wavelets and it can be an easy and fast way of noise suppression in a signal.

DWT has an advantage over DFT in that it accomplishes multi-scale approximation of signals by using time and frequency characteristics. Also, DWT is able to work well with discontinuities in that it requires less wavelet vectors to achieve an approximation as compared to DFT.

However, DWT cannot be completely described with a single equation since it is composed of a variety of unique but related transformations. As an alternative, a set of parameters of varying frequency are used to characterize it. For example, if the scaling function $\phi(x,y)$ is 2-D, and $\psi(x)$ and $\psi(y)$ are its corresponding wavelets, then the relationship is as given below. The scaling function can be separated into two components:

$$\phi(x,y) = \phi(x)\phi(y) \tag{3.49}$$

The directional components of these wavelets can be represented as:

$$\begin{aligned} \psi^H(x,y) &= \phi(x)\psi(y) \\ \psi^V(x,y) &= \psi(x)\phi(y) \\ \psi^D(x,y) &= \psi(x)\psi(y) \end{aligned} \tag{3.50}$$

where;

$\psi^H(x,y)$ represents horizontal wavelets components,

$\psi^V(x,y)$ represents vertical wavelets components and,

$\psi^D(x,y)$ represents diagonal wavelets components.

They measure the intensity variations of images along the gray-levels in different directions. Take an example of a 2-D scaling function, then the wavelet transform can be obtained easily as shown below. The scaling and the translating functions are represented by:

$$\phi_{j,m,n}(x,y) = 2^{j/2}\phi\left(2^j x - m, 2^j y - n\right) \tag{3.51}$$

$$\psi^i{}_{j,m,n}(x,y) = 2^{j/2}\psi^i\left(2^j x - m, 2^j y - n\right) \quad ; \; i = \{H,V,D\} \tag{3.52}$$

where;

i represents directional wavelets,

j controls the width of $\phi_{j,m,n}(x,y)$,

$2^{j/2}$ controls the amplitude of $\phi_{j,m,n}(x,y)$,

m and n determine the position of $\phi_{j,m,n}(x,y)$ along the major axis.

For a two-dimensional image, the DWT is represented as:

$$W_{\phi}(j_0, m, n) = \frac{1}{\sqrt{MN}} \sum_{x=0}^{M-1} \sum_{y=0}^{N-1} f(x, y) \phi_{j_0,m,n}(x, y) \tag{3.53}$$

$$W^{i}{}_{\psi}(j, m, n) = \frac{1}{\sqrt{MN}} \sum_{x=0}^{M-1} \sum_{y=0}^{N-1} f(x, y) \psi^{i}{}_{j,m,n}(x, y) \tag{3.54}$$

where;

j_0 is the arbitrary initial scale of the scaling function,

$W_{\phi}(j_0, m, n)$ approximates the coefficients of image at scale j_0,

$W^{i}{}_{\psi}(j, m, n)$ adds details of horizontal, vertical, and diagonal for $j \geq j_0$.

To recover the 2-D image, the inverse DWT is performed as follows:

$$f(x, y) = \frac{1}{\sqrt{MN}} \sum_{m} \sum_{n} W_{\phi}(j_0, m, n)\, \phi_{j_0,m,n}(x, y) \; + \; \frac{1}{\sqrt{MN}} \sum_{i=H,V,D} \sum_{j=j_0}^{\infty} \sum_{m} \sum_{n} W^{i}{}_{\psi}(j, m, n)\, \psi^{i}{}_{j,m,n}(x, y) \tag{3.55}$$

When DWT is applied to an image, the image is decomposed into four sub-bands having two rows and two columns of low-low (LL), low-high (LH), high-low (HL) and high-high (HH) (Rajput *et al.*, 2012) as shown in Figure 3.8. This is called the first level of decomposition and it has one approximation coefficient and three detail coefficients. The approximation coefficients contains the average image information which is the most significant while the details coefficients carry directional information for the spatial orientation.

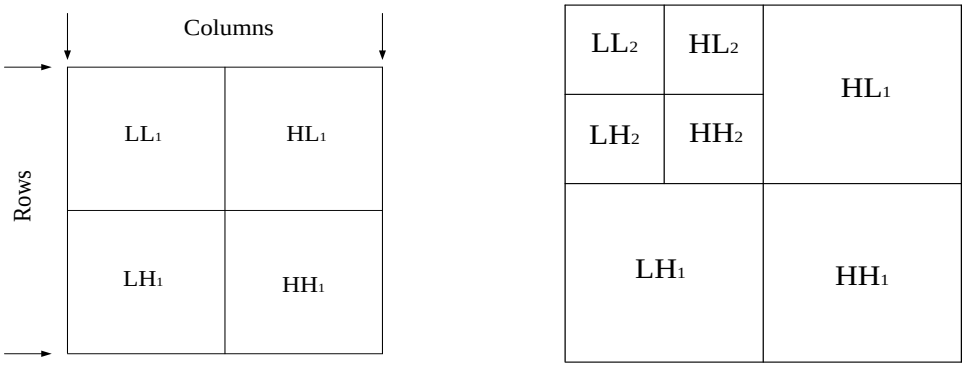

Figure 3.8: Discrete Wavelet Transform Decomposition

Wavelet-based image processing allows an image to undergo decomposition into various coefficients while still preserving the information of the image (Sahu and Parsai, 2012). These coefficients can be altered accordingly before recombining them to obtain the final fused image through the inverse DWT. The inverse DWT requires up-sampling and filtering differentiating it with DWT.

The down-sampling operation happens by using a factor of two and is used to protect the even-numbered constituents in a data matrix. The process is shown in Figure 3.9 below.

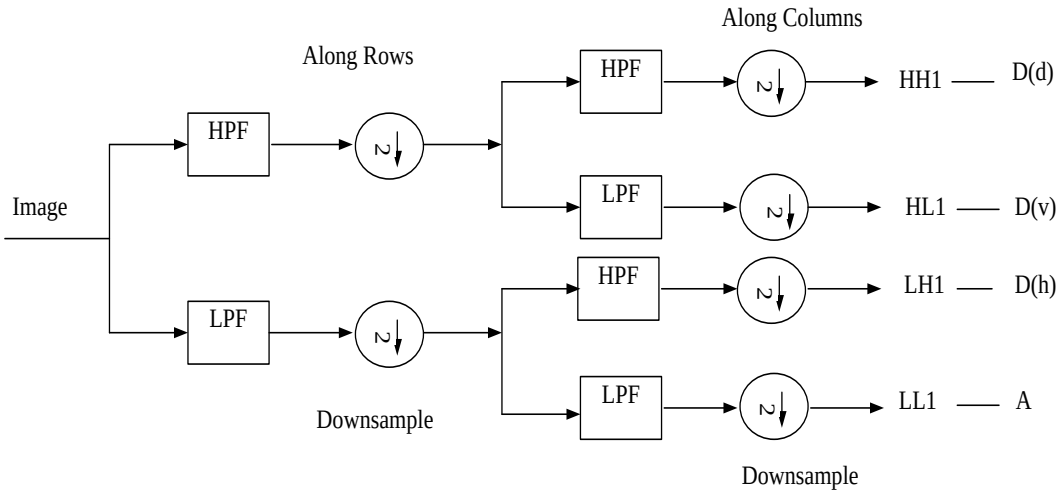

Key:

A – Approximation coefficient

D (h), D (v) and D (d) represents the detail coefficients in horizontal, vertical and diagonal directions respectively

Figure 3.9: Wavelet decomposition structure

On the other hand, the up-sampling by the same factor of two entails expanding through insertion of zeros among the odd-numbered constituents in a data matrix. Figure 3.10 shows the up-sampling process.

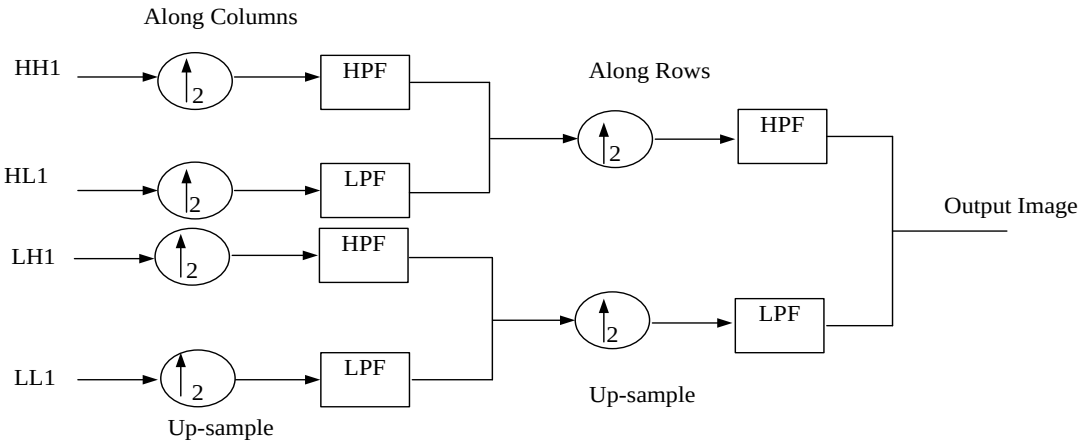

Figure 3.10: Wavelet reconstruction structure

Wavelet transform is a powerful and important tool in image denoising and signal characterization. This is because wavelets offer an instantaneous localization in frequency and time domain and they are computationally fast particularly when using the fast wavelet transform. In addition, wavelets can separate fine details in a signal. Moreover, by using wavelets it is possible to reveal features of data that other signal analysis techniques miss out like discontinuities in higher derivatives. Furthermore, it is possible to obtain an excellent approximation of any function by using fewer factors in comparison to Fourier technique. Finally, signal compression or de-noising is achievable without significant degradation (Sifuzzaman *et al.*, 2009).

3.3.3.2 Haar wavelet transform

This is one of the oldest wavelet and was suggested by Alfred Haar in 1909 (Arora *et al.*, 2014). It defines a family of orthogonal wavelets and it is the simplest of all wavelets with an easy to understand operation. The Haar wavelets are associated with the Haar transform in discrete mathematical operation. In its operation, the Haar wavelet crumbles a discrete signal into two. One sub-signal runs the average and other sub-signal runs the difference.

The Haar wavelet scaling (ϕ) and wavelet functions (ψ) have lengths of 1 and are symmetrical. The scaling function (father wavelet) is written mathematically as:

$$\phi(x) = \begin{cases} 1, & if\ 0 \le x < 1 \\ 0, & otherwise. \end{cases} \tag{3.56}$$

A one dimensional Haar scaling function is illustrated below in Figure 3.11.

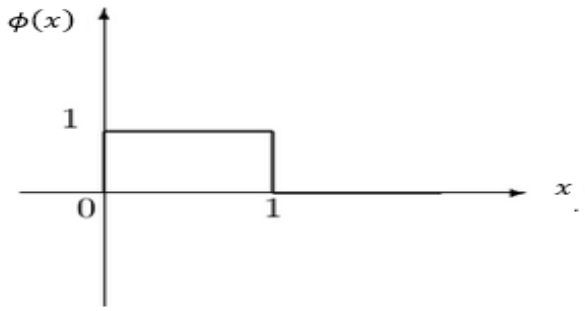

Figure 3.11: 1-D Haar Scaling function

The Haar wavelet's mother function is a bipolar step function defined as $\psi(x) = \phi(2x) - \phi(2x-1)$ and can be written as;

$$\psi(x) = \begin{cases} 1, & 0 \leq x < 0.5, \\ -1, & 0.5 \leq x < 1, \\ 0, & otherwise. \end{cases} \tag{3.57}$$

A one-dimensional Haar wavelet mother function is given in Figure 3.12. It can be noted that the area is zero and that it has only a finite duration.

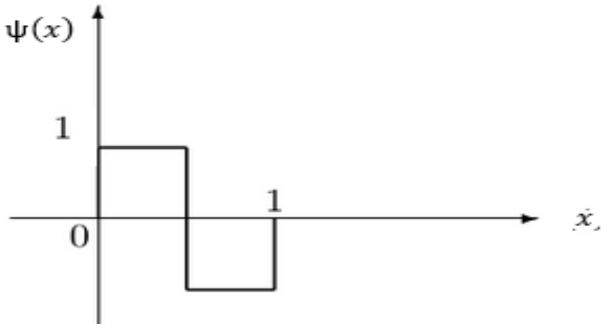

Figure 3.12: 1-D Haar mother function

The Haar wavelet transform is very simple and fast in its operation, efficient in memory usage as it performs calculations without temporary arrays and it is precisely reversible with negligible edge effects.

3.3.4 Image Denoising

Image denoising endeavours to reduce noise levels in an image at the same time maintaining the significant image features. The wavelet domain has noise evenly distributed throughout its coefficients while most of the image information is focussed in a few larger coefficients. To distinguish information from noise, wavelet thresholding of its coefficients is performed. This is done through a series of steps where the image is

passed first through the linear forward wavelet transformation then through the nonlinear thresholding technique and finally recovered by using the linear inverse wavelet transformation. Successful usage of the wavelet transform might lessen the noise effect or even overcome it completely (Ruikar and Doye, 2011).

Image denoising is different from image enhancement in that the latter is objective while the former is subjective (Gonzalez and Woods, 2008). An important technique in denoising is that one has previous information regarding the degradation process. This is in contrast to image enhancement which deals with image characteristics manipulation so as to achieve an attractive image to the observer.

A noisy image can be disintegrated into an original image fragment and a noisy image fragment as shown in Equation 3.58 (Ruikar and Doye, 2011).

$$g(x,y) = f(x,y) + n(x,y) \tag{3.58}$$

where;

$f(x,y)$ and $g(x,y)$ represents the native and noisy images respectively,

$n(x,y)$ represents the Gaussian noise.

Since wavelet transformation is a linear operation, the wavelet factors are made up of two portions as shown below;

$$W_g = W_f + W_n \tag{3.59}$$

where;

W_f represents the wavelet coefficients of the original image,

W_n represents the noise wavelet coefficients and,

W_g represents the wavelet coefficients of the noisy image.

For denoising to take place, the image wavelet coefficients must be greater than the noise wavelet coefficients. This facilitates the choice of a suitable threshold value, T. Section 3.3.5 expands further on this.

3.3.5 Wavelets Thresholding

Thresholding is a technique for image denoising. It is mainly applied in image segmentation where the image pixels that are above a certain criteria are grouped together as the foreground while the other pixels are grouped as the background.

In the wavelet domain, the energy distribution of the signal is mainly concentrated in the limited coefficients of the wavelet, whereas the noise's energy is distributed throughout the wavelet. Therefore, the signal coefficients are superior to those of the noise after wavelet decomposition. A suitable threshold can be found, where the amplitudes of wavelet coefficients that are less than the pre-set threshold, are considered to be caused by noise and their amplitudes set to zero. The other amplitudes which are greater than the set threshold, are considered to be the amplitudes of the signal and they are preserved or revised. The image is reconstructed by the processed wavelet coefficients to achieve the purpose of image denoising. This algorithm is simple, has better visual effects, and can keep the edge information.

The steps involved in a simple de-noising process are described in Figure 3.13. The degraded image is first passed through Haar transformation. A threshold is then set. Thereafter, inverse Haar transformation is performed to reveal the enhanced image.

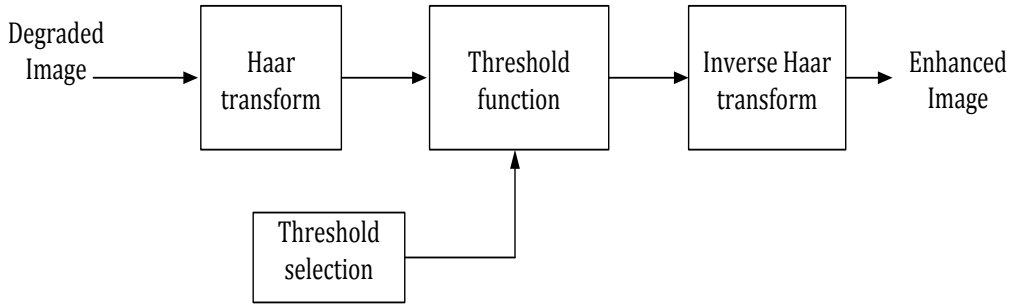

Figure 3.13: Block diagram for image de-noising

There are two main ways of wavelet thresholding, namely the hard thresholding and the soft thresholding methods.

3.3.5.1 Hard Thresholding

Hard thresholding converts all the pixels that are lesser than the specified criteria to zero and retains the other pixels unaffected (Hui *et al.*, 2013). It is indicated as:

$$g(x,y) = \begin{cases} f(x,y) & |f(x,y)| > T \\ 0 & |f(x,y)| \leq T \end{cases} \tag{3.60}$$

where;

$f(x, y)$ represents wavelet coefficients of the noisy image,

T is the set threshold.

Hard thresholding can create discontinuities, and thus significantly amplifies minor variances that have their values closer to the set threshold. (Gonzalez and Woods, 2008). For example, values that are just marginally less than the set threshold are converted to zero while those that are somewhat greater than the threshold are left unchanged. Hence, making it unsuitable for noise removal.

3.3.5.2 Soft Thresholding Method

To overcome the demerits of hard thresholding, an alternative technique referred to as soft thresholding was developed. The coefficients that have their absolute coefficients lesser than the set threshold are all converted to zero and the other values which are non-zero are scaled towards zero by subtracting them from the set threshold (Gonzalez and Woods, 2008). The general soft shrinkage rule is defined by:

$$g(x,y) = \begin{cases} sgn(f(x,y)(|f(x,y)| - T)) & |f(x,y)| > T \\ 0 & |f(x,y)| \leq T \end{cases} \quad (3.61)$$

where;

$f(x, y)$ represents the noisy image,

T represents the threshold value,

$sgn\, f(x, y)$ represents the sign of $f(x, y)$,

$g(x, y)$ represents the result of the wavelet coefficients processed by the improved soft threshold denoising function.

This method removes image discontinuities by smoothening the time series through image blurring which improves on the objects and shape perception. This reduces the edges and thus improves on the smooth transition (Gonzalez and Woods, 2008).

CHAPTER FOUR

MATERIALS AND METHODS

This chapter gives a presentation of the hardware and software materials that were used in the research. The procedure of the image enhancement and defect detection methods are discussed. Finally, an outline of the subjective and objective image quality measures are presented.

4.1 Materials

The software platform used for data analysis in this study is MATLAB 8.0 (R2012b). It has its own programming language and powerful graphics capabilities. The MATLAB platform gives a wide range of remarkable support programs, referred to as toolboxes that considerably increases the number of built-in features into the main program. These toolboxes encompass almost all primary areas in system simulation but the major emphasis will be placed on the image processing toolbox (IPT). This toolbox provides some standard algorithms and graphical tools that are used for image analysis. These include image segmentation algorithms, edge detection algorithms, image transformation algorithms and tools for computing statistical functions and determining image features. In addition, objective quality measures such as Coefficient of Correlation (CoC), PSNR and SSIM have been computed according to the functional codes written in the editor window for various images.

Implementing the automation algorithms discussed in this project requires the creation of a complete development environment. The environment is responsible for the entire work flow, from creation of a gray-image, through running the algorithms, gathering results and performing analysis. The development environment is based on MATLAB. The main reason for using MATLAB was to shorten development time, as MATLAB supports many required features, such as image loading, saving, spatial filters, minimum spanning tree module, and more.

A personal laptop was used as the workstation with the following specifications: Intel (R) Core(TM) i3-3110M CPU @ 2.40 GHz processor, 4.00 GB installed memory (RAM) and 64-bit Windows 8.1-professional operating system.

The X-ray images used were obtained from Quality Inspectors Limited, Kenya Bureau of Standards (KEBS) and from various internet sites such as http://www.x-rayfilmrecycling.com/industrial-non-destructive-testing-ndt.html and https://www.nde-ed.org/EducationResources/CommunityCollege/Radiography/TechCalibrations/RadiographInterp.htm. They were used in the enhancement and defect detection automation techniques discussed previously to compare results, both visually and quantitatively. The images obtained from Quality Inspectors Limited were in XRYX file format. This format is unreadable in MATLAB. Therefore, the images had to be converted to file formats compatible with MATLAB like GIF, JPEG and PNG. Most of the images used are gray-scale in the JPEG file format. This constitutes about 80% of the data base, the rest are in the other file format indicated above.

4.2 Methods

In this section, the proposed enhancement methods are presented. The objective is to enhance the digital X-ray images and later to develop an automated method for the detection of defects that is precise and objective. The following series of steps were followed;

Step i: This involves the process of acquiring the image. The images used here were mainly obtained from the internet or from either Quality Inspectors or KEBS. There were then stored in a data-base.

Step ii: The images were read and converted to gray-scale image using MATLAB image processing toolbox.

Step iii: The resultant 2-D image had to be de-noised so as to remove noise specks.

Step iv: The noise free images were enhanced by either contrast stretching or through histogram equalization techniques to improve on the image contrast and brightness. Mathematical image measurement tools of SSIM and PSNR were applied in determining the changes in the enhanced image in comparison to the input image.

Step v: Once the image was enhanced, the Canny edge detection technique was then applied as it is superior in comparison to other edge detection techniques. It can identify tiny defects in an image.

Step vi: Image thresholding was then performed with an objective of grouping the image into areas with similar characteristics. The method of image thresholding used include: Otsu's thresholding and percolation thresholding.

Step vii: A method for automated recognition of defects was presented. This involved the use of a template matching technique. The Coefficient of Correlation between the original image and the template used was also obtained.

Step viii: Finally, the defect detected was displayed on the screen for user identification.

The block diagram in Figure 4.1 gives the fundamental sequence involved in an image processing system. Once the image is obtained, it is de-noised to eradicate noise. The resulting image is then enhanced using the various enhancement techniques discussed previously. The enhanced image is then segmented so as to extract the required defects from the image. Finally, image measurements techniques are applied on the enhanced image and a comparison made with the original image.

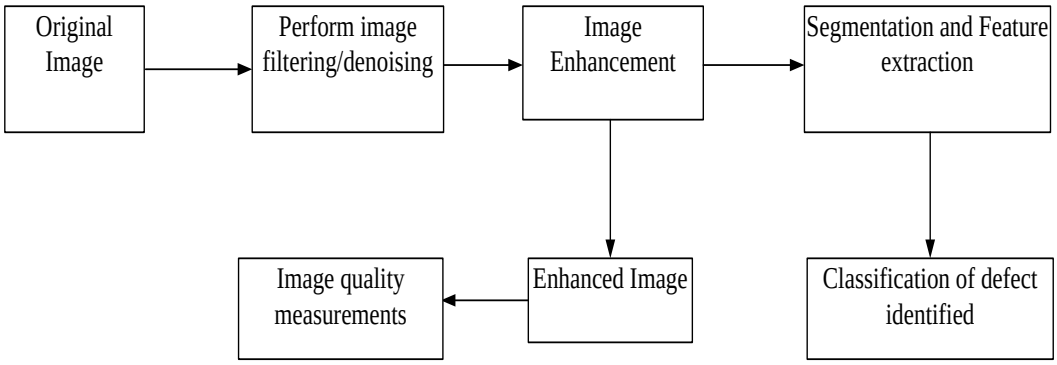

Figure 4.1: System Architecture

4.2.1 Contrast stretching

Contrast stretching improves the image brightness distinguishing various regions with defects in the image. The proposed algorithm used to improve on the image contrast is summarized in Figure 4.2, whereby, an image is read in MATLAB and then contrast stretching is applied on the image as given in the following algorithm.

The algorithm has the following procedure;

i) Reading the X-ray images from the various sources and converting them to gray-scale using the *'im2gray'* function in MATLAB 8.0. The outputs of the conversion are 8-bit gray-scale images.

ii) The gray-scale image was then enhanced by contrast stretching. This expands the range of the gray-levels to span the full intensity range (0 to 255 for the 8-bit images). This highlights and distinguishes features in an image. The linear contrast stretching method described in section 3.2.1 has been used.

iii) The PSNR and SSIM values for the enhanced image were obtained.

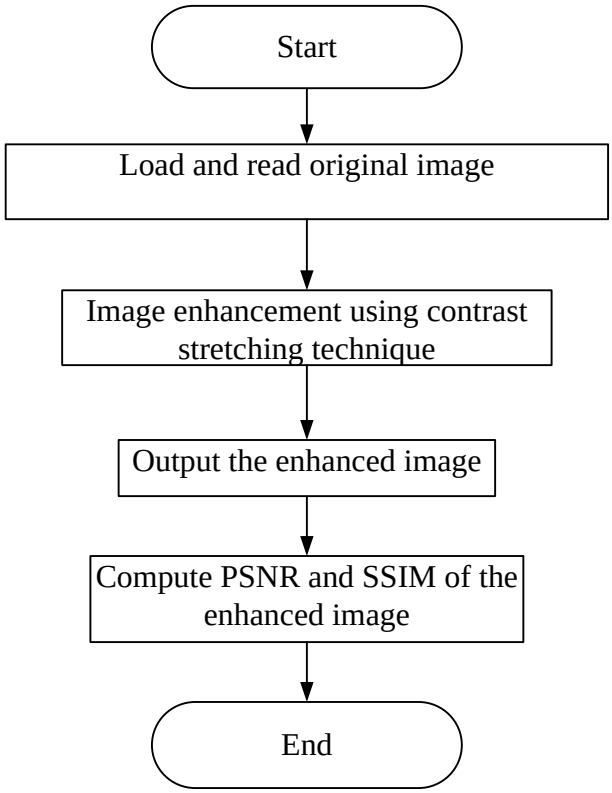

Figure 4.2: Contrast stretching flow chart

4.2.2 Histogram processing

Image enhancement improves image contrast making the image superior than the original image for a particular usage. The main techniques that were used were the Adaptive Histogram Equalization (AHE) algorithm, the Recursive Mean-Separate Histogram Equalization (RMSHE) algorithm, the Classical Histogram Equalization (CHE) algorithm, the Brightness Preserving Bi-Histogram Equalization (BPBHE) algorithm and Dynamic Histogram Equalization (DHE) algorithm. Figure 4.3 gives the proposed procedure. It involves noise removal before image enhancement using the above techniques and finally highlighting of the edges of the enhanced image.

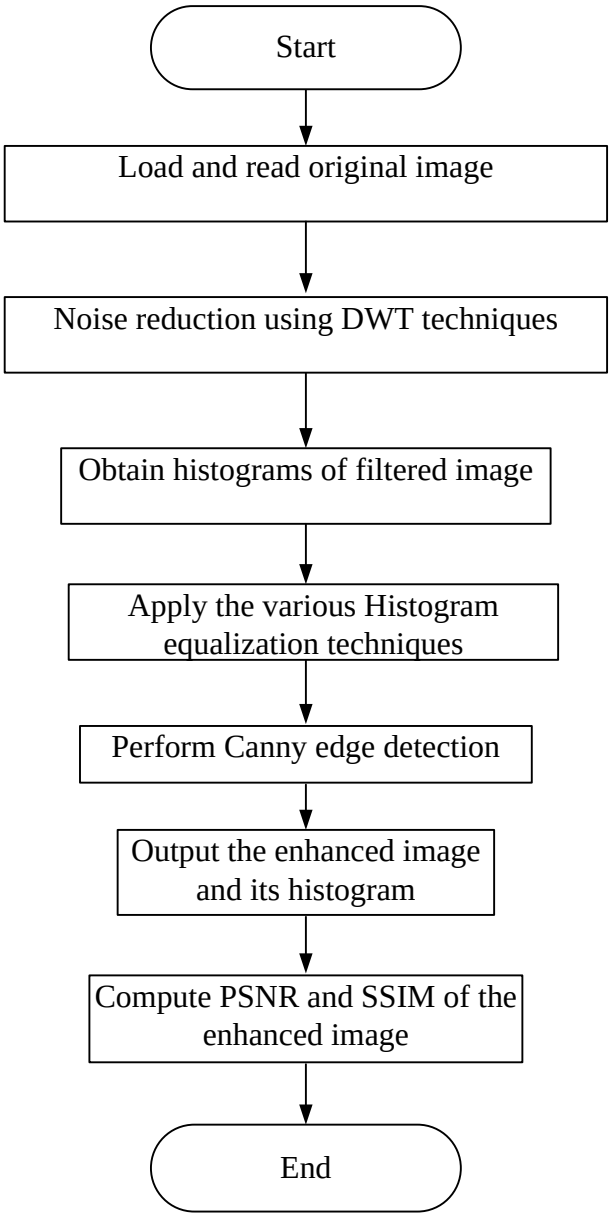

Figure 4.3: Histogram equalization flow chart

The process consists of the following procedure;

i) Reading the X-ray images from the various sources and converting them to gray-scale using the *'im2gray'* function in MATLAB 8.0.The outputs of the conversion were 8-bit gray-scale images.

ii) The gray-scale image was passed through the DWT filter functions for noise reduction.

iii) The filtered image was then enhanced using the various histogram equalization methods discussed in section 3.2.2.2.
iv) Canny filters were finally applied to the enhanced image to extract edges.
v) The PSNR and SSIM values for the enhanced image were obtained and compared.

4.2.3 Automatic defect detection

Otsu's and percolation thresholding techniques have been used in eliminating irrelevant information, leaving only the objects of interest in the image. Finally, template matching was applied in defect detection as shown in Figure 4.4.

Here, an image is loaded in MATLAB where it is converted to gray-scale. Binarization process using either Otsu's thresholding or percolation thresholding is then applied to remove unnecessary information from the image. The main process of defect detection using template matching is then performed by using correlation. This involves a direct comparison of the image template and the input image and then evaluating the degree to which the two images are similar. This is recorded as the Coefficient of Correlation (CoC). A threshold value is set for CoC and value above the threshold indicates the presence of a defect and this is shown on a screen, otherwise, the defect is not major.

The method consists of the following procedure;

i) Reading either the original or the enhanced X-ray images from the stored database.
ii) Performing either Otsu's or percolation thresholding.
iii) The results obtained by segmentation are used for further higher-level methods of feature extraction. Defects were detected by using template matching.
iv) A threshold value is set for CoC and value above the set threshold shows the existence of a defect, otherwise, the defect present is not major. A comparison between Percolation and Otsu's thresholding techniques at the same threshold values was done. For percolation to occur, the threshold value should be higher than 0.59. Since only the major defects are needed in this case, the value was raised to 0.7
v) Finally, the existence or absence of any defect is shown on a screen.

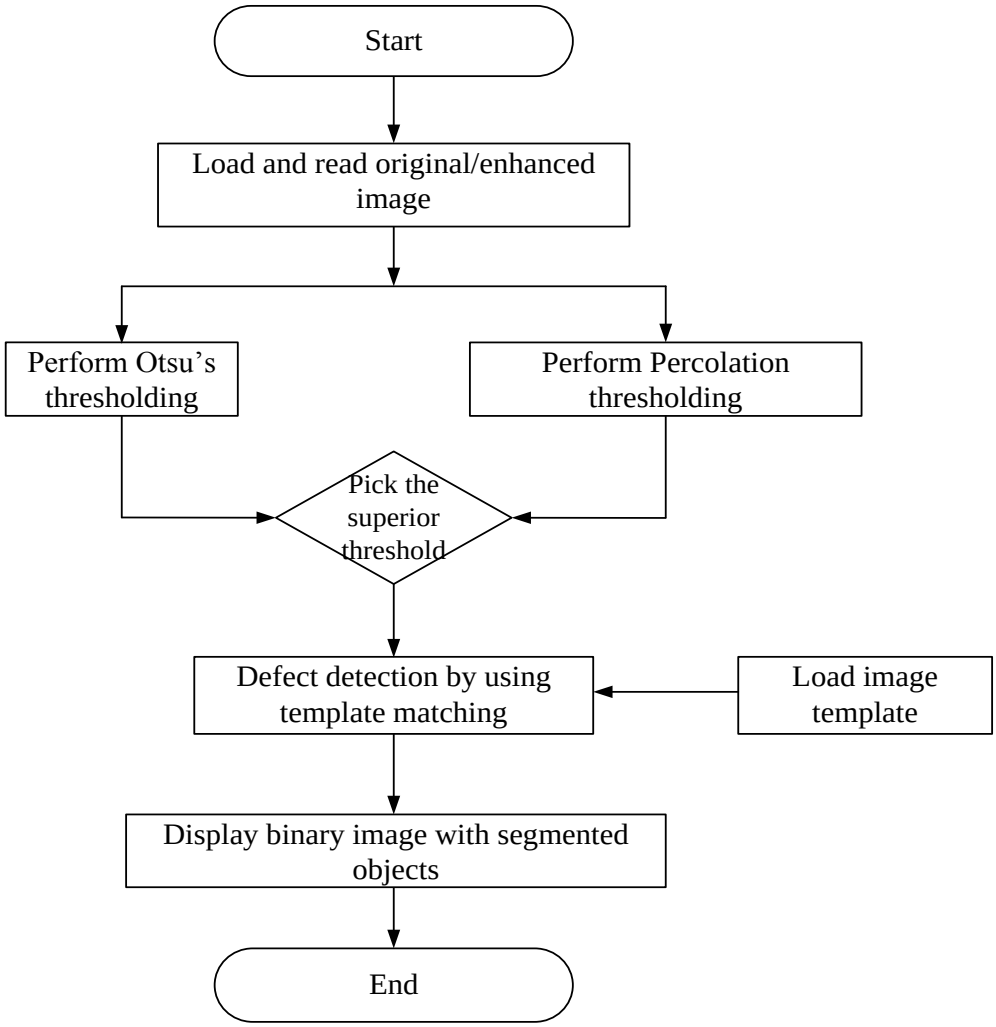

Figure 4.4: Defect detection flow chart

4.3 Image Quality Measures

The general requirement of an image enhancement and fusing technique is that it must preserve the significant information from an image without introducing any artifacts that could interfere with the image analysis (Sahu and Parsai, 2012). The performance measures commonly used can either be subjective or objective.

Image Quality Assessment (IQA) is key to in image processing applications with its main aim being the automatic evaluation of image superiority in a manner that is unswerving with human visual judgment.

4.3.1 Subjective measurement

To begin with, subjective measurement gives opinions of the observer where the performance measures are influenced by personal judgement. By visual observation, it is

possible to give the difference of the primary image in comparison to the resultant image, and hence, evaluate the performance of the enhancement technique (Rajesh *et al*., 2011). Subjective measure evaluates the acceptability of a digital image to the human eyes and also assess its natural appearance. On the other hand, subjective tests are expensive to carry out since they involve interviewing observers. In addition, they are difficult to reproduce and verify.

The scoring can have a grading scale like 5 is good and 1 is undesirable. This can be represented as;

$$Score = \frac{1}{N}\sum_{i=0}^{N} iP_i \tag{4.1}$$

where;

i is an image score,

P_i is image score probability and,

N is the number of observers interviewed.

4.3.2 Objective measurement

On the other hand, an objective quality measure, in contrast to its subjective counterpart, is conducted by the image quality metric that counts some sense of variance between the enhanced image and the original image. Objective measurement gives facts where the performance involves an impartial measurement where personal opinion or interpretations of results are not used. Here a mathematical approach is used and two prominent examples relied on are the PSNR and the SSIM techniques.

These measures plays an important role in image processing techniques by dynamically controlling and adjusting the quality of the image in real-time. Also, they are applied in algorithms optimization and parameter settings for image processing systems. Finally, they are applied in benchmarking a specific image processing system.

a) Peak Signal to Noise Ratio

The Peak Signal to Noise Ratio (PSNR) gives the relationship amongst optimal signal values and the power of the deforming noise which interrupts the quality of the signal

(Sahu and Parsai, 2012). PSNR is mostly conveyed through the logarithmic decibel scale (dB) to counter the wide dynamic range of most signals.

The mathematical representation of the PSNR is;

$$PSNR\ (dB) = 20\ log_{10}\left({MAX_f}/{\sqrt{MSE}}\right) \tag{4.2}$$

where;

MAX_f represents the maximum pixel range of intensities, for example 255 for an 8-bits image,

MSE gives the Mean Square Error amid the native and enhanced image.

The MSE denotes the power of distortion and is obtained from the mean of the squared differences of the intensities of the original and the enhanced image (Mohammadi *et al.*, 2015). It can be represented as;

$$MSE = \frac{1}{MN}\sum_{x=1}^{M-1}\sum_{y=1}^{N-1}|f(x,y) - g(x,y)|^2 \tag{4.3}$$

and;

$f(x,y)$ and $g(x,y)$ are the native and resultant images individually and,

$M \times N$ represents the original image size.

If the value of PSNR is high, it shows that the reconstruction of the degraded image is good.

b) Structural Similarity Index Measure

The Structural Similarity Index Measure (SSIM) technique was designed to improve on methods like PSNR which have proven to be unreliable when it comes to the Human Visual System (HVS). It works by comparing the structural match between images. As such, image degradation is alleged to be the change in the structural information of the pixels which have strong interdependencies particularly when they are spatially close (Sampat *et al.*, 2009). This reliance convey decisive information in regard to an image structure (Mohammadi *et al.*, 2015).

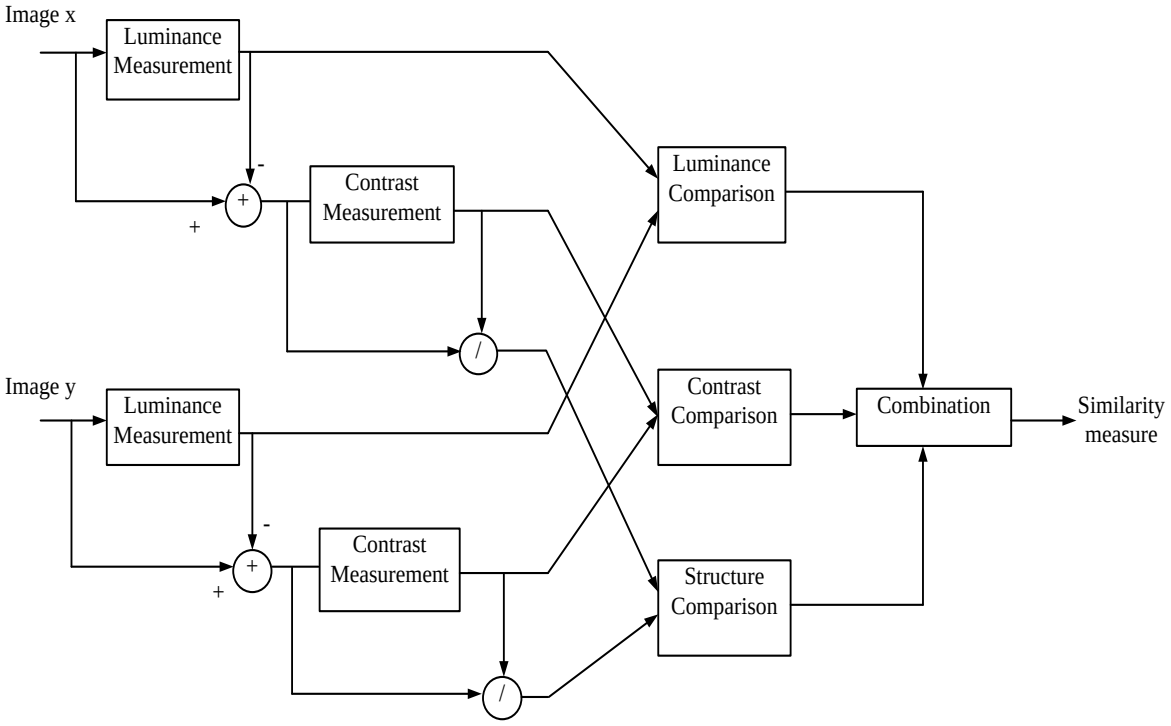

Figure 4.5: SSIM processes block diagram

In an image, the structural information is obtained from the distinguishing characteristics that symbolises it like image contrast and its local luminance. These measurements are performed through contrast comparison, luminance comparison and finally through structure comparison as shown in Figure 4.5 (Mohammadi *et al.*, 2015). This quality assessment index does the calculations of these terms and the final term combination of the three.

The SSIM measurements for two images is given by;

$$SIMM(x,y) = [l(x,y)]^{\alpha}.[c(x,y)]^{\beta}.[s(x,y)]^{\gamma} \tag{4.4}$$

where

x range from $[x_i - M]$ and y range from $[y_i - M]$,

$\alpha > 0, \beta > 0$ and $\gamma > 0$ dictate the relative significance of each terms of the index.

The three terms are distinct in their definition and calculations. The luminance comparison function is;

$$l(x,y) = \frac{\left(2\mu_x\mu_y + C_1\right)}{\left(\mu_x^2 + \mu_y^2 + C_1\right)} \tag{4.5}$$

where C_1 is a constant included to avoid instability and is given as;

$$C_1 = (K_1 L)^2 \tag{4.6}$$

where;

L represents image pixels range,

$K_1 \ll 1$ represents a small constant.

The function indicating the comparison in contrast is obtained as;

$$c(x, y) = \frac{(2\sigma_x \sigma_y + C_2)}{(\sigma_x^2 + \sigma_y^2 + C_2)} \tag{4.7}$$

where $C_2$is non-negative constant having value:

$$C_2 = (K_2 L)^2 \tag{4.8}$$

and K_2 satisfies $K_2 \ll 1$.

The structure comparison function is then conducted as shown below;

$$s(x, y) = \frac{(\sigma_{xy} + C_3)}{(\sigma_x \sigma_y + C_3)} \tag{4.9}$$

The local mean intensity of discrete signals is as follow;

$$\mu_x = \frac{1}{M} \sum_{i=1}^{M} x_i \tag{4.10}$$

Signal contrast is estimated by the use of standard deviation. This is obtained by;

$$\sigma_x = \{\frac{1}{M} \sum_{i=1}^{M} (x_i - \mu_x)^2\}^{1/2} \tag{4.11}$$

The cross-covariance, σ_{xy}, for images x and y is given as;

$$\sigma_{xy} = \frac{1}{M} \sum_{i=1}^{M} (x_i - \mu_x)(y_i - \mu_y) \tag{4.12}$$

SSIM has a maximum value of 1 and this is only possible when the two images are alike. Also, since the three components are quite autonomous, a change in contrast or luminance has minimal effect on the image structure. (Kaur *et al*, 2012). Finally, a map

of quality for the image that carries additional data regarding the degradation extent can be produced by applying the SSIM index locally.

c) Coefficient of Correlation

Karl Pearson (1895) defined the Pearson correlation coefficient γ. This coefficient is extensively used in imaging, statistical analysis and in identifying patterns (Kaur *et al,* 2012). The normalized cross-correlation (NCC) used for finding matches between two images is written mathematically as;

$$\gamma = \frac{\sum_i (x_i - x_m)(y_i - y_m)}{\sqrt{\sum_i (x_i - x_m)^2}\sqrt{\sum_i (y_i - y_m)^2}} \tag{4.13}$$

where;

x_i represents native image pixel values,

y_i represents mask pixel values,

x_m and y_m are mean pixel values of original image and mask respectively

The NCC summarizes the assessment of 2-D images by a single scalar value, γ. Also, since NCC is unmoved by uniform variations in contrast across the image. In contrast, the coefficient of correlation is computationally intensive limiting its usefulness to image registration. If one image has uniform intensity, NCC becomes indeterminate in some practical presentations because of the division by zero.

CHAPTER FIVE

RESULTS AND DISCUSSIONS

This chapter presents the results that were obtained from a series of experiments conducted through computer simulations based on MATLAB. Section 5.1 gives the results obtained using spatial domain image enhancement techniques, while section 5.2 gives the results which were obtained using wavelet frequency domain enhancement techniques. Section 5.3 gives the results from the standard weld images obtained from Kenya Bureau of Standards. Finally, section 5.4 gives a comparison of the image enhancement technique results using the PSNR, the SSIM and the subjective measures discussed earlier. A total of forty four images and fifteen templates were used in conducting the simulations.

5.1 Spatial Domain Enhancement Results

Computer simulation results of tests performed in the spatial domain are presented in this section.

5.1.1 Contrast stretching

a) Linear contrast stretching

Figures 5.1 and 5.2 show the results of contrast stretching enhancement of two different gray-scale images. The linear contrast stretching method used is as discussed in section 3.2.1. The images presented in Figures 5.1(b) and 5.2(b) are the results of using linear contrast stretching method on the original images. These results have better contrast compared to the native images in Figures 5.1(a) and 5.2(a). Here the available pixels have been stretched to fit into the entire available pixel range. This improvement in contrast is indicated by the ease with which defects are recognised in the enhanced images compared to the original images.

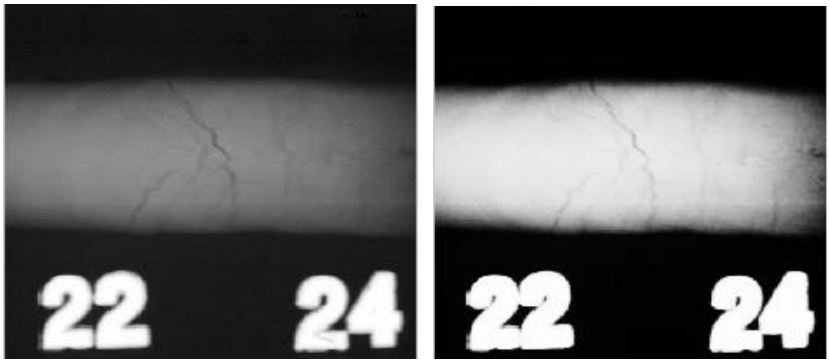

a) b)

Figure 5.1: Contrast stretching results (a) Native image (b) Enhanced image

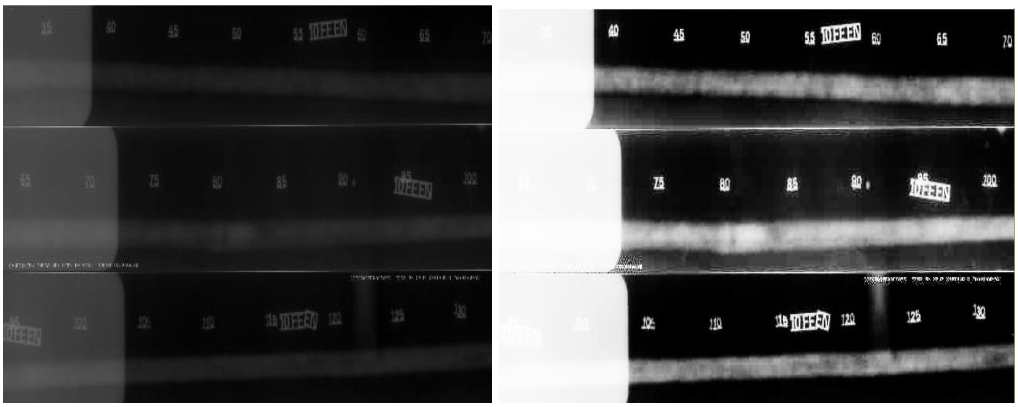

a) b)

Figure 5.2: Contrast stretching results (a) Native image (b) Enhanced image

b) Linear Negative Transformation

Figures 5.3 and 5.4 show the results of using linear negative transformation on gray-scale images. Figures 5.3(a) and 5.4(a) are the original images while Figures 5.3(b) and 5.4(b) are the enhanced images using negative transformation. This reverses the effect of the linear contrast stretching by making lighter pixels become dark and the darker picture becomes lighter. This technique is particularly suitable for improving white details that are fixed in dominant dark areas of the image. Although the visual content is similar in both images of Figures 5.3 and 5.4, it is much easier to analyse the defects in the negative images.

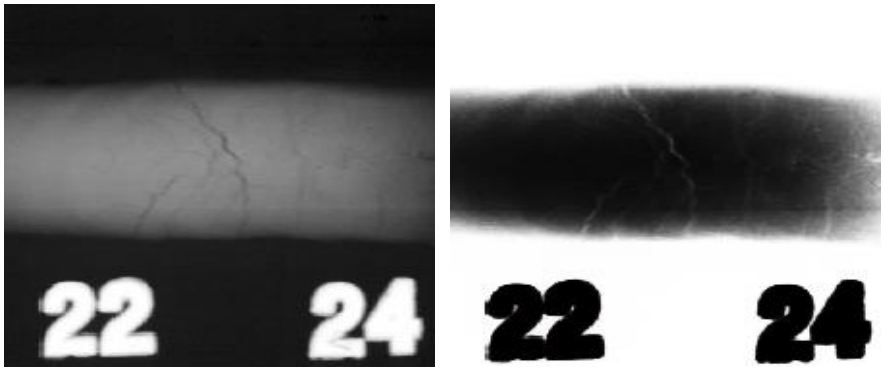

a) b)

Figure 5.3: Linear negative transformation. (a) Native image. (b) Enhanced image.

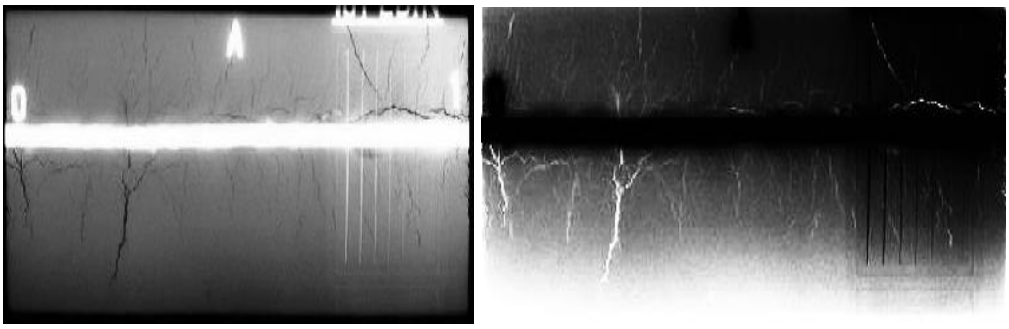

a) b)

Figure 5.4: Linear negative transformation. (a) Native image. (b) Enhanced image.

c) Logarithmic Transformation

Figures 5.5 and 5.6 show the results of using logarithmic transformation on gray-scale images. The darker image pixels are expanded while the lighter image pixels are compressed. The images presented in Figures 5.5(b) and 5.6(b) are the results of applying logarithmic transformation on Figures 5.5(a) and 5.6(a) which are the original images and these results have better contrast compared to the original images. The value of the positive constant used is 5.

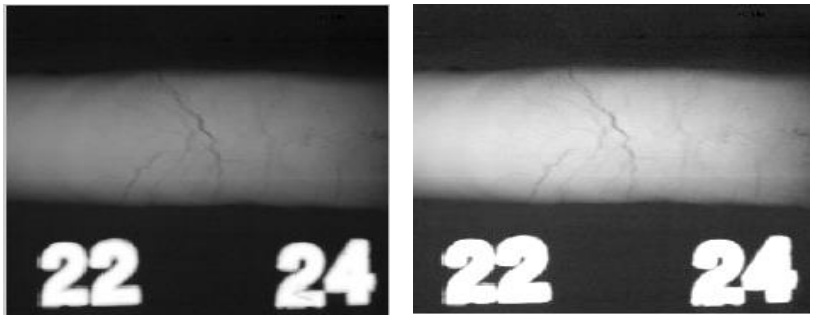

a) b)

Figure 5.5: Logarithmic transformation (a) Native image (b) Resultant image

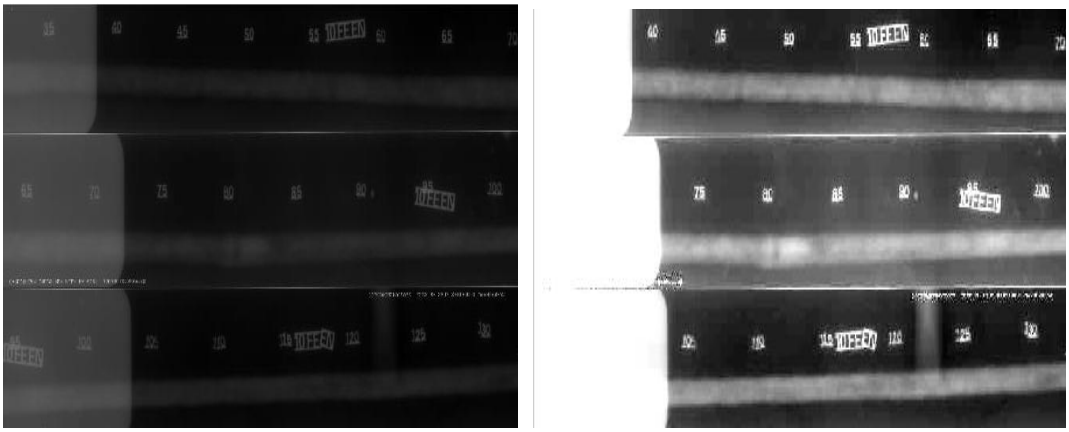

a) b)

Figure 5.6: Logarithmic transformation (a) Native image (b) Resultant image

5.1.2 Histogram Equalization

The main histogram equalization techniques that were used in image enhancement are the Classical Histogram Equalization (CHE) technique, the Adaptive Histogram Equalization (AHE) technique, the Recursive Mean-Separate Histogram Equalization (RMSHE) technique, the Brightness Preserving Bi-Histogram Equalization (BPBHE) technique and the Dynamic Histogram Equalization (DHE) technique. Their results are illustrated here.

a) Classical Histogram Equalization

Figure 5.7 displays the result of applying the Classical Histogram Equalization (CHE) function on a gray-scale image. Figure 5.7(b) shows the result which have altered the image brightness of the original image, Figure 5.7(a), significantly, and has flooded the output image with bright or dark intensity values. This technique therefore affects the visual quality of processed image making it unsatisfactory and leads to loss of contrast.

Also it does not preserve image brightness. Figure 5.7(c) and 5.7(d) shows the image histograms of the native and enhanced images respectively.

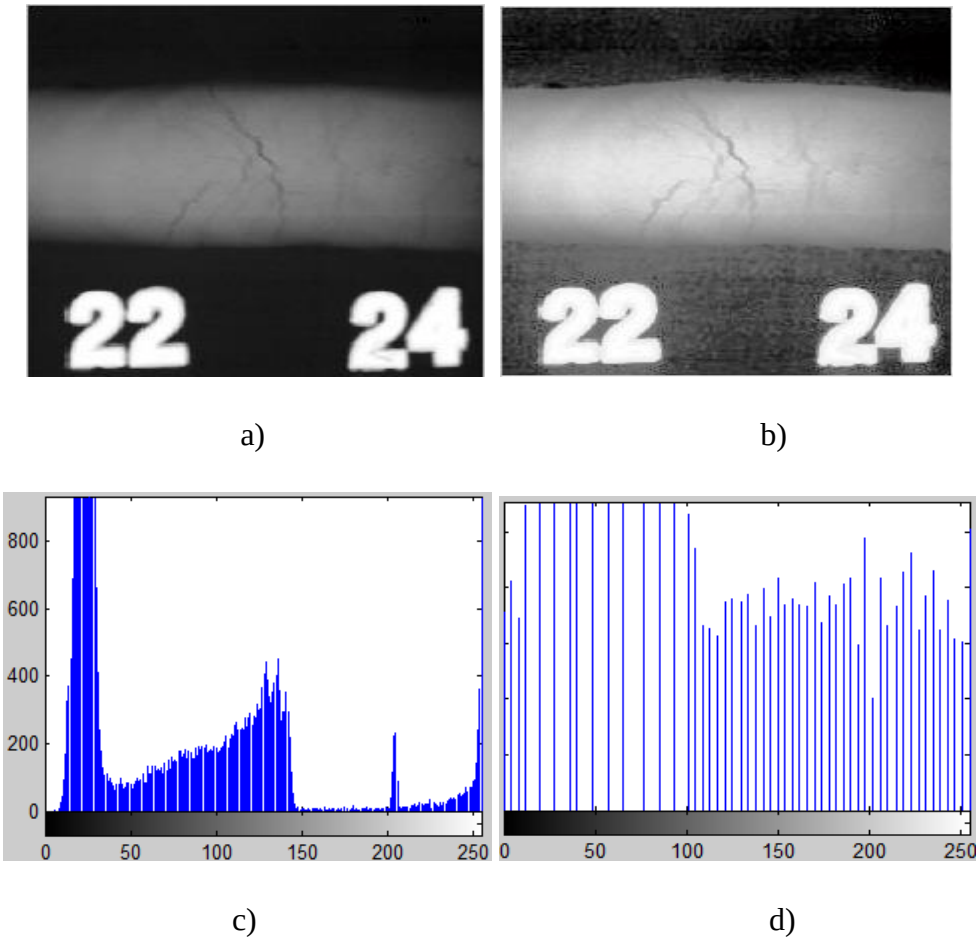

Figure 5.7: CHE results. (a) Native image. (b) CHE enhanced image. (c) Native image histogram (d) CHE image histogram.

b) Adaptive Histogram Equalization

The result of applying Adaptive Histogram Equalization (AHE) function on a gray-scale image is displayed on Figure 5.8. This technique improves the contrast of the image neighbourhood and conveys more details than the CHE. In addition, this technique spreads the histogram systematically and close to the original image histogram. Therefore, it does not add unnecessary artifacts to the output image. Figure 5.8(a) indicates the native image while Figure 5.8(b) is the enhanced result. Also Figure 5.8(c) indicates the original image histogram while 5.8(d) shows the enhanced image histogram.

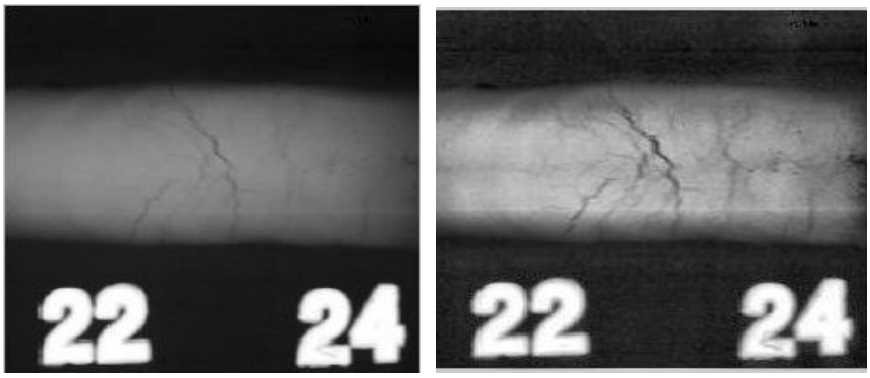

a) b)

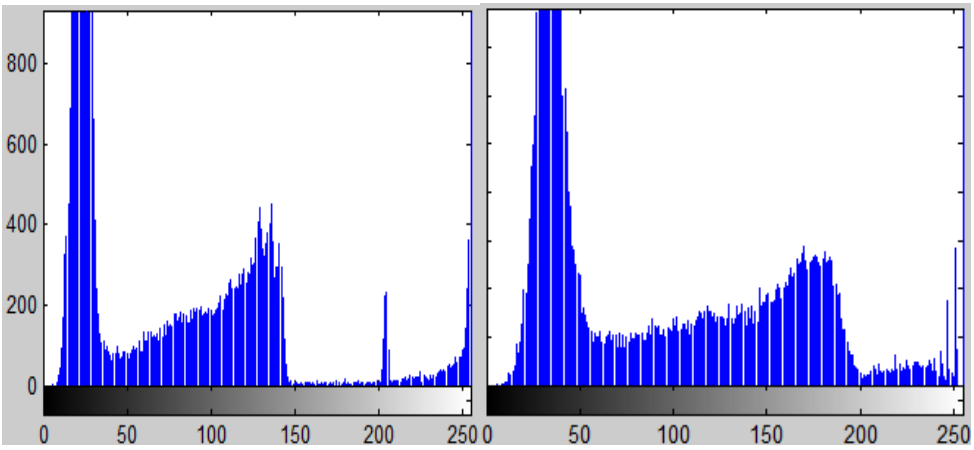

c) d)

Figure 5.8: AHE results. (a) Native image. (b) AHE enhanced image. (c) Native image histogram. (d) AHE image histogram.

c) Brightness Preserving Bi-Histogram Equalization

Figures 5.9 and 5.10 show the result of applying the Brightness Preserving Bi-Histogram Equalization (BPBHE) function on two gray-scale images. As can be noted from the outputs in Figures 5.9 (b) and 5.10 (b), this procedure conserves mean brightness of an image considerably well in comparison to CHE. In addition, there are no major changes on the resultant histograms but they are stretched out uniformly on the entire range as shown on Figures 5.9 (d) and 5.10(d) as compared to Figures 5.9 (c) and 5.10(c).

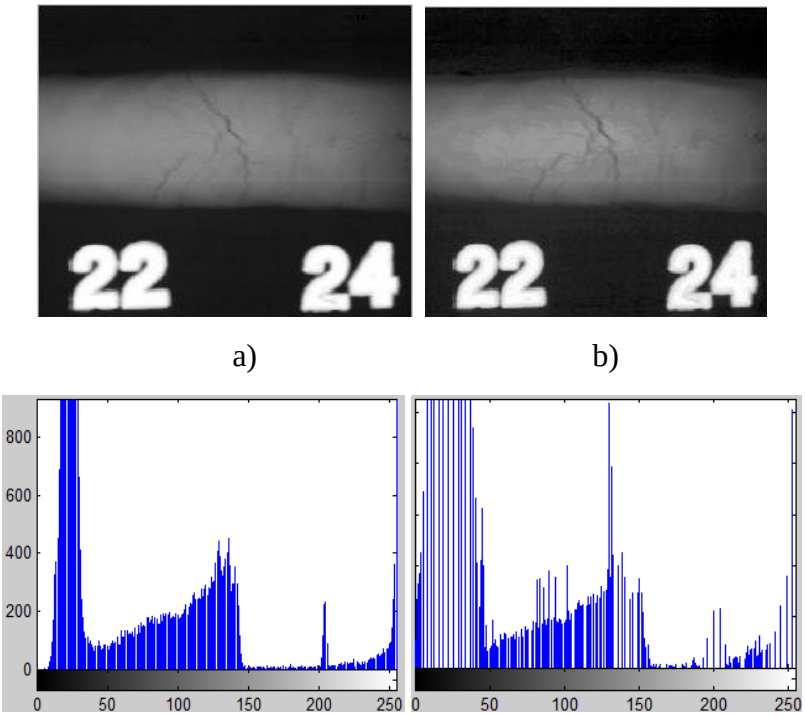

Figure 5.9: BPBHE results. (a) Native image. (b) BPBHE enhanced image. (c) Native image histogram. (d) BPBHE histogram.

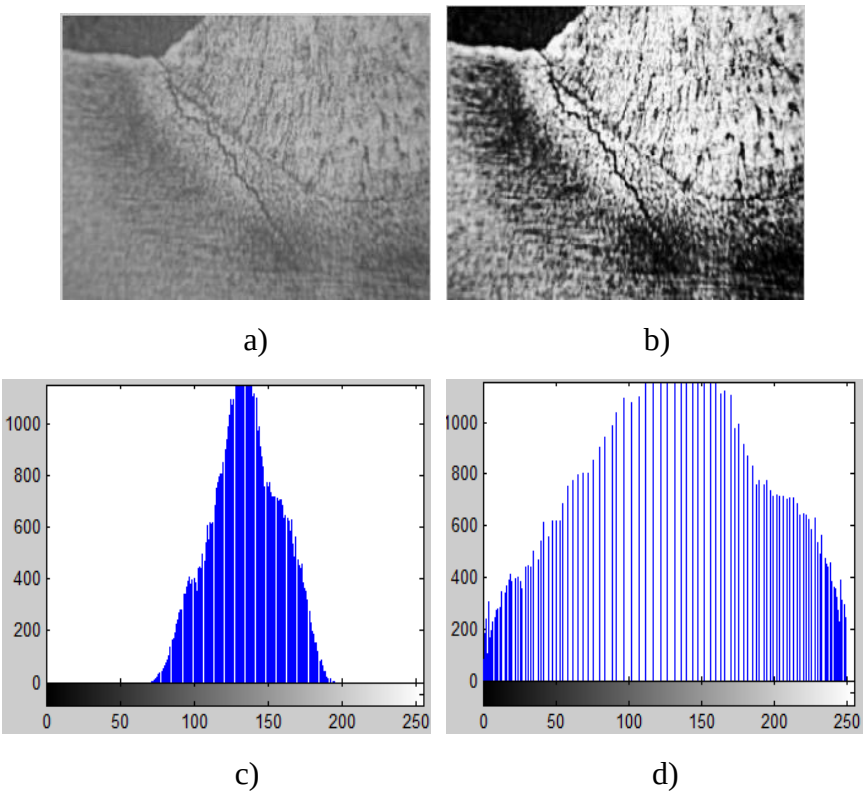

Figure 5.10: BPBHE results. (a) Native image. (b) BPBHE enhanced image. (c) Native image histogram. (d) BPBHE histogram.

d) Recursive Mean-Separate Histogram Equalization

Figures 5.11 and 5.12 show the result of applying the Recursive Mean-Separate Histogram Equalization (RMSHE) function on two gray-scale images, Figures 5.11(a) and 5.12(a). Due to the fact that this technique uses multi-separation of the histogram, it is in a position to achieve virtuous brightness preservation. This clearly outlines the defects as presented in Figures 5.11(b) and 5.12(b) as compared to 5.11(a) and 5.12(a). Also, the resultant histograms are presented in Figures 5.11(d) and 5.12(d).

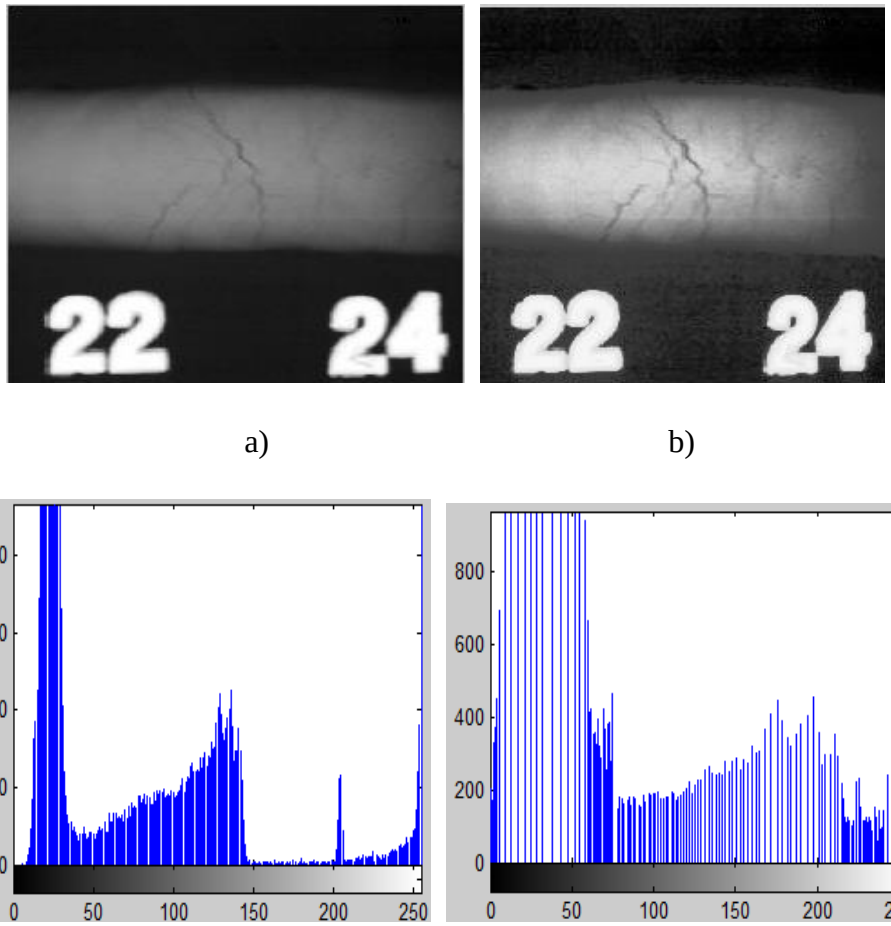

a) b)

c) d)

Figure 5.11: RMSHE results. (a) Native image. (b) RMSHE enhanced image. (c) Native image histogram. (d) RHSHE histogram.

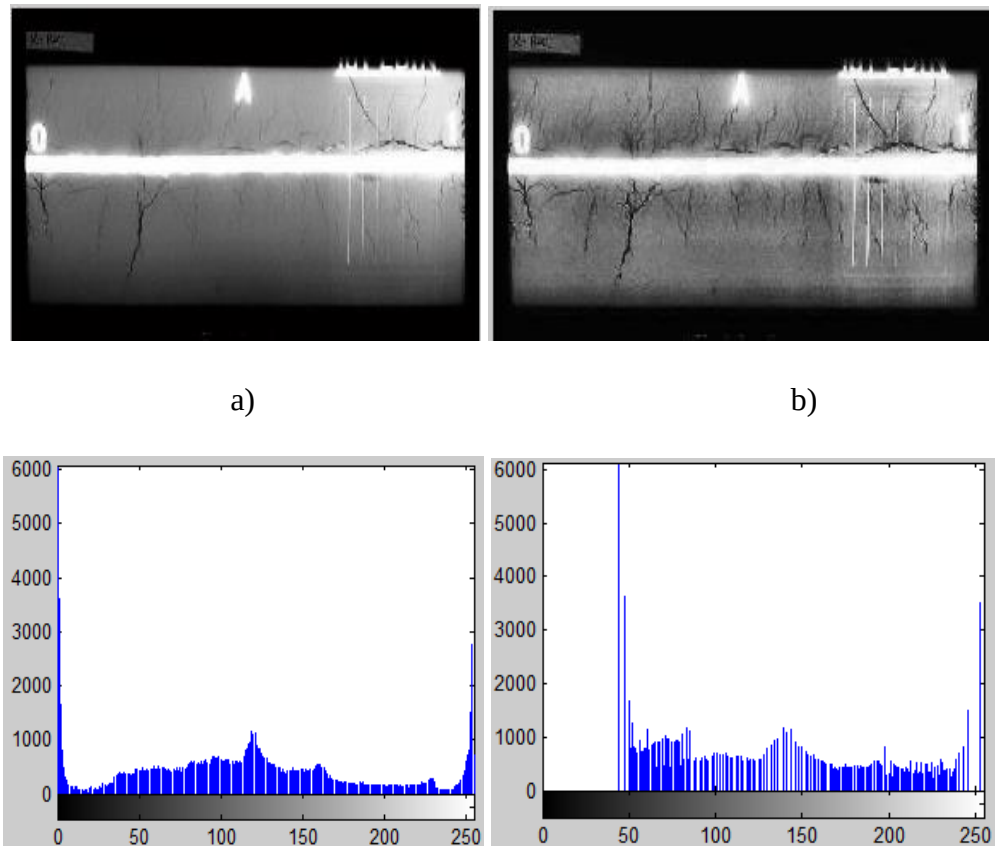

Figure 5.12: RMSHE results. (a) Native image. (b) RMSHE enhanced image. (c) Native image histogram. (d) RHSHE histogram.

e) Dynamic Histogram Equalization

Figure 5.13 presents the results of applying the Dynamic Histogram Equalization (DHE) function on a gray-scale image, Figure 5.13(a). This method preserves the image details well and does not have any severe side effects as shown in the output image of 5.13(b). This technique eliminates the dominance of upper histogram constituents on lower histogram constituents and it's able to control the extent of gray-level stretching for rational image features enhancement as presented in Figure 5.13(d) in comparison to 5.13(c).

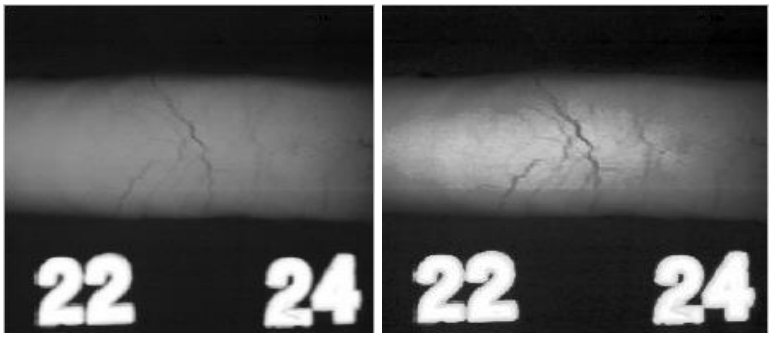

a) b)

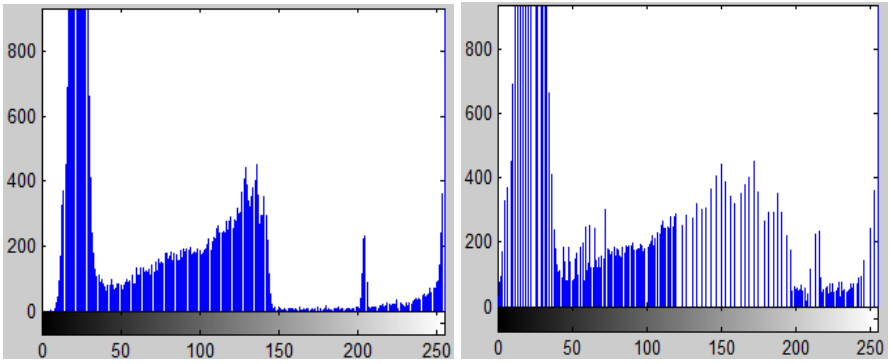

c) d)

Figure 5.13: DHE results. (a) Native image. (b) DHE enhanced image. (c) Native image histogram. (d) DHE image histogram.

5.1.3 Spatial filtering

Figures 5.14 and 5.15 show the results of performing spatial filtering by using unsharp masking to sharpen the edges of an image. Sharpness makes image edges clear and distinct without adding any artifacts or noise to the image. The images in Figures 5.14(a) and 5.15(a) are input images, while the results in Figures 5.14(b) and 5.15(b) are the sharpened images using the unsharp mask filter. The resultant images have their edges, points and thin lines clearly highlighted.

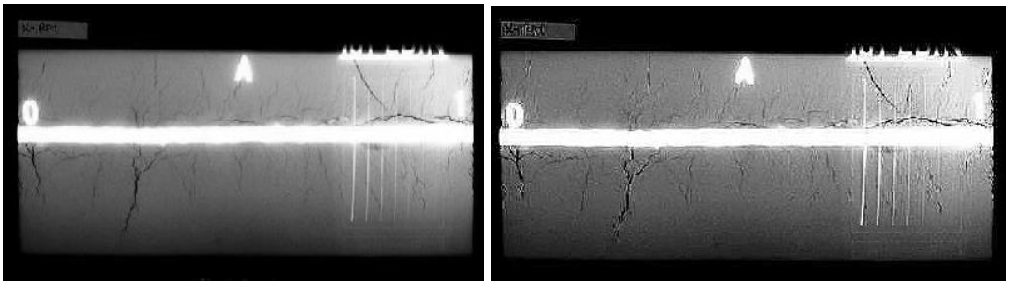

a) b)

Figure 5.14: Edge sharpening. (a) Native image. (b) Unsharp mask sharpening result.

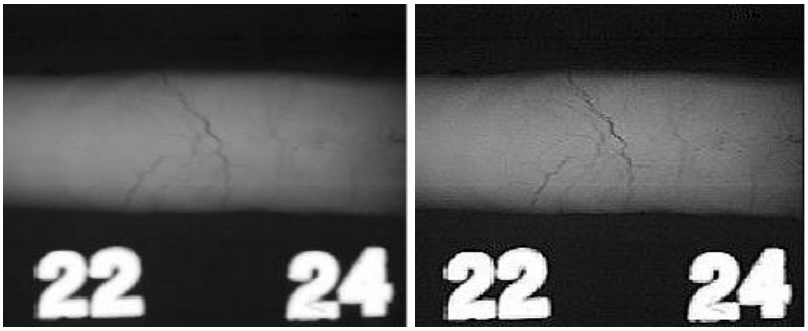

a) b)

Figure 5.15: Edge sharpening. (a) Input image. (b) Unsharp mask sharpening result.

5.1.4 Image Segmentation

a) Otsu's Thresholding

Otsu's thresholding performs automatic clustering-based image segmentation. This reduces gray-level images to binary images as shown below. Figures 5.16(a) and 5.17(a) are the original images while Figures 5.16(b) and 5.17(b) show the results after applying Otsu's thresholding. This techniques clears shows the background, and preserves all the thin details which are of interest. This helps in extracting detail points during the feature extraction process.

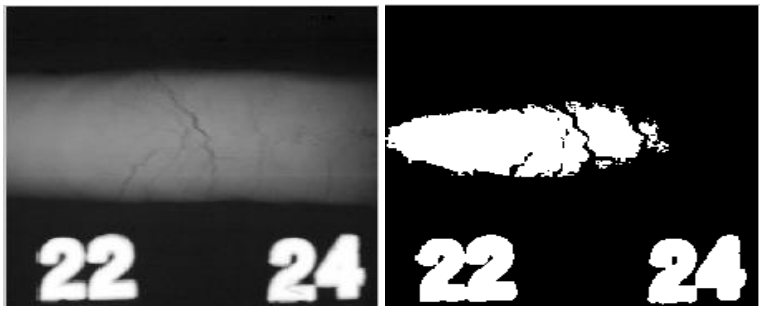

a) b)

Figure 5.16: Otsu's results. (a) Native image. (b) Resultant image

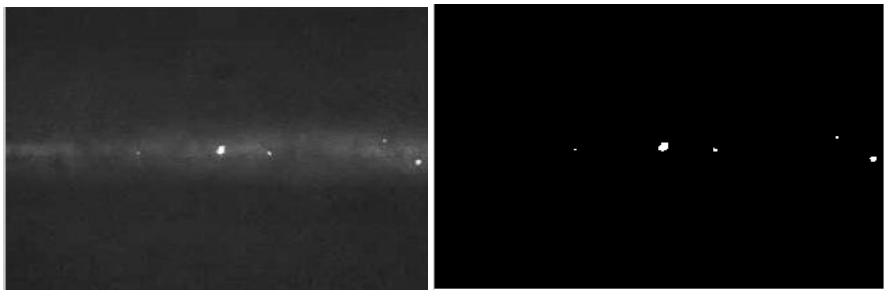

a) b)

Figure 5.17: Otsu's results. (a) Native image. (b) Resultant image

a) Percolation Thresholding

Percolation thresholding is related to percolation theory, which describes the behaviour of connected clusters. The identified defects are detected by using connectivity of the surrounding binary images. This method detects defects not only in the enhanced cases but also in noisy cases. The results of using percolation thresholding on original images, Figures 5.18(a) and 5.19(a), are presented in 5.18(b) and 5.19(b).

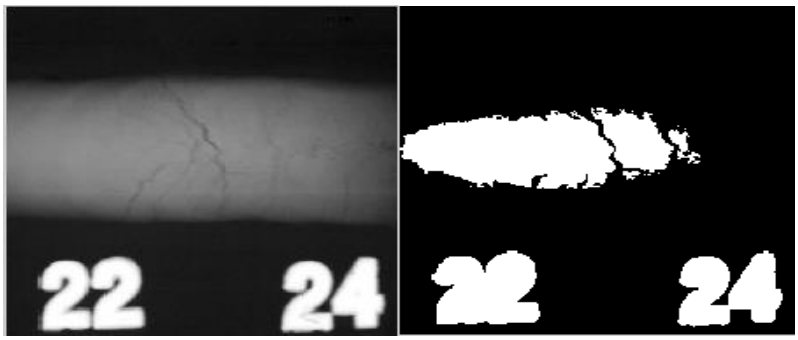

a) b)

Figure 5.18: Percolation results. (a) Native image. (b) Resultant image

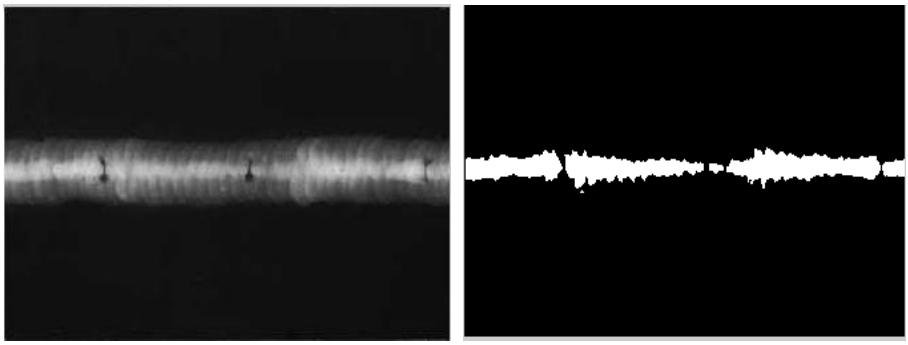

a) b)

Figure 5.19: Percolation results. (a) Native image. (b) Resultant image

5.1.5 Automatic Defect Detection

There is an agreement that manual inspection of defects is not consistent and lack reliability. This hinders its application in preventive maintenance. As such, an automatic defect detection technique has been developed to help solve this problem. This development has improved the performance in the detection rate, the detection accuracy and the detection efficiency.

a) Control experiment

Six images without defects were used as control experiments to test the proposed algorithm. Out of these, one image was selected as shown in Figure 5.20(a) and several templates (with faults such as pores and cracks) were presented as in Figures 5.20(b), 5.20(c) and 5.20(d) were passed over it to try and obtain regions of similar defects by using image correlation. The templates used were from different locations or images and not from the main images. This was done so as to achieve template independence. After passing all the templates over the original image, the results in Figures 5.20(e), 5.20(f) and 5.20(g) were obtained. These results show that no defect were identified.

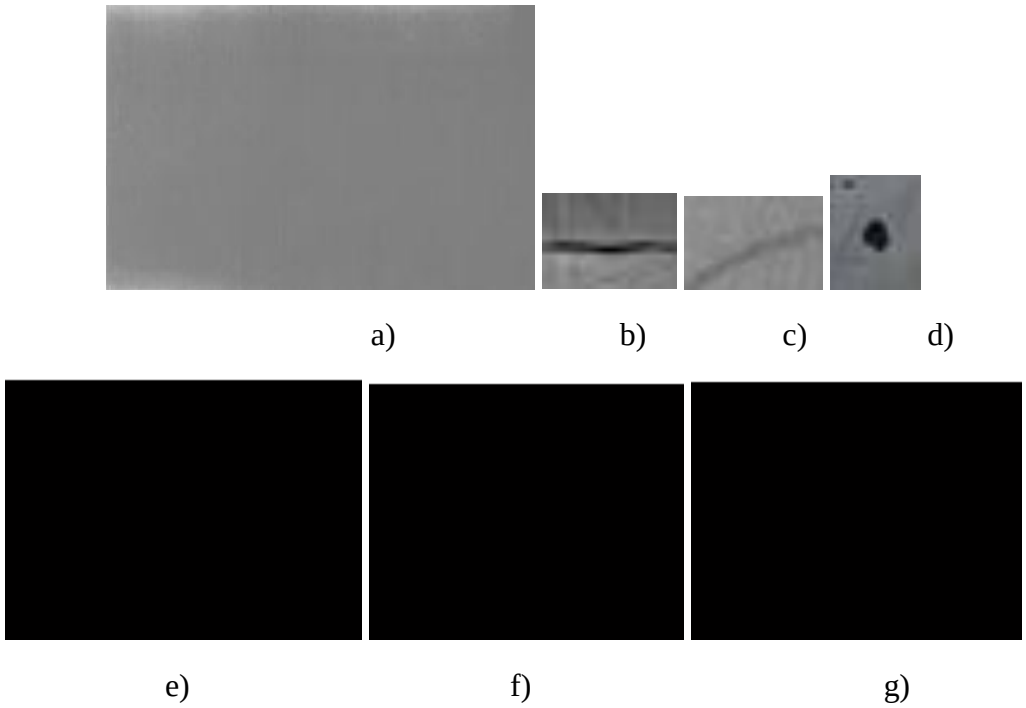

Figure 5.20: Control experiment results (a) Native image. (b) Horizontal crack template. c) Lateral crack template (d) Pore template (e) Horizontal template result (f) Lateral template result (g) Pore template result

A defect analysis and interpretation algorithm was developed. This was implemented by using the Coefficient of Correlation (CoC). A series of experiments have shown a threshold of 0.7 to be suitable. This is higher than the critical threshold required for percolation to occur (Sukop *et al.*, 2002). Also, a value of 0.7 eliminates unnecessary thresholded information as proved after several experiments. For the control experiment, the following was obtained.

```
>>
If maxValue (CoC) is > 0.70, there is a defect
Results
******************
First Template
There is no defect
******************
Second Template
There is no defect
******************
Third Template
There is no defect
>>
```

b) Metal crack

Eighteen metal crack images were used in the process of testing the applicability of the proposed algorithm. Out of these, two images have been discussed. The first is a metal image with a cracks as shown in Figure 5.21(a). Two templates (with defects) as presented in Figure 5.21(b) and 5.21(c) were passed over it in order to identify regions of similar defects by using correlation. The results in Figure 5.21(d) and 5.21(e) were obtained indicating the presence of a defect.

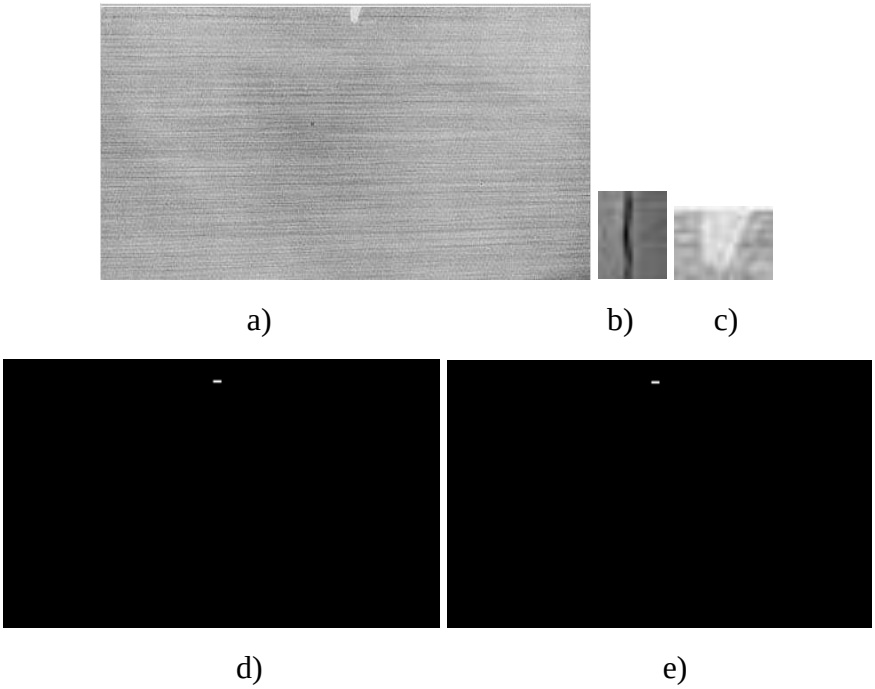

Figure 5.21: Metal crack results. (a) Native image (b) Vertical crack template (c) Pore crack template (d) Vertical template result (e) Pore template result

From the developed algorithm, the following results were displayed on the screen.

```
>>
If maxValue (CoC) is > 0.70, there is a defect
Results
*************
First Template
There is a defect
*************
Second Template
There is a defect
>>
```

The second metal image with a cracks is presented in Figure 5.22(a). Two templates as indicated in Figure 5.22(b) and 5.22(c) were passed over it in order to identify regions of similar defects using correlation. The results in Figure 5.22(d) and 5.22(e) were obtained indicating that Figure 5.22(b) did not identify any defect but Figure 5.22(c) identified.

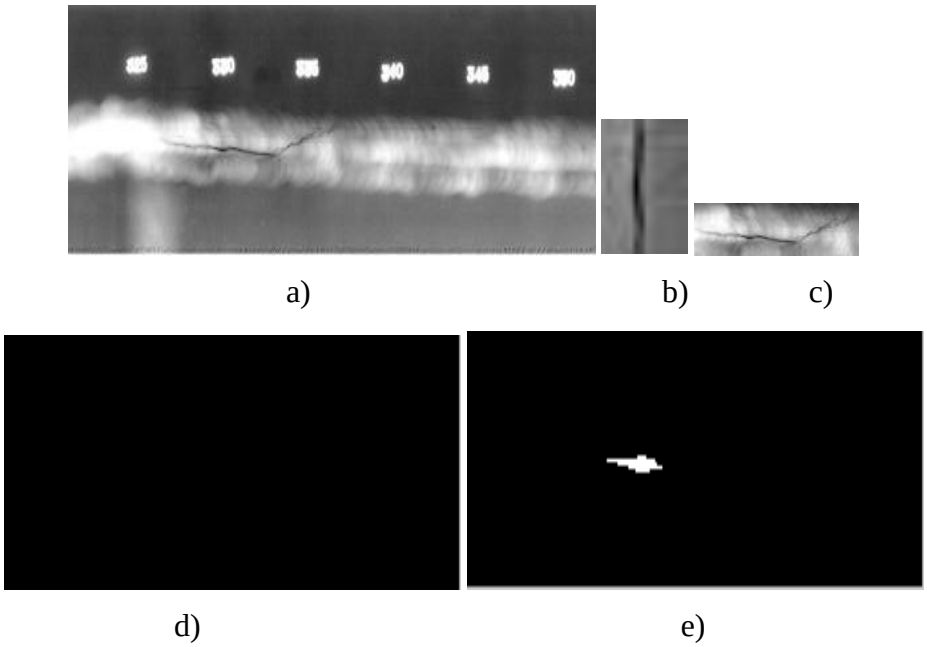

a) b) c)

d) e)

Figure 5.22: Second Metal crack results. (a) Native image (b) Vertical template crack (c) Horizontal template crack (d) Vertical template result (e) Horizontal template result

From the developed algorithm, the following results were displayed on the screen.

```
>>
If maxValue (CoC) is > 0.70, there is a defect
Results
*************
First Template
There is no defect
*************
Second Template
There is a defect
```

c) Weld Pore

Twenty weld pore images were used in the process of testing the applicability of the proposed algorithm. Out of these, two images have been discussed and their results presented. The first is a weld pore image with a defect as presented in Figure 5.23(a). Two templates as presented in Figure 5.23(b) and 5.23(c) were passed over it in order to identify regions of similar defects by using correlation. The results in Figure 5.23(d) and 5.23(e) were obtained indicating the presence of defects.

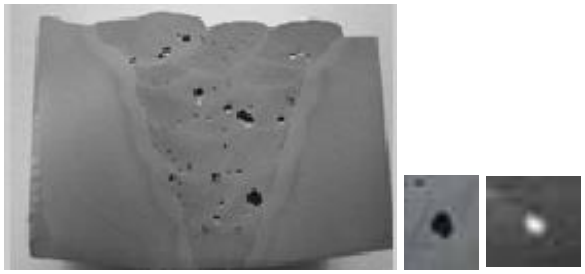

a) b) c)

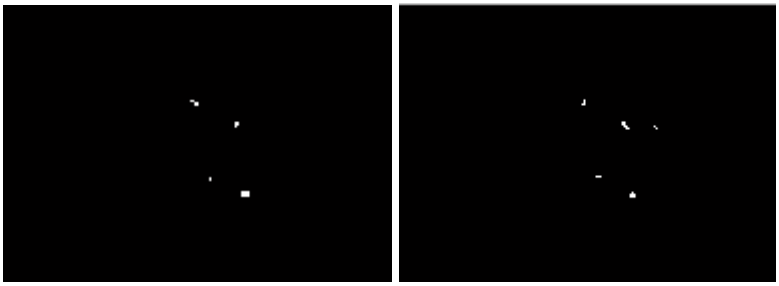

d) e)

Figure 5.23: Weld pore results. (a) Native image (b) Pore 1 template (c) Pore 2 template (d) Pore 1 result (e) Pore 2 result

From the developed algorithm, the following results were displayed on the screen.

```
>>
If maxValue (CoC) is > 0.70, there is a defect
Results
**************
First Template
There is a defect
**************
Second Template
There is a defect
>>
```

The second was a weld image with a defect of a slag inclusion as presented in Figure 5.24(a). Two templates Figure 5.24(b) and 5.24(c) were passed over it in order to identify regions of similar defects by using correlation. The results in Figure 5.24(d) and 5.24(e) were obtained. These results indicates the presence of defects.

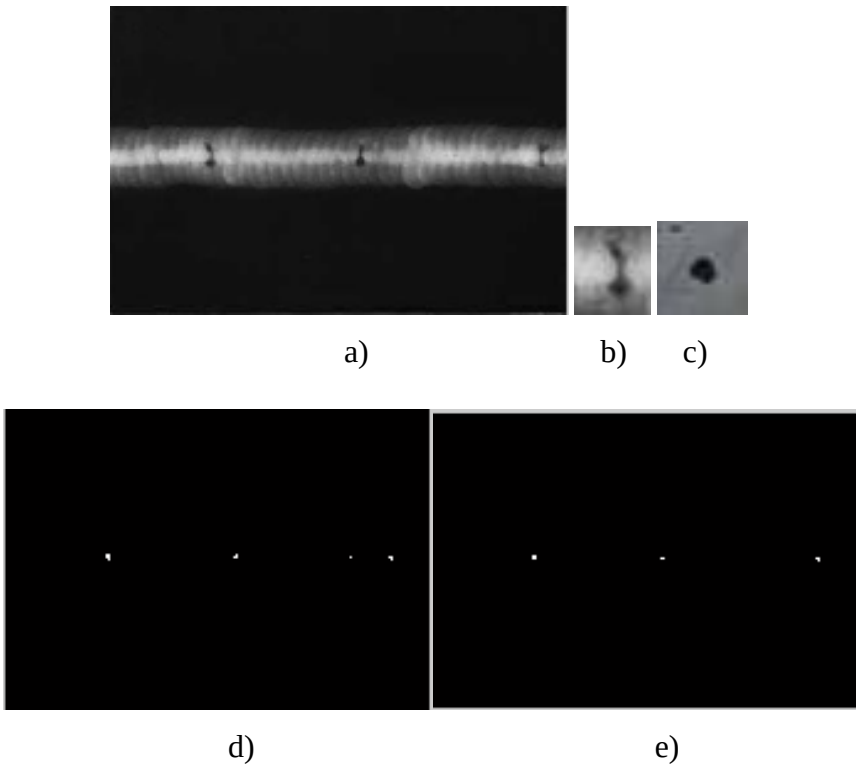

a) b) c)

d) e)

Figure 5.24: Slag inclusion results. (a) Native image (b) Slag template (c) Pore template (d) Slag results (e) Pore results

From the developed algorithm, the following results were displayed on the screen.

```
>>
If maxValue (CoC) is > 0.70, there is a defect
Results
*************
First Template
There is a defect
*************
Second Template
There is a defect
>>
```

d) Template addition

Two templates, Figure 5.25(b) and 5.25(c), were added as shown in Figure 5.25(d) and then passed over the original image to try and identify detect on the original image,

Figure 5.25(a). The outcomes in Figure 5.25(e), 5.25(f) and 5.25(g) were obtained indicating the presence of a defect on the original image. Figure 5.25(g) clearly shows that addition of templates can identify defects on an image. A total of twelve images were used to test this technique.

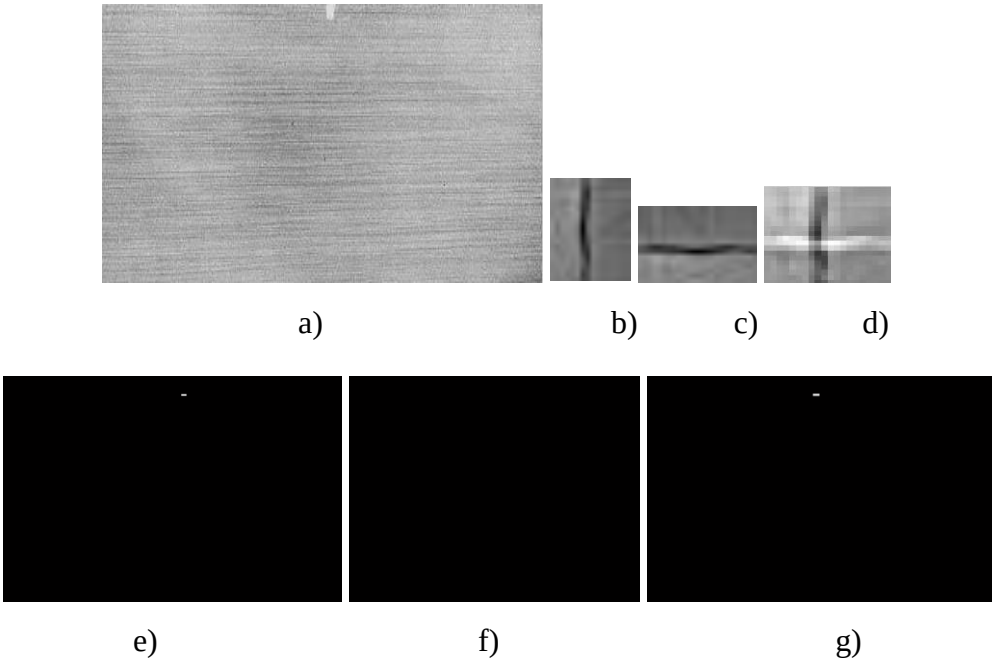

Figure 5.25: Template addition results. (a) Native image (b) Vertical template crack (c) Horizontal template crack (d) Addition of vertical and horizontal templates (e) Vertical template result (f) Horizontal result (g) Addition of (b) and (c) result

From the developed algorithm, the following results were displayed on the screen.

```
>>
If maxValue (CoC) is > 0.70, there is a defect
Results
**********
First Template
There is a defect
**********
Second Template
There is no defect
**********
Third Template
There is a defect
>>
```

5.2 Frequency Domain Enhancement Results

Here, computer simulation results obtained using wavelet transforms are presented.

5.2.1 Image Denoising

Image denoising removes noise present in an image and attempts to retain the significant part of the information, notwithstanding the frequency contents of the signal. This was implemented using a Haar wavelet transform technique as it is simple in operation and perfect in reconstruction. Figure 5.26 and 5.27 shows the result of applying Haar wavelet on gray-scale images. The results in Figures 5.26(b) and 5.27(b) display the de-noised images while Figure 5.26(a) and Figure 5.27(a) are the original gray-scale images

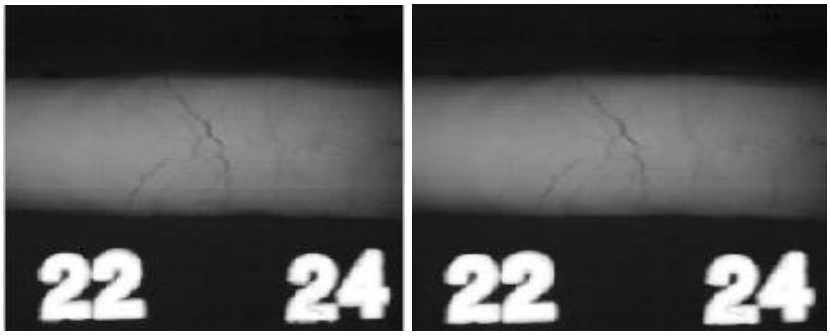

a) b)

Figure 5.26: Haar de-noised results. (a) Native image. (b) Resultant image.

a) b)

Figure 5.27: Haar de-noised results. (a) Native image. (b) Resultant image.

5.2.2 Edge Detection

The effects of applying the Canny's edge detection algorithm on gray-scale images is shown in Figures 5.28 and 5.29. Figures 5.28(a) and 5.29(b) presents the gray-scale input images. Figure 5.28(b) and 5.28(c) shows the outputs of AHE and CHE, while those in Figure 5.29(b) and 5.29(c) are the outputs of DHE and RMSHE respectively. The edges detected are presented in Figure 5.28(d), 5.28(e) and 5.28(f) for the Figure 5.28(a), and Figure 5.29(d), 5.29(e) and 5.29(f) for Figure 5.29(a).

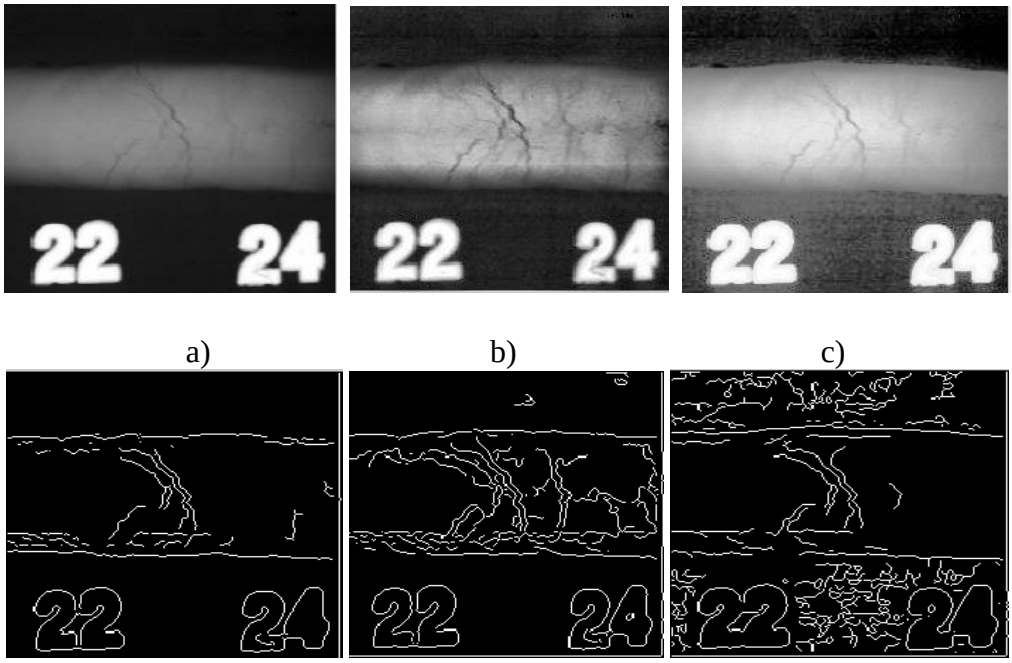

a) b) c)

d) e) f)

Figure 5.28: Canny results. (a) Native image. (b) AHE image. (c) CHE image. (d) Native image edges (e) AHE edges (f) CHE edges

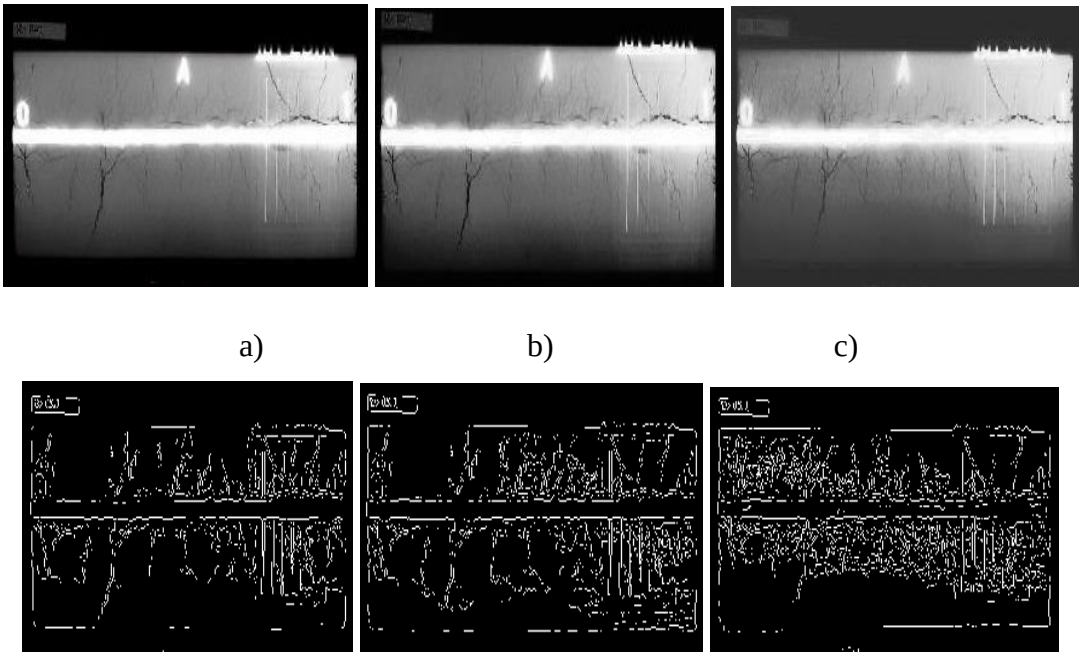

a) b) c)

d) e) f)

Figure 5.29: Canny results. (a) Native image. (b) DHE image (c) RMSHE image. (d) Native edges (e) DHE edges (f) RMSHE edges

5.3 Imaging Standardization

To test the efficacy of the algorithm proposed, six standard welded pipes with defects were obtained from Kenya Bureau of Standard (KEBS). This regulator prepares standards relating to various products. The pipes were X-rayed using the machines from Quality Inspectors Limited and the images obtained were enhanced using the above discussed techniques. The results obtained compared very well with those discussed from Quality Inspector Limited and from the internet.

For example, Figure 5.30(a) presents one of the images obtained from KEBS. It has been enhanced using RMSHE to obtain Figure 5.30(b). The histograms of the native and enhanced images are in Figure 5.30(c) and 5.30(d) respectively. This technique spreads out the histograms uniformly.

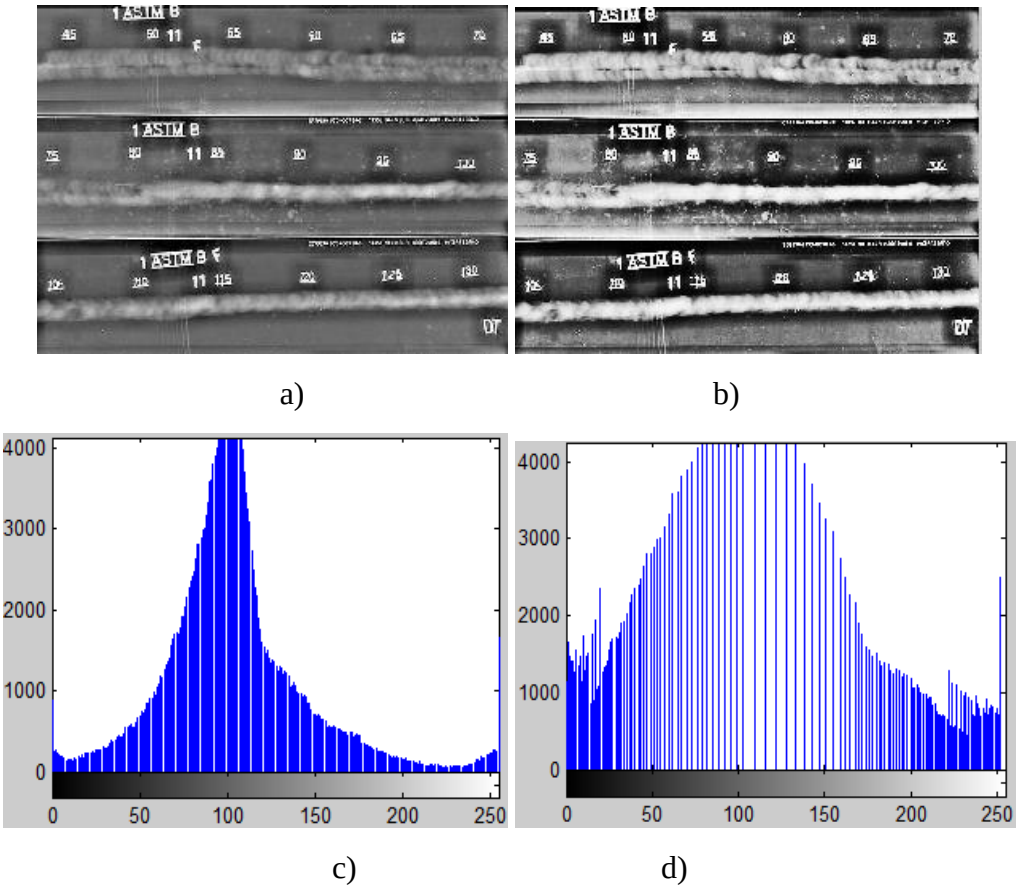

Figure 5.30: KEBS image1. (a) Native image. (b) RMSHE enhanced image. (c) Native image histogram. (d) RMSHE histogram.

Also, Figure 5.31(a) displays a second image gotten from KEBS. It has been enhanced using Adaptive Histogram Equalization (AHE) to obtain Figure 5.31(b). This has improved the neighbourhood contrast.

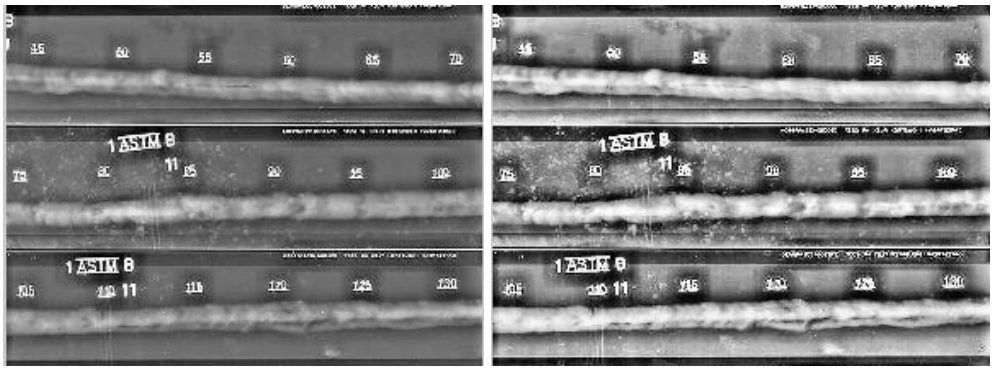

a) b)

Figure 5.31: KEBS image2. (a) Native image. (b) AHE enhanced image.

5.4 Performance Test Results

5.4.1 Subjective measurements

The subjective test was performed using twenty observers who were asked to choose the best output image from amongst the outputs of the five enhancement techniques discussed. These were CHE, AHE, DHE, RMSHE and BPBHE. Subjective scales that were evaluated included contrast, sharpness and image distortion. The subjective assessment results are given in Table 5.1. For example, the tabulated data shows that 14 observers preferred images enhanced using AHE and RMSHE in terms of image sharpness, while only 1 observer chose the result of the CHE based technique. Out of the 20 observers, 13 of them said that the CHE technique added distortion to the original image. In regard to background brightness preservation, the BPBHE and RMSHE had the support of 15 observers.

Table 5.1: Subjective analysis results

Scales evaluated	**CHE**	**AHE**	**RMSHE**	**BPBHE**	**DHE**
Contrast	3	7	8	0	2
Sharpness	1	8	6	2	3
Background preservation	0	2	7	8	3
Distortion	13	3	1	0	3

Subjective testing was also applied between Otsu's thresholding and percolation thresholding. Of the 20 observers interviewed, 14 of the correspondent preferred Otsu's to percolation thresholding. They observed that Otsu's technique displayed more results from the binarized image as compared to percolation based technique.

5.4.2 Objective measurements

Objective tests use mathematical analysis in their comparison. As such they are not subject to human variation. A total of thirty two images were used in this analysis using both the SSIM and PSNR. Table 5.2 compares image enhancement using CHE, AHE, RMSHE, BPBHE and DHE by using the PSNR technique. If the results have a higher PSNR value, then the enhanced image and the original image are closer in resemblance and the enhanced image has not changed so much from the original image and background brightness has been preserved. From Table 5.2, the BPBHE technique has the overall highest value of PSNR at 32.91 dB while CHE has the lowest PSNR at 6.31 dB.

Table 5.2: Objective analysis results using PSNR

Objective Technique	**PSNR (dB)**				
Images used	**CHE**	**AHE**	**RMSHE**	**BPBHE**	**DHE**
QIL WELD 1	7.56	17.21	13.00	30.60	16.10
QIL WELD 3	6.31	18.38	12.71	28.91	14.82
QIL WELD 4	19.91	16.55	22.45	30.06	23.35
CRACK 2	12.89	20.16	19.54	32.91	25.48
CRACK 3	13.74	18.23	24.11	14.36	18.12
PIPE 1	13.94	20.50	18.67	27.98	31.58
SLAG INCLUSION	7.52	21.39	22.06	29.33	20.64
WELD 7 CRACK	7.45	18.95	20.63	25.05	17.61
KEBS IMAGE 1	14.30	17.53	14.82	20.44	22.55
KEBS IMAGE 2	14.65	16.39	16.24	19.03	23.50

Table 5.3 compares image enhancement using CHE, AHE, RMSHE, BPBHE and DHE by using the Structural Similarity Image Metric (SSIM) technique. The highest value of

SSIM is unity and is obtained when the compared images are similar. From Table 5.3, the BPBHE seems to have the highest SSIM value at 0.98. This shows that the enhanced image is almost akin to the original image. The CHE technique has the lowest SSIM value at 0.24. This indicates that CHE changed the structural information of the image more than the other techniques.

Table 5.3: Objective analysis results using SSIM

Objective Technique	**SSIM**				
Images used	**CHE**	**AHE**	**RMSHE**	**BPBHE**	**DHE**
QIL WELD 1	0.40	0.70	0.80	0.96	0.90
QIL WELD 3	0.24	0.70	0.52	0.87	0.68
QIL WELD 4	0.88	0.88	0.90	0.98	0.93
CRACK 2	0.66	0.82	0.82	0.93	0.93
CRACK 3	0.51	0.59	0.87	0.55	0.73
PIPE 1	0.64	0.67	0.68	0.74	0.89
SLAG INCLUSION	0.30	0.89	0.90	0.92	0.94
WELD 7 CRACK	0.30	0.82	0.85	0.90	0.89
KEBS IMAGE 1	0.58	0.73	0.59	0.78	0.90
KEBS IMAGE 2	0.68	0.75	0.69	0.76	0.94

Table 5.4 compares images de-noised using Haar wavelet transform by using the PSNR and the SSIM techniques. Seventeen images were used in testing the suitability of the techniques proposed. From Table 5.4 both objective technique seems to have higher value than when the image is enhanced (comparing with Tables 5.2 and 5.3). This is because de-noising an image does not change the image pixels significantly as compared to image enhancement. For example, weld 1 crack has a PSNR value of 77.76 dB and SSIM value of 0.998.

Table 5.4: Image de-noising results for quality measurement using PSNR and SSIM

Images	**PSNR (dB)**	**SSIM**
CRACK 1	42.63	0.986
CRACK 2	52.03	0.988
PIPE 1	66.01	0.998
QIL WELD 3	46.17	0.978
WELD 1 CRACK	77.76	0.998

The number of experiments performed and the rate of correct defect detections are summarized in Table 5.5. From the table, template addition had the highest rate of defect detection with 10 out of the 12 samples having their defects being identified correctly. This represents an 83.3% of correct defect identification.

Table 5.5: Percentage of correct defect detection

Defect type	**Number of images used**	**Correct defect detected**	**% of correct detection**
Weld spot detection	16	13	81.3%
Crack detection	15	12	80.0%
Slag inclusion	10	9	90.0%
Template addition	12	10	83.3%

CHAPTER SIX

CONCLUSION AND RECOMMENDATIONS

6.1 Conclusion

In this thesis, image enhancement procedures and automatic defect detection technique have been proposed. The enhancement techniques addresses the effects of poor image contrast and noise while the defect detection technique addresses the limitations of manual inspection of defects which include lack of reliability and consistency. Herein, several well-known algorithms for image enhancement have been implemented, investigated and their performance comparatively assessed. These techniques are CHE, AHE, RMSHE, BPBHE and DHE. A technique like CHE does improve the image contrast significantly. However, it adds some undesirable artifacts and washed-out appearances to the image hence amplifying the noise level of the images. The BPBHE technique adds some unnatural look and adds some insignificant enhancement to the resultant image. The RMSHE technique shows good contrast enhancement and aims to bring more extends of brightness preservation than CHE and BBHE techniques. The DHE technique improves the contrast stretching range and precludes minor attributes of the original image from being flooded and then concealed. It also makes sure that each portion of the image obtains moderate contrast. In summary, image enhancement ensures that the output image looks better in appearance and that the mean brightness is preserved.

The usefulness of the proposed algorithms have been illustrated with test results for each of the proposed techniques. Both subjective and objective image quality measurement techniques have been used to compare various methods of image denoising and enhancement.

In automatic defect detection, Otsu's thresholding and percolation model were compared in regard to the connectivity among neighbourhood pixels. Otsu's technique proved to be superior to percolation thresholding through experiments. Other results of the automatic defect detection technique revealed that the method proposed produces reliable results which can be used in industries relying on X-ray images to reduce the effect of errors in detection and to overcome the challenge of always relying on skilled operators to identify defects in an image. The proposed technique relies on "learned" features from the

template image. The accuracy and robustness of the technique can be easily improved by re-training using an extended set of templates.

The prompt and accurate detection of defects has a direct benefit-cost in terms of time saving as well as preventing rejections generated downstream from being generated in large numbers. In addition, automated inspection techniques usage are essential so as to improve the quality of products at each level of production as well as to eliminate the need of human intervention in a hazardous environment. This has a clear benefit in terms of quality assurance.

The Haar wavelet transform is a simple method due to its low computing requirements. It is an efficient tool in image denoising and also helps when extracting high-frequency components from an image. Finally, Haar transformation helps an image to keep its details and sharpness.

6.2 Recommendation

There exists some spaces for future work so as to enhance the performance of the proposed algorithm especially on automatic defect detection. For example, to apply the algorithm to a video sequence, instead of static images, by exploiting the motion information and optical flow in tracking and verifying defects over the image sequence. Also, the study does not cover the identification of cracks in terms of their length or the number of cracks available in a certain cluster. This need to be pursued further.

The SSIM value change when the image is rotated. More work need to be performed to identify the structural changes that occurs when an image is flipped.

Several other issues remain to be addressed. For example, the increasing number of colour digital images is becoming a new challenge for binarization and segmentation. In addition, more work is required in image enhancement so as to identify which specific technique produces superior results for both colour images and gray-scale images.

REFERENCES

Anandakrishnan, N. and, Baboo, S.S., (2014), "A Novel Improved Gradient Noise Tolerant Method for Enhanced Edge Detection" *Journal of Theoretical and Applied Information Technology*, Vol. 66 No.2, pp. (521-532).

Arora, S., Brar, Y. and Kumar S., (2014), "Haar Wavelet Matrices for the Numerical Solutions of Differential Equations" *International Journal of Computer Applications (0975 –8887)*, Volume 97–No.18, pp. (33-36).

Canny, J.F., (1986), "A computational approach to edge detection", *IEEE Transaction on Pattern Analysis and Machine Intelligence*, 8, pp. (679-714).

Carasso, A.S., (2013), "Alternative Methods of Latent Fingerprint Enhancement and Metrics for Comparing Them", National Institute of Standards and Technology, U.S. Department of Commerce, pp. (1-21).

Das, S., Rana, M.S., Sebastian, B., Mukherjee D. and Abdulla K.K., (2013), "Examination of Pipe Welds by Image Plate Based Computed Radiography System", Atomic Fuels Division, Bhabha Atomic Research Centre, Mumbai, India, pp (1-7).

Domingo, M. (2014), "X-ray Testing by Computer Vision", *The British Institute of Non-Destructive Testing*, Manchester, UK, pp. (9-11).

Galatsanos, N.P., Segall, C.A. and Katsaggelos, A.K., (2003), "Digital Image Enhancement", *Encyclopedia of Optical Engineering*, pp. (388-402).

Gonzalez, R.C. and Woods, R.E., (2008), *Digital Image Processing*, Third Edition, Pearson Education, Inc., Upper Saddle River, New Jersey, USA.

Halfawy, M.R. and Hengmeechai, J., (2014), "Automated Defect Detection in Sewer Closed Circuit Television Images using Histograms of Oriented Gradients and Support Vector Machine", *Automation in Construction*, 38, pp. (1-13).

Hellier, C.J., (2003), *Handbook of Non-destructive Evaluation*, McGraw-Hill Companies, Inc. New York, USA.

Hui, T., Lin, C., Zengli, L. and Zaiyu, C., (2013) "Wavelet Image Denoising Based on the New Threshold Function", *Second International Conference on Computer Science and Electronics Engineering (ICCSEE)*, Atlantis Press, Paris, France, pp. (2749-2752).

Iyer, S. and Sinha, S.K., (2005), "Automated Condition Assessment of Buried Sewer Pipes Based on Digital Imaging Techniques", *Indian Institute of Science*, Vol-85, pp. (235–252).

Jin, L., Wei, W.Y., Lei, W., Jie, W., and Da, W.D., (2011), "Industrial X-ray Image Enhancement Algorithm based on Adaptive Histogram and Wavelet", *The 6th International Forum on Strategic Technology*, pp. (836-839).

Juneja, M. and Sandhu, P.S., (2009) "Performance Evaluation of Edge Detection Techniques for Images in Spatial Domain", *International Journal of Computer Theory and Engineering*, Vol. 1, No. 5, pp. (614-621).

Karsten, E., Goebbels, J., Meinel, D., Paetsch, O., Prohaska, S. and Zobel, V., (2011), "Comparison of Crack Detection Methods for Analyzing Damage Processes in Concrete with Computed Tomography" *International Symposium on Digital Industrial Radiology and Computed Tomography – Poster 2*, Berlin, Germany, pp. (1-8).

Kaur, A., Kaur, L. and Gupta S., (2012), "Image Recognition using Coefficient of Correlation and Structural SIMilarity Index in Uncontrolled Environment", *International Journal of Computer Applications (0975 – 8887)*, Volume 59– No.5, pp. (32-39).

Khan, S.U. and Chai, W.Y., (2012), "An Image Enhancement Technique of X-ray Carry-on-Luggage for Detection of Contraband/Illicit Object(s)", *IJCSI International Journal of Computer Science Issues*, Vol. 9, Issue 5, No 1, pp. (205-211).

Khurana, K. and Awasthi, R., (2013), "Techniques for Object Recognition in Images and Multi-Object Detection", *International Journal of Advanced Research in Computer Engineering and Technology*, Volume 2, Issue 4, pp. (1383-1388).

Liao, P., Chen, T. and Chung, P., (2001), "A Fast Algorithm for Multilevel Thresholding", *Journal of Information Science and Engineering*, 17, pp. (713-727).

Longkumer, N., Kumar, M. and Saxena, R., (2014), "Contrast Enhancement Techniques using Histogram Equalization: A Survey", *International Journal of Current Engineering and Technology*, Vol.4, No.3, pp. (1561-1565).

McAndrew, A., (2004), *An Introduction to Digital Image Processing with MATLAB*, Course Technology Press, Boston, MA, USA, 1st Edition.

Mohammadi, P., Moghadam, A.E. and Shirani, S., (2015), "Subjective and Objective Quality Assessment of Image: A Survey", *Majlesi Journal of Electrical Engineering*, Vol. 9, No. 1, pp. (55-83).

Otsu, N., (1979), "A threshold selection method from gray-level histograms", *IEEE Trans. Sys., Man and Cybern*, SMC-9(1): pp. (62-66).

Pai, R.D., Halvi, S. and Hiremath, B., (2015), "Medical Colour Image Enhancement using Wavelet Transform and Contrast Stretching Technique", *International Journal of Scientific and Research Publications*, Volume 5, Issue 7, pp. (1-7).

Rajesh, G., Mittal, B. and Garg, S., (2011), "Histogram Equalization Techniques for Image Enhancement", *International Journal of Electronics and Communication Technology*, Vol. 2, pp. (107-111).

Rajput, Y., Rajput, V., Thakur, A. and Vyas, G., (2012), "Advanced Image Enhancement Based on Wavelet and Histogram Equalization for Medical Images*" IOSR Journal of Electronics and Communication Engineering (IOSRJECE)*, Vol. 2, Issue 6, pp (12-16).

Raju, A., Dwarakish, G.S. and Reddy, D.V., (2013), "A State-of-the-Art and Comparative Analysis of Mean Brightness Preserving Histogram Equalization based Contrast Enhancement Techniques" *International Journal of Remote Sensing and GIS*, Volume 2, Issue 1, pp. (41-51).

Romen, T.S., Roy, S., Imocha, O.S., Sinam, T. and Singh, K., (2011), "A New Local Adaptive Thresholding Technique in Binarization*" IJCSI International Journal of Computer Science Issues*, Vol. 8, Issue 6, No 2, pp. (271-277).

Ruikar, S.D. and Doye, D.D., (2011), "Wavelet Based Image De-noising Technique", *International Journal of Advanced Computer Science and Applications,* Volume 2, Issue No.3, pp. (49-53).

Sahu, D.K. and Parsai, M.P., (2012), "Different Image Fusion Techniques – A Critical Review", *International Journal of Modern Engineering Research*, Vol. 2, Issue 5, pp (4298-4301).

Sampat, M.P., Wang, Z., Gupta, S., Bovik, A. and Markey, K., (2009), "Complex Wavelet Structural Similarity: A New Image Similarity Index", *IEEE Transactions on Image Processing,* Vol. 18, No. 11, pp, (2385-2401).

Santhi, B., Krishnamurthy, G., Siddharth, S. and Ramakrishnan, P.K., (2012), "Automatic Detection of Cracks in Pavements using Edge Detection Operator" *Journal of Theoretical and Applied Information Technology,* Vol 36, No. 2, pp. (199-205).

Saravanan, S. and Kumar, P.S., (2014), "Image Contrast Enhancement Using Histogram Equalization Techniques: Review", *International Journal of Advances in Computer Science and Technology*, ISSN 2320 – 2602, Volume 3, No.3, pp. (163-172).

Sargunar, P.N.J. and Sukanesh, R., (2010), "Automatic Detection of Porosity and Slag Inclusion in Boilers using Statistical Pattern Recognition Techniques", *International Journal of Computer Applications (0975 - 8887),* Volume 1 – No. 21, pp. (75-81).

Satish, D.K., Victor, M. and Nagesha, (2013), "Characterization of brazing defects in oxygen free high thermal conductivity copper using non-destructive testing techniques" *International Journal of Combined Research and Development (IJCRD),* Volume: 1; Issue: 7; pp. (17-24).

Sezgin, M. and Sankur, B., (2004), "Survey over Image Thresholding Techniques and Quantitative Performance Evaluation", *Journal of Electronic Imaging*, Volume 13(1), pp. (146–165).

Sifuzzaman, M., Islam, M.R. and Ali, M.Z., (2009) "Application of Wavelet Transform and its Advantages Compared to Fourier Transform" *Journal of Physical Sciences*, Vol. 13, pp. (121-134).

Singh, G.M., Kohli, M.S. and Diwakar, M., (2013), "A Review of Image Enhancement Techniques in Image Processing" *HCTL Open International Journal of Technology Innovations and Research*, Volume 5, pp. (1-13).

Sinha, S.K. and Fieguth, P.W., (2006), "Segmentation of Buried Concrete Pipe Images", *Automation in Construction,* Vol -15, pp. (47 – 57).

Solomon, C. and Breckon, T., (2011), *Fundamentals of Digital Image Processing – A Practical Approach with Examples in MATLAB*, John Wiley and Sons Ltd, Chichester, UK.

Sukop, M.C., Dijk, G. V., Perfect, E. and Loon, W.P.V., (2002), "Percolation Thresholds in 2-Dimensional Prefractal Models of Porous Media" *Transport in Porous Media*, Vol-48: pp. (187–208).

The MathWorks, Inc., (2009), *Image Processing Tool Box Users Guide*.

Thiruganam, M., Anouncia, M. and Kantipudi, S., (2010), "Automatic Defect Detection and Counting in Radiographic Weldment Images", *International Journal of Computer Applications (0975 – 8887)*, Vol 10– No.2, pp. (1-5).

Tsai, D.M. and Lin, C.T., (2003), "The evaluation of normalized cross correlations for defect detection", *Pattern Recognition Letters*, Vol. 24, pp. (2525-2535).

Vinoth, M. and Jayalakshmi, B., (2014), "Analysis of Edge Detection Algorithms and De-noising Filters on Digital X-ray Images", *International Journal of Science and Technology*, Vol. 2 Issue 2, pp. (42-49).

Weeks, A.R. Jr, (1998), *Fundamentals of Electronic Image Processing*, Second Edition, SPIE Optical Engineering Press, Bellingham, Washington, USA.

Yamaguchi, T., (2008), "*A Study on Image Processing Method for Crack Inspection of Real Concrete Surfaces*", Unpublished PhD thesis, Graduate School of Science and Engineering, Waseda University, Tokyo, Japan.

Yamaguchi, T., Nakamura, S., Saegusa, R. and Hashimoto, S., (2008), "Image-Based Crack Detection for Real Concrete Surfaces", *IEEJ Transactions on Electrical and Electronic Engineering*, Vol - 3: pp. (128–135).

Zhong, Q., Lin, L., Guo, Y. and Wang, N., (2015), "An Improved Algorithm for Image Crack Detection Based on Percolation Model", *IEEJ Transactions on Electrical and Electronic Engineering*; Vol. 10: pp. (214–221).

Other resources:

Advanced Non-Destructive Testing Solutions, accessed 02 March 2015 [online] available from <http://www.ansndt.com/standard-ndt-services/radiography>

Aegleteq Limited, accessed 01 May 2015 [online] available from <http://www.aegleteq.com/Pages/systems.html>

NDT Resource Center, 2001-2014, The Collaboration for NDT Education, accessed 01 May 2015 [online] available from <https://www.ndeed.org/EducationResources/CommunityCollege/Radiography/TechCalibrations/RadiographInterp.htm>

Radiography Film Digitization, accessed 16 March 2015 [online] available from <http://www.buffaloinspection.com/inspection-services/film-digitization>

Radiograph panoramic Gamma Ir-192 pipe 5G weld, accessed 02 March 2015 [online] available from <http://www.weldsmith.co.uk/tech/radiography_ndt/100610_radiog_panopipe/radiogpano5G.html>

Subsea Pipeline Arbitration [online] available from <http://www.exponent.com/Subsea-Pipeline-Arbitration>

U.S. Environmental Protection Agency, accessed 16 March 2015 [online] available from <http://www3.epa.gov/radtown/industrial-radiography.html>, last updated on 10/26/2015.

X-ray film recycling, accessed 01 May 2015 [online] available from <http://www.x-rayfilmrecycling.com/industrial-non-destructive-testing-ndt.html>

APPENDIX

This appendix is divided into two parts. Appendix 1 presents the MATLAB code simulations that were used to generate the results presented in chapter six of this thesis while Appendix 2 contains a paper that was published during the research.

Appendix 1: Selected Algorithms in MATLAB

This segment provides some of the algorithms used in this thesis. These algorithms were implemented as MATLAB functions (scripts) and the programs were used to create the various examples and figures in this thesis. This form of implementation is computationally more efficient and enables experimentation on the multi-dimensional data.

```
%% Project: ENHANCEMENT OF X-RAY IMAGES FOR INDUSTRIAL APPLICATIONS
%%Programmers: NJOGU, KIMANI PETER
%%Date: January, 2015 - April, 2016
%%This code enhances digital radiographic images and also detects
cracks
%%using correlation

%%reading the original image from the stored data base
clc;clear all;close all;
%read image from stored location/folder
image = imread('pipe1.jpg');
if numel(size(image))>2
   image=rgb2gray(image);
end

%performing wavelet decomposition
[ac,hc,vc,dc] = dwt2(image,'haar');
% coefficients construction
all= upcoef2('all', ac, 'haar', 1);
hor= upcoef2('hor', hc, 'haar', 1);
ver= upcoef2('ver', vc, 'haar', 1);
dia= upcoef2('dia', dc, 'haar', 1);
%performing multilevel wavelet decomposition
[r,c]=wavedec2(image,1,'haar');
%coeffiecients extraction
[hc,vc,dc] = detcoef2('all',r,c,1);
%reconstruct decomposed values
hor=wrcoef2('hor',r,c,'haar',1);
ver=wrcoef2('ver',r,c,'haar',1);
dia=wrcoef2('dia',r,c,'haar',1);
%reconstruct the image using multilevel decomposition
Output_image = waverec2(r,c,'haar');
%image compression
img = image_comp(image)
%performing adaptive histogram equalization
image1 = adapthisteq(img);
%performing classical histogram equalization
image2 = histeq(img);
% performing Brigntness preserving bi-histogram equalization
image3 = Brigntness_preserving(img);
```

```
%% performing RMSHE
imaget = Recursive_Mean(img)
% performing DHE
DHE_img = Dynamic_equ(img)

%sharpening of images using the unsharp masking
H = fspecial('unsharp');
sharp = imfilter(img,H);
sharp1 = imfilter(image1,H);
sharp2 = imfilter(image2,H);
sharp3 = imfilter(image3,H);
sharp4 = imfilter(imaget,H);
sharp5 = imfilter(DHE_img,H);

%edge detection using the Canny edge detection technique
% Original edges
edge(img,'canny');
% adaptive HE edges
edge(image1,'canny');
% Classical HE edges
edge(image2,'canny');
% BPDFHE edges
edge(image3,'canny');
% RMSHE edges
edge(imaget,'canny');
% Dyanamic HE edges
edge(DHE_img,'canny');

%Objective measurement of image enhancement
%psnr of Adaptive H.E
disp('Adaptive PSNR, dB')
a = double(img); b = double(image1);
d = sum((a(:)-b(:)).^2) / numel(a);
psnr = 10*log10(255*255/d)

%%Comparioson of percolation and Otsu
clc;clear all;close all;
I = double (image/255);
p = 0.7;
I = I<p;
cc = bwconncomp(I,8);
stats = regionprops(cc,'Image');

%Proposed technique
%Crack detection automation
%%reading the original image from the stored data base
clc;clear all;close all;
image = imread('new1.jpg');
if numel(size(image))>2
    image = rgb2gray(image);
end

% reading the tempale image from the stored data base
img = imread('test1.jpg');
if numel(size(img))>2
    img = rgb2gray(img);
end
score = normxcorr2(img,image);
h = fspecial('unsharp');
I2 = imfilter(score,h);
```

```
sharp = imfilter(score,h,'replicate');

% performing image Thresholding
[c d] = size(sharp);
opim = zeros(c,d);
%op=zeros(ht,wd,'uint8');                              % Take Output
variable
for k = 1:c
    for m = 1:d
        int = sharp(k,m);
        if int < 1.2
            % Define Threshol level
            opim(k,m) = 0;
        else                                           % Thresholding
            opim(k,m) = d;
        end;
    end;
end;
%second comparison
im = imread('test2.jpg');
if numel(size(im))>2
    im = rgb2gray(im);
end
score1 = normxcorr2(im,image);
h = fspecial('unsharp');
I3 = imfilter(score1,h);
shar = imfilter(score1,h,'replicate');
% Thresholding
[a b] = size(shar);
opm = zeros(a,b);                              % Take Output variable
for x = 1:a
    for y = 1:b
        int = shar(x,y);
        if int < 1.5
            % Define Threshol level
            opm(x,y) = 0;
        else                                           % Thresholding
            opm(x,y) = b;
        end;
    end;
end;
%third comparison
img1 = imread('pore.jpg');
if numel(size(img1))>2
    img1 = rgb2gray(img1);
end
score2 = normxcorr2(img1,image);
h = fspecial('unsharp');
I4 = imfilter(score2,h);
sharp1 = imfilter(score2,h,'replicate');
% Thresholding
[e f] = size(sharp1);
opim1 = zeros(e,f);
%op=zeros(ht,wd,'uint8');                              % Take Output
variable
for p = 1:e
    for q = 1:f
        int = sharp1(p,q);
        if int < 1.2
            % Define Threshol level
```

```
            opim1(p,q) = 0;
        else                                        % Thresholding
            opim1(p,q) = f;
        end;
    end;
end;
%fourth comparison
img2 = imread('weld.jpg');
if numel(size(img2))>2
    img2 = rgb2gray(img2);
end
score3 = normxcorr2(img2,image);
h = fspecial('unsharp');
I5 = imfilter(score3,h);
sharp2 = imfilter(score3,h,'replicate');
% Thresholding
[g h] = size(sharp2);
opm1 = zeros(g,h);                          % Take Output variable
for r = 1:g
    for s = 1:h
        int = sharp2(r,s);
        if int < 0.85
            % Define Threshol level
            opm1(r,s) = 0;
        else                                        % Thresholding
            opm1(r,s) = h;
        end;
    end;
end;

%displaying cracks detected on the screen
%CoC decision
disp('If maxValue (CoC) is > 0.7, there is a defect')
%CoC
maxValue = max(max(score));
maxValue1 = max(max(score1));
maxValue2 = max(max(score2));
maxValue3 = max(max(score3));
  disp('Results')
  disp('**************')
  disp('First Template')
% first comparison
if maxValue >= 0.70
    disp('There is a defect')
else
    disp('There is no defect')
end
 % second comparison
   disp('**************')
  disp('Second Template')
if maxValue1 >= 0.70
    disp('There is a defect')
else
    disp('There is no defect')
end
 % third comparison
   disp('**************')
  disp('Third Template')
if maxValue2 >= 0.70
    disp('There is a defect')
```

```
else
    disp('There is no defect')
end
 % Fourth comparison
   disp('**************')
  disp('Fourth Template')
if maxValue1 >= 0.70
    disp('There is a defect')
else
    disp('There is no defect')
end
```

Functions used:

```
%% function for image compression
function img = image_comp(image)
[hrt, orhs, papp]=ddencmp('cmp','wv', image);
[comp_image,CXC,LXC,PERF0,PERFL2]=wdencmp('gbl',r,c,'haar',1, hrt,orhs,
papp);
[ca,ch,cv,cd] = dwt2(comp_image,'haar');
%idwt2 to obtain denoised image
m = idwt2(ac,hc,vc,dc,'haar');
img = uint8(m);
end

%% function for Adaptive SSIM
function ssim = SSIM(img1,img2)
dow = fspecial('gaussian', 10, 1.4);
   U(1) = 0.01;
   U(2) = 0.03;
   L = 255;
   D1 = (U(1)*P)^2;
   D2 = (U(2)*P)^2;
dow = dow/sum(sum(dow));
 %Adaptive SSIM
image1 = double(img);
image2 = double(imag1);
u1   = filter2(dow, image1, 'valid');
u2   = filter2(dow, image2, 'valid');
u1_sq = u1.*u1;
u2_sq = u2.*u2;
u1_u2 = u1.*u2;
gma1_sq = filter2(dow, image1.* image1, 'valid') - u1_sq;
gma2_sq = filter2(dow, image2.* image2, 'valid') - u2_sq;
gma12 = filter2(dow, image1.* image2, 'valid') - u1_u2;

if (D1 > 0 && D2 > 0)
ssim_map = ((2*u1_u2 + D1).*(2*gma12 + D2))./((mu1_sq + u2_sq +
D1).*(gma1_sq + gma2_sq + D2));
else
   numer1 = 2*u1_u2 + D1;
   numer2 = 2*gma12 + D2;
   denom1 = u1_sq + u2_sq + D1;
   denom2 = gma1_sq + gma2_sq + D2;
   map_ssim = ones(size(u1));
   pix = (denom1.*denom2 > 0);
   map_ssim(pix) = (numer1(pix).*numer2(pix))./(denom1(pix).*
denom2(pix));
   pix = (denom1 ~= 0) & (denom2 == 0);
   map_ssim(pix) = numer1(pix)./denom1(pix);
```

```
end
disp('Adaptive SSIM')
ssim = mean2(map_ssim)
end
%% function for Recursive Mean Separate Histogram Equalization
function imaget = Recursive_Mean(img)
h=imhist(img);
[m,n]=size(img); imaget=zeros(m,n);
maxx = double(max(max(img)));
minn = double(min(min(img)));
r=1; length=2^r; Xm=zeros(1,length); Xm(1)=maxx+1; Xm(2)=minn+1;
for i=1:r
    for j=1:2^(i-1)
        Xm(2^(i-1)+j+1)= averpixcal(h,Xm(2^(i-1)-j+2),Xm(2^(i-1)-j+1));
    end
    Xm=sort(Xm,'descend');
end
Xm=sort(Xm);
for i=2:2^r
    [row,col]=find((img>=Xm(i-1)-1)&(img<=Xm(i)-2));
    imaget=FuncHE(img,imaget,row,col,h,Xm(i-1)-1,Xm(i)-2,m,n);
end
[row,col]=find((img>=Xm(2^r)-1)&(img<=Xm(2^r+1)-1));
imaget=FuncHE(img,imaget,row,col,h,Xm(2^r)-1,Xm(2^r+1)-1,m,n);
imaget=uint8(imaget);
h1=imhist(imaget);
end
```

Appendix 2: Published Paper

Automation of Defect Detection in Digital Radiographic Images

Kimani Njogu
Institute of Nuclear Science and Technology, University of Nairobi, Kenya.

David Maina
Institute of Nuclear Science and Technology, University of Nairobi, Kenya.

Elijah Mwangi
School of Engineering, University of Nairobi, Kenya.

ABSTRACT

Conventionally, diagnosis of defects in an object depends mainly on experience of the operator. But this process is error prone and liable to subjective considerations such as fatigue, boredom and lapses in operator concentration. This reduces the reliability and consistency of the process thus precluding the undertaking of preventive maintenance with confidence. Also, the process is time consuming and expensive. In this paper, a new automatic defect detection algorithm has been developed in order to identify defects in digital radiographic images. Percolation and Otsu's thresholding and segmentation algorithms have been used and a new procedure for displaying defects on a screen has been developed. Computer simulation based experiments have been used to demonstrate the effectiveness of the proposed algorithm. The performance of the proposed algorithm is found to be better than the existing defect detection algorithms as the results obtained are impressive with respect to the defect detection rate.

Keywords

Binarization, Non-Destructive Testing, Crack detection, Correlation, Percolation.

1. INTRODUCTION

In engineering, Industrial Non-Destructive Testing (NDT) is concerned with all techniques that examine, test, detect and evaluate materials for defects or discontinuities that may affect the usefulness or serviceability of an object without causing any physical damage to the material [1]. In the past, humans have been identifying these defects. However, manual detection is a very complicated and a time consuming process. With the advance of science and technology, automated systems have been developed to detect artifacts and defects like cracks [2]. System automation has significantly improved the accuracy of defect detection.

In recent years, numerous algorithms have been proposed and developed in the field of automated systems. For example, an efficient and simple image segmentation algorithm for automated analysis of scanned images from underground pipes has been developed by Sinha and Fieguth [3]. However, they did not integrate a way of indicating the severity of the crack. Thiruganam [4] *et al.* proposed a segmentation method of radiographic welds combining global and local thresholding. This gave the defect count and significantly improved the efficiency in terms of computational complexity. Yamaguchi [5] *et al.,* introduced a unique image-based approach to detect cracks on concrete surfaces by using percolation thresholding. This model could easily detect simple cracks but it could not detect complex cracks accurately because the window for percolation processing was fixed. Zhong [6] *et al.,* developed an improvement to Yamaguchi [5] *et al.,* on crack detection procedure based on the percolation model by introducing a reduction on the number of iterations during percolation processing. This led to reduction in the computation time and improved the efficiency of crack detection. Karsten [7] *et al.,* did a comparison of the three crack detection techniques of template matching, a sheet filter based on Hessian eigenvalues and percolation thresholding. From these techniques it was found out that it might be relevant to consider template matching when thin cracks are considered. Halfawy and Hengmeechai [8] developed an algorithm for an efficient pattern recognition to support automated detection and classification of pipe defects in images obtained from conventional sewer closed-circuit television (CCTV). The algorithm uses histograms of oriented gradients and support vector machine to identify defects in pipes. The method was only applicable on a few defects and CCTV inspections are known to be costly, time consuming, labour intensive and error prone. Finally, Santhi [2] *et al.* has proposed an automation model for crack detection in pavements using edge detection techniques. However, this algorithm has a limitation in that the given image had to be pre-processed to obtain a gray-scale image with square sized dimension before any detection was done. In addition the performance of the algorithm in comparison to other techniques was not investigated.

This paper proposes an automatic defect detection algorithm based on template matching, percolation with a flexible window and Otsu's thresholding techniques. This would eliminate the need of manual operation to identify defects on surfaces. The proposed algorithm is helpful in regard to the reduction of the computational cost and increasing the accuracy of defect detection. In addition, it can detect a large variety of defects like cracks and fractures. We have also demonstrated that it is possible to have an algorithm for classification of defects. This algorithm incorporates a way of indicating the severity of the defect by having to set a threshold. If the crack is above a certain threshold, it is severe and it will be indicated by the system. This fulfils the primary goal of NDT for discontinuities in engineering materials, which

is to determine whether or not the continuity and homogeneity of a component are adequate for its use.

The rest of this paper is structured as follows: section 2 gives an outline on the theory that is used in coming up with the algorithm proposed. The theory includes: Otsu's and percolation thresholding techniques. Section 3 is a presentation of the proposed method while section 4 gives a presentation of the experimental results obtained using the proposed algorithm. Finally, section 5 gives a conclusion and suggestions on how the work could be extended.

2. THEORETICAL BACKGROUND

2.1 Correlation

In image processing, correlation is a technique used to establish whether a linear relationship exists between two variables. It the process of moving a filter mask over the image and computing the sum of the products in each location. It has found its usage in localizing features in one image that appear in another image.

The correlation of the two functions $f(x,y)$ and a mask $h(x,y)$ is defined as:

$$g(x,y) = \sum_{i=1}^{m}\sum_{j=1}^{n} f(i,j)h(x+i,y+j) \quad (1)$$

where the limits of summation are taken over the region shared by f and h.

In template matching applications, a small reference template with the target defect is found in a large scene image by sliding the template window in a pixel–by–pixel basis. The normalized correlation is then calculated by multiplying the pixels that are overlaid. The correlation of the two images, the template h and the original image f, will be maximum if they match [9].

The term cross correlation is often used in place of correlation to clarify that the images being correlated are different [10]. Normalized Cross Correlation (NCC) has been commonly used as a metric to evaluate the degree of similarity between two images. The main advantage of the normalized cross correlation over the cross correlation is that it is less sensitive to linear changes in the amplitude of illumination in the two compared images. Furthermore, the NCC is confined in the range between -1 and 1. The setting of detection threshold value is much easier than the cross correlation.

The NCC used for finding matches between two images is defined as;

$$\gamma = \frac{\sum_i (x_i - x_m)(y_i - y_m)}{\sqrt{\sum_i (x_i - x_m)^2}\sqrt{\sum_i (y_i - y_m)^2}} \quad (2)$$

where;
x_i and y_i are the intensity values of the pixel in the original and mask images respectively.

x_m and y_m are the mean intensity values of the pixel in the original and mask images respectively.

The NCC is independent of scale changes in the amplitude of f and h. The correlation coefficient has the value $\gamma = 1$ if the two images are absolutely identical while a value of $\gamma = -1$ indicates that the two images have the same shape except that they have the opposite signs. A value of $\gamma = 0$ shows that they are completely uncorrelated [10].

2.2 Image Thresholding

Thresholding is an important technique for image segmentation that tries to identify and extract a target from its background on the basis of the distribution of gray-levels or texture in image objects. The threshold of an image is set manually at a specific value or automatically set by an application. Pixels below the set threshold value are converted to black and pixels above the threshold value are converted to white. The thresholding process is sometimes described as separating an image into foreground values and background values and is referred to as binarization [11].

This can be represented as;

$$g(x,y) = \begin{cases} G_a, & f(x,y) \le T \\ G_b, & f(x,y) > T \end{cases} \quad (3)$$

where;

T is the set threshold,

G_a and G_b are the desired gray levels in thresholded image.

Thresholding can be categorized into either global or local thresholding. Global thresholding consists of setting an intensity value (threshold) such that all pixels having intensity value below the threshold belong to one phase and the remainder belong to the other. This is shown in Equation 4. It tries to find a single threshold value for the whole image. Global thresholding is as good as the degree of intensity separation between the two peaks in the image. It is mostly used in images with uniform contrast distribution of background and foreground [11]. This method is very fast in its operation but it tends to produce marginal noise along the page borders of the image. To overcome these complexities, local thresholding techniques have been proposed for image binarization [10].

A global threshold is a value such that:

$$g(x,y) = \begin{cases} 0 & if\ f(x,y) \le T) \\ 1 & otherwise \end{cases} \quad (4)$$

where;

T is the threshold value,
$g(x,y)$ is the binarized image and
$f(x,y) \in [0,1]$ be the intensity of a pixel at location (x,y) of the image *f*.

Local thresholding splits the original image into various sub-images each with a different threshold. At pixel levels (in comparison with neighbouring pixels), local thresholding yields highly superior results in comparison to global thresholding, particularly for images with varying contrast levels. This achieves good results even on severely degraded images, though it is slow since the computation of image

features from the local neighbourhood is done for each image pixel [12]. This approach is given in Equation 5, where the image is segmented into three gray-regions G_a, G_b and G_c.

$$g(x,y) = \begin{cases} G_a, & 0 \le f(x,y) < T_1 \\ G_b, & T_1 \le f(x,y) < T_2 \\ G_c, & T_2 \le f(x,y) \le G_{max} \end{cases} \quad (5)$$

where $G_{max}$is the maximum allowable gray level of the image $f(x,y)$.

2.2.1 Otsu's Thresholding

Otsu's thresholding was proposed by N. Otsu in 1979 [13] making it one of the oldest techniques in image segmentation. It is a global thresholding selection method and it is popular because of its simplicity and low computational requirements. The basic principle in Otsu's method is to split the image into two classes which are the objects and the background. The automatic threshold is obtained through finding the maximum variance between the two classes. This is done by performing several iterations for all the possible threshold values and calculating a measure of spread for the pixel levels. The purpose of this calculation is to find the threshold value where the sum of foreground and background spreads is minimum or look the point where the variance is maximum. This is important as well-thresholded classes should be distinct with respect to the intensity values of their pixels [10]. In addition to its optimality, Otsu's method is based entirely on computations performed on the histogram of the image, which is easily obtained.

Consider a digital image of size $M \times N$ pixels with intensity levels {0, 1, 2… L-1}. Let n_i denote the number of pixels with intensity i. The normalized histogram has components $p_i = {n_i}/{MN}$, it then follows that:

$$\sum_{i=0}^{L-1} p_i = 1 \qquad p_i \ge 0 \quad (6)$$

Considering a case of bi-level thresholding, $T(k) = k, 0 < k < L-1$, provides a threshold which divides the input image into two classes $C_1$and C_2, where C_1 consists of all the pixels in the image with intensity values in the range $[0,k]$ and C_2 consists of the pixels in the values in the range $[k+1, L-1]$ [14]. The probability, $P_1(k)$, of a pixel being in class C_1 is:

$$P_1(k) = \sum_{i=0}^{k} p_i \quad (7)$$

Similarly, the probability of class C_2 occurring is:

$$P_2(k) = \sum_{i=k+1}^{L-1} p_i = 1 - P_1(k) \quad (8)$$

The effectiveness of a threshold value at a specific level k is obtained as:

$$\eta = {\sigma_B{}^2}/{\sigma_G{}^2} \quad (9)$$

where $\sigma_G{}^2$ is the global variance. The intensity variance of all the pixels in the image is obtained as:

$$\sigma_G{}^2 = \sum_{i=0}^{L-1} (i - m_G)^2 \, p_i \quad (10)$$

m_G is the global mean denoted as:

$$m_G = \sum_{i=0}^{L-1} i p_i \quad (11)$$

and $\sigma_B{}^2$ is the between-class variance, defined as:

$$\sigma_B{}^2 = P_1 \, (m_1 - m_G)^2 + P_2 (m_2 - m_G)^2 \quad (12)$$

where m_1 and m_2 are the mean intensity values of the pixels assigned to class C_1 and C_2 respectively.

From these computations, the further the two means m_1 and m_2 are from each other, the larger $\sigma_B{}^2$ will be. Therefore, the optimal threshold value, k, should maximize the between-class variance. The above equations can easily be extended for multi-level thresholding of an image [14].

2.2.2 Percolation Thresholding

Percolation is a physical model founded on the natural phenomenon of liquid permeation and is effective for describing various phenomena such as electricity conductivity in materials, ferromagnetism and the spread of epidemics [5]. Percolation theory involves the study of discrete objects and their association with each other. This is specifically done by investigating image clusters, their statistics and properties.

For percolation to occur, it must originate from an initial location, and then extends to the surroundings areas according to a probability p. This probability measures the ease of percolation to the nearest neighbouring region. The region with the maximum value of p is percolated. As the percolation process is repeated, the region covered continues to grow and extends until it reaches the border [16]. Generally, for percolation to occur the critical probability must be higher than 0.5927 otherwise percolation is highly unlikely. This value has been determined empirically [15]. In image processing based-percolation model, the points with related and similar gray-values are percolated and eventually form an image cluster [6].

Percolation thresholding entails four steps.

i) The size of the local window is fixed and the initial pixel at the center of the local window is set. These initial pixels belong to a percolated region D_p, and the initial threshold is set to the value of the initial pixel brightness.

ii) The threshold T is updated as indicated below [6]:

$$T = \max\left(\max_{p \in D_p}(V(p)), T\right) + \omega \quad (13)$$

where;

$V(p)$ represents the brightness of the pixel p,

ω represents the acceleration parameter, which accelerate percolation.

iii) The eight neighbouring pixels of D_p are indicated in the region D_c. The pixels whose brightness is below the threshold T are percolated and included as part of D_p. Else, the pixel with the lowest brightness in D_c is regarded as a part of D_p.

iv) Termination occurs here when D_p reaches the boundary of the local window. Else, the process goes back to stage two. Therefore, the final D_p is defined, and a cluster is formed by the percolation process. By describing the percolated (D_p), the focal pixel obtained is assessed to determine whether it belongs to a defect. This is done by using the circularity (F_c) as an attribute of D_p as:

$$F_c = {4C_{count}}/{(4{C_{max}}^2)} \quad (14)$$

where,

C_{count} is the number of pixels in cluster D_p and,

C_{max} is the diameter of the circumcircle in the percolated cluster that is formed by the proposed scalable window processing.

The value of Fc is close to zero if the pixels at the centre of the local window belongs to crack area. This makes the percolation region to grow linearly. Otherwise, the center pixel belongs to the background region and the value of the circularity (F_c) is close to 1. Therefore, the value of F_c ranges from 0 to 1, and it can determined whether the center pixel belongs to cracks according to the feature quantity of F_c [6].

Percolation process can be improved by modifying the acceleration parameter, ω. This improved parameter ω' is given as [5];

$$\omega' = F_c.\omega \quad (15)$$

3. PROPOSED METHOD

Automatic Defect Detection

Thresholding together with correlation were used for automatic defect detection. Otsu's and percolation thresholding techniques were used to eliminate irrelevant information, leaving only the objects of interest in the image. Finally, template matching was used in defect detection as illustrated in Figure 1.

From Figure 1, an image is loaded in MATLAB where it is converted to gray-scale. A binarization process using either Otsu's thresholding or percolation thresholding is then applied to remove unnecessary information in the image. The main process of defect detection using template matching is then performed by using correlation. This involves a direct comparison between the image template and the original image and evaluating the degree to which the two images are similar. This is recorded as the Coefficient of Correlation (CoC), which gives mathematically the degree of correlation between two images. A threshold value is set for CoC and value above the threshold indicates the presence of a defect and it is shown on a screen, otherwise, the defect is not major.

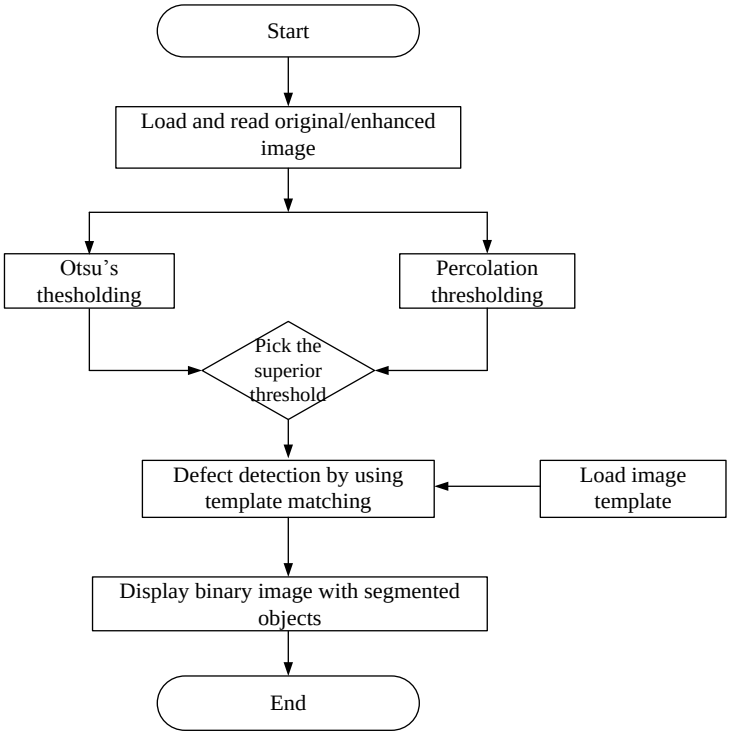

Figure 1: Defect detection flow chart

The method consists of the following procedure;

vi) Reading the original X-ray images from the stored database.
vii) Performing either Otsu's or percolation thresholding.
viii) The results obtained by segmentation are used for further higher-level methods of feature extraction. Defects were detected by using template matching.
ix) A threshold value is set for CoC and value above the threshold indicates the presence of a defect, otherwise, the defect is not major.
x) Finally, the presence or absence of a defect is shown on a screen.

4. RESULTS AND DISCUSSION

The results that were obtained from a series of experiments conducted through computer simulations based on MATLAB are presented. A total of twenty nine samples were tested using the proposed methodology. The X-ray images used were obtained from various internet sites. These images have been used by other researches working in the same field [4, 17].

4.1 Image Segmentation

The results in Figure 2 shows the comparison between Otsu's and percolation thresholding. Otsu's thresholding perform clustering-based image thresholding while percolation

thresholding describes the behaviour of connected clusters. The identified defects are detected by using connectivity of the surrounding binary images. Figure 2(b) and 2(c) clearly shows the results of Otsu's and percolation thresholded images respectively.

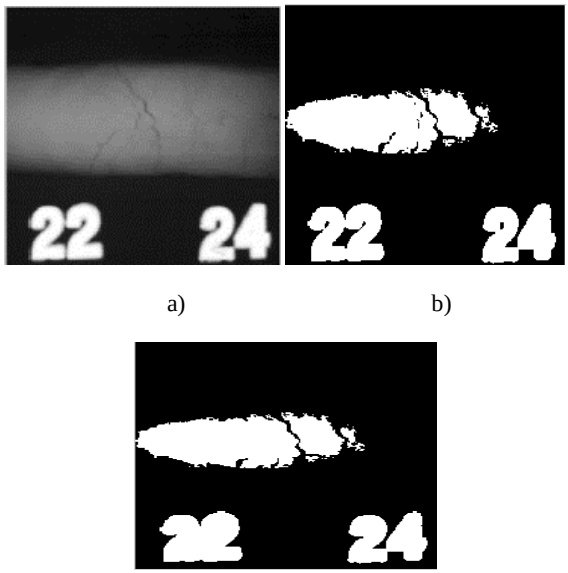

a) b)

c)

Figure 2: Image segmentation. (a) Input image. (b) Otsu's Thresholding (c) Percolation Thresholding.

4.2 Automatic Crack Detection

Manual inspection of defects have been noted to lack reliability and consistency, making it impossible to undertake the process of preventive maintenance with sureness. Therefore, developing an automatic crack detection and classification method is the inevitable way to solving this problem. This development would be expected to achieve high performance in detection rate, detection accuracy and detection efficiency.

4.2.1 Control experiment

Two images without cracks were used as control experiments. One image as shown in Figure 3(a) was selected and several templates as shown in Figure 3(b), 3(c) and 3(d) were passed over it to try and obtain regions of similar defects by using image correlation. The templates used were from different images and not from the main images. This was done so as to achieve template independence. After passing all the templates over the image, the results in Figure 3(e), 3(f) and 3(g) were obtained. From these results it shows no defect were identified.

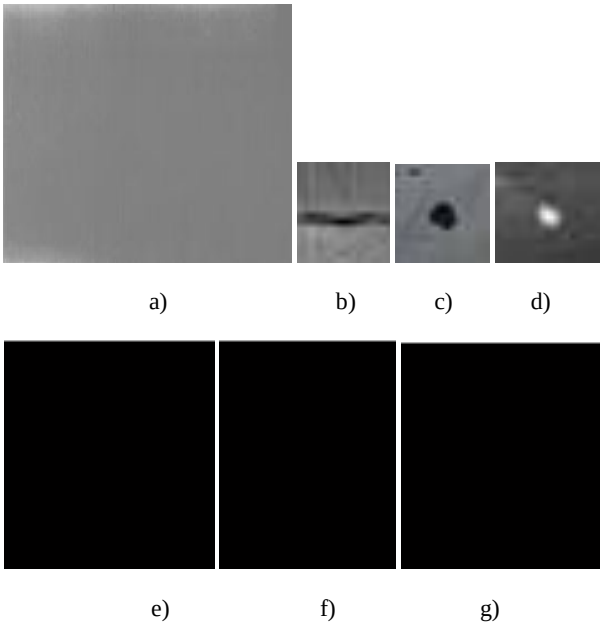

a) b) c) d)

e) f) g)

Figure 3: Control experiment (a) Input image. (b) Horizontal crack template image. (c) Pore1 template image (d) Pore2 template image (e) Horizontal crack result (f) Pore1 template result (g) Pore2 template result

A defect analysis and interpretation algorithm has been developed. This has been implemented by using the Coefficient of Correlation (CoC), which indicates how the two images resemble each other. A series of experiments have shown a threshold of 0.7 to be appropriate. This is higher than the critical threshold required for percolation to occur [15]. Also, a value of 0.7 eliminates unnecessary thresholded information as proved after several experiments. From the proposed algorithm, a value of CoC that is above 0.7 identifies a defect and it is indicates on the screen as shown below.

```
>>
If maxValue (CoC) is > 0.70, there is a defect
Results
******************
First Template a)
There is no defect
******************
Second Template b)
There is no defect
******************
Third Template c)
There is no defect
>>
```

4.2.2 Weld Pore

Twelve weld pores spot images were used to test the proposed algorithm. A weld pore image with a defect as shown in Figure 4(a) was selected. Two templates as shown in Figure 4(b) and 4(c) were passed over it in order to identify regions of similar defects by using correlation. The results in Figure 4(d) and 4(e) were obtained indicating the presence of a defect.

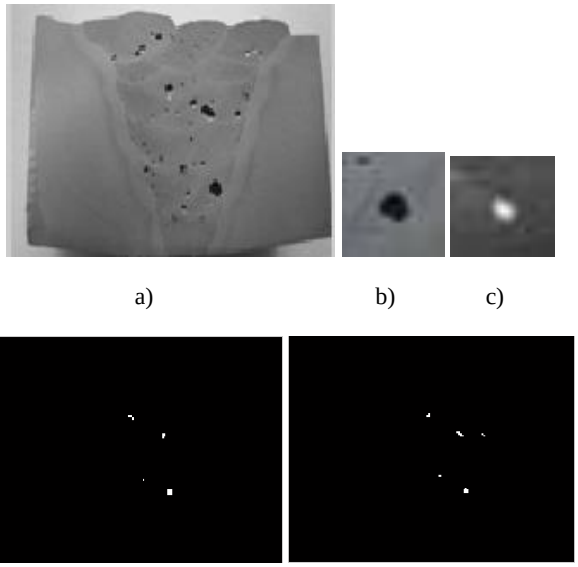

a) b) c)

d) e)

Figure 4: Weld pore results. a) Original image b) Pore 1 image c) Pore 2 image d) Pore 1 results e) Pore 2 results

From the algorithm that was developed, the following results were displayed on the screen.

```
>>
If maxValue (CoC) is > 0.70, there is a defect
Results
**************
First Template
There is a defect
**************
Second Template
There is a defect
>>
```

4.2.3 Slag Inclusion

Five weld images with slag inclusions as shown in Figure 5(a) were also used. A template as shown in Figure 5(b) was passed over Figure 5(a) in order to identify regions of similar defects by using correlation. The results in Figure 5(c) were obtained. These results indicates the presence of defects on the original image.

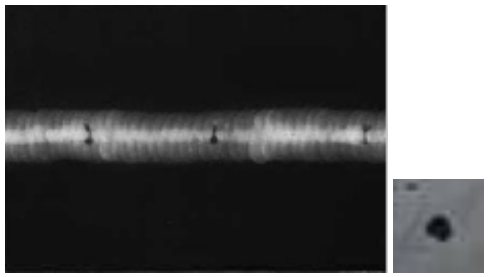

a) b)

c)

Figure 5: Slag inclusion results. a) Original image b) Slag template image c) Slag template results

From the algorithm that was developed, the following results were displayed on the screen.

```
>>
If maxValue (CoC) is > 0.70, there is a defect
Results
**************
First Template
There is a defect
**************
>>
```

4.2.4 Metal Cracks

Ten metal crack images were used to test the applicability of the proposed algorithm. A metal image with a cracks as shown in Figure 6(a) is discussed. Two templates (with defects) as shown in Figure 6(b) and 6(c) were passed over it in order to identify regions of similar defects by using correlation. The results in Figure 6(d) and 6(e) were obtained indicating the presence of a defect on the original image.

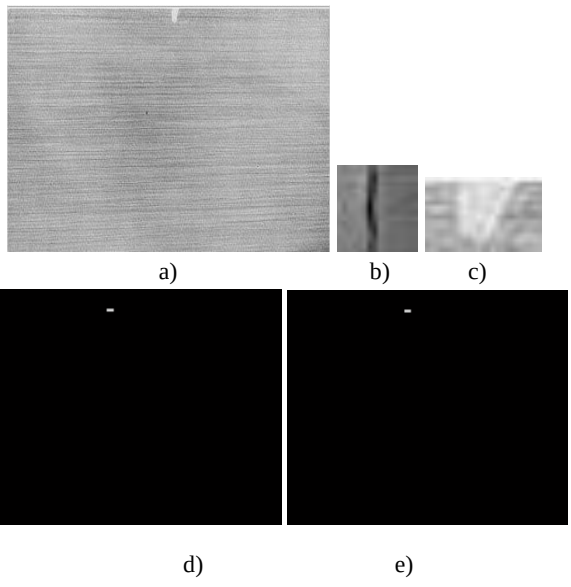

a) b) c)

d) e)

Figure 6: Metal crack results. a) Original image b) Vertical template crack c) Pore template image d) Vertical template result e) Pore template result

From the algorithm that was developed, the following results were displayed on the screen.

```
>>
If maxValue (CoC) is > 0.70, there is a defect
Results
**********
First Template
There is a defect
**********
Second Template
There is a defect
>>
```

4.2.5 Template addition

Two templates, Figure 7(b) and 7(c), were added as shown in Figure 7(d) and then passed over Figure 7(a), the original image, to try and identify detect on the original image. The results in Figure 7(e) and 7(g) were obtained indicating the presence of a defect on the original image. Figure 7(f) did not indicate any defect. Figure 7(g) clearly shows that addition of templates can identify defects on an image. A total of ten images were used to test the applicability of this technique.

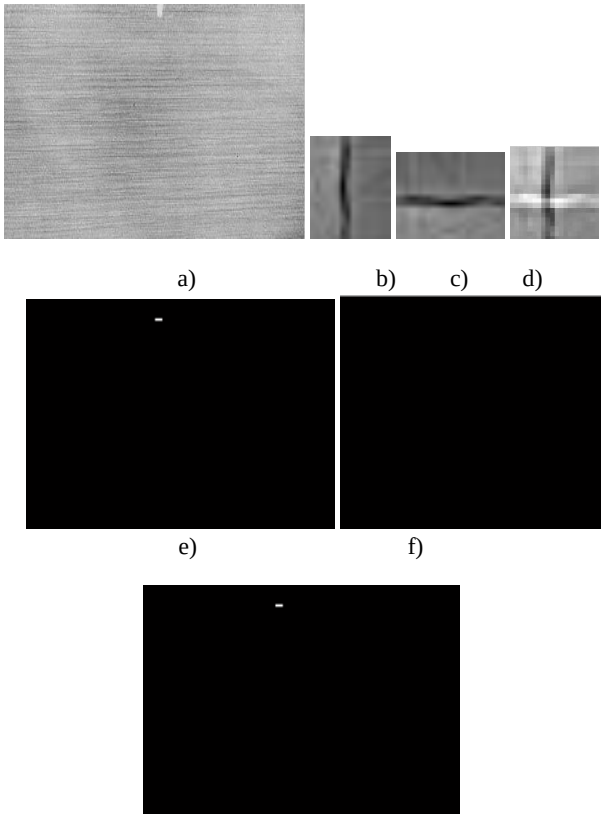

Figure 7: Results of template addition. a) Original image. b) Vertical template crack. c) Horizontal template crack. d) Addition of vertical and horizontal templates. e) Result of template (b). f) Result of template (c). g) Result of addition of template (d).

The following results were displayed on the screen.

```
If maxValue (CoC) is > 0.70, there is a defect
Results
**********
First Template
There is a defect
**********
Second Template
There is no defect
**********
Third Template
There is a defect
>>
```

The number of experiments performed and the rate of correct defect detection are summarized in Table 1.

Table 1: Experiments performed and the percentage of correct detection

	Number of images used	**% of correct detection**
Weld spot detection	12	83.3%
Crack detection	10	80.0%
Slag inclusion	5	100%
Template addition	10	90.0%

5. ACKNOWLEDGMENT

The authors of this paper would like to acknowledge the International Science Programme, Uppsala University, Sweden, for their research support at the Institute of Nuclear Science and Technology as well as Prof. M. J. Gatari for his suggestions and help. The authors are also grateful to the anonymous reviewers and associate editor for their valuable comments.

6. CONCLUSION

In automatic defect detection, a formulation of a novel image processing method which takes into account the connectivity among neighbourhoods based on either Otsu's thresholding or percolation model were compared. Otsu's techniques proved to be superior through experiments. The results of the automatic defect detection method show that the proposed method produces reliable results which can be used in industries to reduce the effect of errors in detection and to overcome the challenge of always relying on trained operators to identify defects in an image.

There exist much space for future work in order to improve the performance of the proposed algorithm especially on automatic defect detection. For example, to apply the algorithm to a video sequence, instead of static images, by exploiting the motion information and optical flow in tracking and verifying defects over the image sequence.

7. REFERENCES

[1] C. J. Hellier, *Handbook of Non-destructive Evaluation*, McGraw-Hill Companies, Inc., New York, USA, 2003.

[2] B. Santhi, G. Krishnamurthy, S. Siddharth and P. K. Ramakrishnan, "Automatic Detection of Cracks in Pavements using Edge Detection Operator" *Journal of Theoretical and Applied Information Technology*, pp. (199-205), February 2012.

[3] S. K. Sinha and P. W. Fieguth, "Segmentation of Buried Concrete Pipe Images", *Automation in Construction*, 15, (2006), pp. 47 – 57.

[4] M. Thiruganam, S. M. Anouncia and S. Kantipudi, "Automatic Defect Detection and Counting in Radiographic Weldment Images", *International Journal of Computer Applications*, Vol 10– No.2, pp. (1-5), November 2010.

[5] T. Yamaguchi, S. Nakamura, R. Saegusa and S. Hashimoto, "Image-Based Crack Detection for Real Concrete Surfaces", *IEEJ Transactions on Electrical and Electronic Engineering*, 2008; 3: pp. 128–135.

[6] Q. Zhong, L. Lin, Y. Guo and N. Wang, "An Improved Algorithm for Image Crack Detection Based on Percolation Model", *IEEJ Transactions on Electrical and Electronic Engineering*, 2015; 10: pp. 214–221.

[7] E. Karsten, J. Goebbels, D. Meinel, O. Paetsch, S. Prohaska and V. Zobel, "Comparison of Crack Detection Methods for Analyzing Damage Processes in Concrete with Computed Tomography" *International Symposium on Digital Industrial Radiology and Computed Tomography*, Berlin, Germany, pp. (1-8), June 2011.

[8] M. R. Halfawy and J. Hengmeechai "Automated Defect Detection in Sewer Closed Circuit Television Images using Histograms of Oriented Gradients and Support Vector Machine", *Automation in Construction*, 38 pp. (1-13), 2014.

[9] D. M. Tsai, and C. T. Lin, "The evaluation of Normalized Cross Correlations for defect detection", *Pattern Recognition Letters*, vol. 24, pp. 2525-2535, 2003.

[10] R. C. Gonzalez and R. E. Woods, *Digital Image Processing*, Third Edition, Pearson Education, Inc., Upper Saddle River, New Jersey, USA, 2008.

[11] T. S. Romen, S. Roy, O. S. Imocha, T. Sinam and K. Singh "A New Local Adaptive Thresholding Technique in Binarization*" IJCSI International Journal of Computer Science Issues*, Vol. 8, Issue 6, No 2, pp. 271-277, November 2011.

[12] A. R. Weeks, Jr, *Fundamentals of Electronic Image Processing*, Second Edition, SPIE Optical Engineering Press, Bellingham, Washington USA, 1998.

[13] N. Otsu. "A threshold selection method from gray-level histograms". *IEEE Trans. Sys., Man and Cybern*, SMC-9(1): pp. 62-66, January 1979.

[14] P. Liao, T. Chen and P. Chung, "A Fast Algorithm for Multilevel Thresholding", *Journal of Information Science and Engineering*, 17, pp. 713-727, 2001.

[15] M. C. Sukop, G. Van Dijk, E. Perfect and W. P. Van Loon, "Percolation Thresholds in 2-Dimensional Prefractal Models of Porous Media" *Transport in Porous Media*, 48: pp. 187–208, 2002.

[16] T. Yamaguchi, "*A Study on Image Processing Method for Crack Inspection of Real Concrete Surfaces*", Unpublished PhD thesis, Graduate School of Science and Engineering, Waseda University, Tokyo, Japan, 2008.

[17] X-ray film recycling, accessed 01 May 2015 [online] available from <http://www.x-rayfilmrecycling.com/industrial-non-destructive-testing-ndt.html>